DESIGN, MANUFACTURING AND TESTING OF AN ETHANOL/LOX BI-PROPELLANT ROCKET ENGINE WITH A FOCUS ON THE MASS FLOW CONTROL

by

İbrahim Safa Uç

B.S., Mechanical Engineering, Boğaziçi University, 2019

Submitted to the Institute for Graduate Studies in
Science and Engineering in partial fulfillment of
the requirements for the degree of
Master of Science

Graduate Program in Mechanical Engineering

Boğaziçi University

2022

ACKNOWLEDGEMENTS

First of all, I would like to express my gratitude to my advisor Prof. Murat ÇELİK for his immense support and guidance throughout my thesis. His enthusiasm and immense knowledge has been a crucial source of motivation during this research. I also want to thank him for allowing me to take part in many interesting experiments in the laboratory.

I would like to thank the members of my thesis committee, Prof. Şebnem ÖZÜPEK and Prof. Tufan Coşkun KARALAR, for the time they spent reading and correcting in the preparation process of this dissertation.

I would like to thank my colleague Enes Oğuz İSKENDER for his invaluable contributions and sincere friendship during our studies. We spent many days full of challenges and fun.

I would like to express my gratitude to my parents. Without their tremendous understanding and encouragement in the past few years, it would be impossible for me to complete my study.

Last but not least, I would like to thank my precious wife Selcen YEDİYILDIZ UÇ who has stood by me through all my travails, good days and bad days. Words cannot express my gratitude to her for her love, support, encouragement, appreciation and keen interest in my research.

ABSTRACT

DESIGN, MANUFACTURING AND TESTING OF AN ETHANOL/LOX BI-PROPELLANT ROCKET ENGINE WITH A FOCUS ON THE MASS FLOW CONTROL

Rocket engines are getting more popular day by day with the involvement of private companies in the space industry. Reusable rockets and lander vehicles are gaining more importance with the upcoming technologies regarding space exploration. Throttleable rocket engine is one of the key components for these rockets and vehicles. In this thesis, a 5 kN pressure fed and water cooled rocket engine was designed, manufactured and tested as a starting point for developing a throttleable and regeneratively cooled rocket engine. %75 concentrated ethanol-water mixture is used as the fuel and liquid oxygen is used as the oxidizer. Engine is designed to work at 30 bar chamber pressure for 1.01 kg/s and 1.26 kg/s fuel and oxidizer mass flow rates, respectively. A preliminary design procedure for the thrust chamber is explained. Cooling channel geometry, and heat transfer between the hot combustion gases and the coolant flow are investigated. Cavitating venturies are used for the mass flow rate control. Their designs and tests are discussed in detail. A test stand is developed to test the engine. Overview of the test stand and pressure control systems are explained. Engine firing test is conducted and achieved mass flow rates are found out to be lower than the expected. 0.89 kg/s fuel and 0.83 kg/s oxidizer mass flow rates are achieved at the final complete thrust chamber test. Possible causes for this situation are investigated.

ÖZET

ETANOL/LOX SIVI YAKITLI ROKET MOTORUNUN KÜTLE AKIŞ KONTROLÜ ODAKLI TASARIMI, ÜRETİMİ VE TESTLERİ

Roket motorları, uzay endüstrisine özel şirketlerin de dahil olmasıyla her geçen gün daha popüler hale geliyor. Yeniden kullanılabilir roketler ve yeryüzü iniş araçları, uzay araştırmaları konusunda gelişen teknolojilerle daha da önem kazanıyor. Ayarlanabilir itkili roket motoru, fırlatma roketleri ve yeryüzü iniş araçları için en önemli parçalardan biridir. Bu tezde, ayarlanabilir itkili ve rejeneratif soğutmalı bir roket motoru geliştirmek için başlangıç noktası olarak 5 kN itki düzeyinde, basınç beslemeli ve su soğutmalı bir roket motoru tasarlanmış, üretilmiş ve test edilmiştir. Yakıt olarak %75 konsantre etanol-su karışımı, oksitleyici olarak sıvı oksijen kullanılmaktadır. Motor, 30 bar yanma odası basıncında sırasıyla 1.01 kg/s ve 1.25 kg/s yakıt ve oksitleyici kütle akış hızları elde edilecek şekilde tasarlanmıştır. İtki odası için bir ön tasarım prosedürü anlatılmıştur. Soğutma kanalı geometrisi ve yanma odasındaki sıcak gazlar ile soğutucu akışı arasındaki ısı transferi incelenmiştir. Kütle akış hızı kontrolü için kavitasyon venturileri kullanılmıştır. Kavitasyon venturilerinin tasarımları ve testleri ayrıntılı olarak açıklanmıştır. Motoru test etmek için bir test standı geliştirilmiştir. Test standı ve basınç kontrol sistemleri ayrıntılarıyla anlatılmıştır. Motor ateşleme testi yapılmış ve elde edilen kütle akış hızlarının beklenenden daha düşük olduğu tespit edilmiştir. Ateşleme testinde 0.89 kg/s yakıt ve 0.83 kg/s oksitleyici kütle akış hızları elde edilmiştir. Bu durumun olası nedenleri incelenmiştir.

TABLE OF CONTENTS

ACKNOWLEDGEMENTS iii
ABSTRACT iv
ÖZET v
LIST OF FIGURES ix
LIST OF TABLES xvi
LIST OF SYMBOLS xvii
LIST OF ACRONYMS/ABBREVIATIONS xx
1. INTRODUCTION 1
1.1. Literature Review 11
1.1.1. Tecnico Lisboa 11
1.1.2. Minerva Project 13
1.1.3. Lulea University of Technology 15
1.1.4. University of Texas at El Paso 16
1.2. Scope of This Study 19
2. THEORETICAL BACKGROUND 21
2.1. Propellants 24
2.1.1. Fuels 25
2.1.1.1. Liquid Hydrogen 25
2.1.1.2. Liquid Methane 25
2.1.1.3. Kerosene 25
2.1.1.4. Ethanol 26
2.1.2. Oxidizers 26
2.1.2.1. Liquid Oxygen (LOX) 26
2.1.2.2. Hydrogen Peroxide (H_2O_2) 26
2.1.2.3. Nitrogen Tetroxide (N_2O_4) 27
2.1.2.4. Nitrous Oxide (NO_2) 27
2.2. Heat Transfer in Cooling Channels 27
3. ENGINE DESIGN 32

3.1. Propellants . . . 33
3.2. Thrust Chamber Characteristics . . . 36
3.3. Thrust Chamber . . . 40
3.3.1. Injector . . . 41
3.3.2. Combustion Chamber . . . 44
3.3.3. Nozzle . . . 46
3.3.4. Cooling Channels . . . 48
3.3.4.1. Calculating Convective Heat Transfer Coefficients . . . 49
3.4. Igniter . . . 52
4. PROPELLANT FEED SYSTEM . . . 53
4.1. Propellant Tanks . . . 55
4.2. Valves . . . 56
4.3. Cavitating Venturi . . . 57
4.3.1. Design of the Venturi . . . 60
4.3.1.1. CFD Benchmark Study . . . 61
4.3.1.2. Sizing of the venturies . . . 63
4.3.2. Manufacturing . . . 73
4.4. Pressure Control . . . 74
5. TEST SETUP . . . 77
5.1. High Pressure Gas System . . . 77
5.2. Control Table . . . 77
5.3. Propellant Tank Systems . . . 78
5.4. Cooling Water System . . . 79
5.5. Engine and Thrust Stand . . . 80
5.6. Flow Diagram . . . 80
6. COMPONENTS AND MATERIAL SELECTION . . . 86
6.1. Combustion Chamber and Nozzle . . . 86
6.2. Injector . . . 90
6.3. Dome . . . 91
6.4. Jacket . . . 93
6.5. Jacket Flange . . . 94

6.6. Saddle . . . 96
6.7. Cover . . . 98
6.8. Sensors . . . 99
6.8.1. Pressure Sensors . . . 99
6.8.2. Flow Meters . . . 100
6.8.3. Load Cells . . . 101
6.9. Actuators . . . 102
6.9.1. Pneumatic Valves . . . 102
6.9.2. Solenoid Valves . . . 102
6.10. Control System . . . 105
7. TESTS . . . 110
7.1. Component Tests . . . 110
7.1.1. Cooling Water Mass Flow Rate Test . . . 110
7.1.2. Injector Water Tests . . . 111
7.2. Thrust Chamber Tests . . . 112
7.2.1. Cold Flow Tests . . . 112
7.2.2. Open Fire Tests . . . 116
7.2.2.1. 30 Bar Test . . . 118
7.2.2.2. 80 Bar Test . . . 120
7.2.3. BUSTLab V1 Complete Thrust Chamber Test . . . 123
8. CONCLUSION . . . 130
8.1. Future Work . . . 134
REFERENCES . . . 137
APPENDIX A: CAVITATING VENTURI TESTS . . . 141
A.1. OCV-V0 Water Tests . . . 141
A.2. FCV-V1 Water Tests . . . 142
APPENDIX B: TECHNICAL DRAWINGS . . . 144
B.1. Fuel Cavitating Venturi FCV-V1 . . . 145
B.2. Oxidizer Cavitating Venturi OCV-V1 . . . 146
B.3. Combustion Chamber . . . 147
B.4. Dome . . . 148

LIST OF FIGURES

Figure 1.1. Schematics of pressure fed, gas generator cycle, expander cycle and staged combustion cycle systems [2]. 5

Figure 1.2. Ideal vacuum exit velocity (v_e or $I_{sp}g_0$) values of common propellant combinations for a range of oxidizer to fuel mixture ratios [2]. . . . 9

Figure 1.3. Schematic of regenerative cooling in rocket engines [5]. 11

Figure 1.4. MLE5K-S1a design with ablative cooling [9]. 14

Figure 1.5. MLE5K-S1b design with calorimetric chamber [9]. 14

Figure 1.6. Cold flow test results of the impinging injector showing the change of discharge coefficient (C_d) with respect to pressure drop (ΔP) [9]. 15

Figure 1.7. Design of the CROME [12]. 17

Figure 1.8. Mission summary of the JANUS [13]. 18

Figure 1.9. CROME-X engine attached to the vehicle interface [13]. 18

Figure 2.1. Sample schematic of regenerative cooling [15]. 28

Figure 3.1. Change of the combustion temperature with the OF ratio for (a) %100-%0 ethanol-water, (b) %85-%15 ethanol-water and (c) %75-%25 ethanol-water concentration. 34

Figure 3.2. Change of the I_{sp} with OF ratio and ethanol concentration. 35

Figure 3.3. Representations of impinging and shower head injectors [3]. 42

Figure 3.4. A sample pintle injector [18]. 43

Figure 3.5. Schematic of a swirl injector [19]. 43

Figure 3.6. Schematic of a shear coaxial injector [20]. 44

Figure 3.7. Exhaust gas behaviour for three different nozzle configurations for sea level test and flight conditions [3]. 47

Figure 3.8. Closer look at the cooling water channels. 48

Figure 3.9. Longitutional cross-section of the rocket engine showing the sections 1,2 and 3 used in the heat transfer calculations (L(1) =0.27 m, L(2) = 0.05 m and L(3) = 0.13 m). 50

Figure 4.1. Overview of the predicted pressures in the system. 53

Figure 4.2. Oxidizer tank (a) before and (b) after the insulation. 56

Figure 4.3. Change of sonic velocity with respect to air volume fraction for water/bubble homogeneous mixture [23]. 59

Figure 4.4. Used quadrilateral mesh in the benchmark study. (a) shows the full model and (b) shows critical region which has a denser mesh. . 61

Figure 4.5. Liquid phase volume fraction contours (a) for 44 bar downstream pressure and (b) for 55 bar downstream pressure. 62

Figure 4.6. Results of the benchmark study. (a) shows the results of Kang et. al. [24] and (b) shows the results of CFD analysis conducted for benchmark study. 63

Figure 4.7. CFD results for 5 bar upstream pressure. 65

Figure 4.8. CFD results for 30 bar upstream pressure. 65

Figure 4.9. Change of mass flow rate for different upstream pressures in cavitating mode. 66

Figure 4.10. Test results of the fuel cavitating venturi FCV-V0 for the upstream pressure of 6 to 9 bar. 68

Figure 4.11. Water test results of the oxidizer cavitating venturi OCV-V0 for the upstream pressure of 4 to 7 bar (OCV-V0 - Test 1). 69

Figure 4.12. Change of mass flow rate with the pressure ratio for OCV-V0 - Test 1. 70

Figure 4.13. Test results of the fuel cavitating venturi FCV-V1 for the upstream pressure of 24.5 bar (FCV-V1 - Test 1). 72

Figure 4.14. Change of mass flow rate with respect to pressure ratio for FCV-V1 at 14 bar upstream pressure. 72

Figure 5.1. Test stand and load cell connection from (a) upper view and (b) side view. 81

Figure 5.2. Diagram of the propellant feed systems and the cooling water system. 82

Figure 6.1. Exploded CAD view of the engine. 86

Figure 6.2. Assembled CAD view of the engine. 87

Figure 6.3. Designed combustion chamber from (a) front, (b) back and (c) cut views. 88

Figure 6.4. Manufactured combustion chamber showing (a) the side of the chamber and (b) the inner surface of the chamber. 89

Figure 6.5. Designed Injector 2 from (a) front, (b) back and (c) cut views. . . 90

Figure 6.6. (a) Dome side and (b) chamber side of the manufactured injector. 90

Figure 6.7. Designed dome from (a) front, (b) back and (c) cut views. 91

Figure 6.8. (a) Injector side and (b) outer side of the manufactured dome. . . 92

Figure 6.9. Designed jacket from (a) front, (b) back and (c) cut views. 93

Figure 6.10. (a) Outside and (b) inside of the manufactured jacket. 94

Figure 6.11. Designed jacket flange from (a) front, (b) back and (c) cut views. . 95

Figure 6.12. (a) Dome side and (b) combustion chamber side of the manufactured jacket flange. 95

Figure 6.13. Designed saddle from (a) front, (b) back and (c) cut views. 96

Figure 6.14. (a) Outer and (b) inner side of the manufactured saddle. 97

Figure 6.15. Saddle and combustion chamber assembly. 97

Figure 6.16. Designed cover from (a) front, (b) back and (c) cut views. 98

Figure 6.17. (a) Combustion chamber side and (b) outer side of the manufactured cover. 99

Figure 6.18. KELLER PA-21Y pressure sensor [25]. 100

Figure 6.19. (a) Beam type and (b) S-type load cells. 101

Figure 6.20. (a) Swagelok 133 spring return type and (b) double acting type pneumatic actuators. 103

Figure 6.21. (a) 3/2 type [26] and (b) 5/2 type [27] solenoid valve schematics are shown, (c) shows a representative solenoid valve [28]. 104

Figure 6.22. Appearance of the LABView panel. 108

Figure 7.1. BUSTLab V1 rocket engine cold flow test. 113

Figure 7.2. Pressure graphs of the cold flow test with 80 bar tank pressures for (a) the fuel line and (b) the oxidizer line. 114

Figure 7.3. Change of the tank masses during the cold flow test with 80 bar tank pressures for (a) the fuel tank and (b) the oxidizer tank. . . . 115

Figure 7.4. BUSTLab V1 rocket engine open fire test setup. 117

Figure 7.5. BUSTLab V1 10 bar open fire test. 118

Figure 7.6. BUSTLab V1 30 bar open fire test. 119

Figure 7.7. Pressure graphs of the open fire test with 30 bar tank pressures for (a) the fuel line and (b) the oxidizer line. 119

Figure 7.8. Pressure graphs of the open fire test with 80 bar tank pressures for (a) the fuel line and (b) the oxidizer line. 121

Figure 7.9. Change of the tank masses during the open fire test with 80 bar tank pressures for (a) the fuel tank and (b) the oxidizer tank. . . . 122

Figure 7.10. BUSTLab V1 80 bar open fire test. 123

Figure 7.11. BUSTLab V1 rocket engine after cooling the system. 124

Figure 7.12. BUSTLab V1 rocket engine complete thrust chamber test setup. . 125

Figure 7.13. Pressure graphs of the engine test with 80 bar tank pressures for (a) the fuel line and (b) the oxidizer line. 126

Figure 7.14. BUSTLab V1 engine firing test. 127

Figure 7.15. Change of the tank masses during the engine test with 80 bar tank pressures for (a) the fuel tank and (b) the oxidizer tank. 128

Figure A.1. Water test results of the oxidizer cavitating venturi OCV-V0 for the upstream pressure of 4 to 6 bar (OCV-V0 - Test 2) 141

Figure A.2. Water test results of the fuel cavitating venturi FCV-V1 for the upstream pressure of 20 bar (FCV-V1 - Test 2). 142

Figure A.3. Test results of the fuel cavitating venturi FCV-V1 for the upstream pressure of 18.5 bar (FCV-V1 - Test 3). 143

Figure B.1. Technical drawing of the fuel cavitating venturi FCV-V1. 145

Figure B.2. Technical drawing of the oxidizer cavitating venturi OCV-V1. . . . 146

Figure B.3. Technical drawing of the combustion chamber. 147

Figure B.4. Technical drawing of the dome. 148

LIST OF TABLES

Table 1.1. Properties of the engine designed at Tecnico Lisboa [8]. 13

Table 1.2. Thrust chamber parameters for three different EFC [10]. 16

Table 3.1. Summary of the initial 10 kN design with Kerosene-GOX propellant combination. 40

Table 3.2. Summary of the final 5kN design with ethanol-LOX propellant combination. 41

Table 3.3. Typical L* values for the rocket engines. 45

Table 4.1. Test results for the cavitating venturies FCV-V0 and OCV-V0. . . 71

Table 4.2. Test results for the cavitating venturies FCV-V1 and OCV-V1. . . 73

Table 6.1. Test sequence that is used in LABView. 106

Table 7.1. Designed and measured mass flow rates in the fuel and the oxidizer lines. 129

LIST OF SYMBOLS

A	Heat transfer area
A_c	Flow cross sectional area
$A_{chamber}$	Chamber cross sectional area
A_e	Nozzle exit area
A_f	Fin surface area
A_{flow}	Flow area
A_{total}	Total surface area
A^*	Throat area
b	Cooling channel width
C_d	Discharge coefficient
C_v	Flow coefficient
c^*	Characteristic Velocity
D	Diameter
D_e	Nozzle exit diameter
D_h	Hydraulic diameter
D_{throat}	Throat diameter
g_0	Standard gravity
h	Convective heat transfer coefficient
h_c	Convective heat transfer coefficient at the coolant side
h_h	Convective heat transfer coefficient at the hot gas side
I_{sp}	Specific Impulse
k	Thermal conductivity
L	Length of the heat transfer area in axial direction
L_{nozzle}	Nozzle length
L^*	Characteristic chamber length
$\mathbb{L}$	Height of the cooling channel
M	Mach number
M_e	Exit Mach number

M_f	Final mass
M_o	Initial mass
m	Mass
$\dot{m}$	Mass flow rate
$\dot{m}_f$	Fuel mass flow rate
$\dot{m}_o$	Oxidizer mass flow rate
$\dot{m}_{water}$	Water mass flow rate
$\mathbb{M}$	Molecular weight
N	Number of fins
Nu_D	Local Nusselt number
P_a	Ambient Pressure
P_c	Combustion chamber pressure
P_{down}	Downstream pressure
P_e	Nozzle exit pressure
P_o	Total pressure
P_{ratio}	Ratio of downstream pressure to upstream pressure
P_{up}	Upstream pressure
P_{vap}	Vapor pressure
Pr	Prandtl number
$\mathbb{P}$	Wetted perimeter
Q	Heat transfer rate
Q_{total}	Total heat transfer rate
Q_{water}	Total heat transfer rate to the water
Q''	Heat transfer rate per unit area
R	Thermal resistance
$R_{cond,wall}$	Conductive thermal resistance due to the chamber wall
$R_{conv,c}$	Convective thermal resistance at the coolant side
$R_{conv,h}$	Convective thermal resistance at the hot gas side
R''	Thermal resistance per unit area
Re_D	Local Reynolds number
$\mathbb{R}$	Specific gas constant

$\mathbb{R}_{univ}$	Universal gas constant
r_1	Inner wall radius
r_2	Outer wall radius
S_w	Combustion chamber internal wall thickness
T_1	Combustion chamber inner wall surface temperature
T_2	Combustion chamber outer wall surface temperature
T_c	Combustion chamber temperature
$T_{c,i}$	Coolant side inlet temperature
$T_{c,o}$	Coolant side outlet temperature
$T_{h,i}$	Hot gas side inlet temperature
$T_{h,o}$	Hot gas side outlet temperature
T_o	Total Temperature
$T_{water,1}$	Water inlet temperature
$T_{water,2}$	Water temperature at the throat
$T_{water,3}$	Water outlet temperature
$T_{water,corrected,3}$	Corrected water outlet temperature
t	Time
t_w	Rib thickness
$\mathbb{T}$	Thrust
U	Overall heat transfer coefficient
$V_{chamber}$	Chamber volume
v_e	Nozzle exit velocity
ΔV	Change in velocity
ΔT_{lm}	Log mean temperature difference
γ	Ratio of specific heats
η_f	Efficiency of single fin
η_0	Overall efficiency of fin array
ρ	Density

LIST OF ACRONYMS/ABBREVIATIONS

1D	One Dimensional
BUSTLab	Bogazici University Space Technologies Laboratory
CAD	Computer-Aided Design
CEA	Chemical Equilibrium with Applications
CFD	Computational Fluid Dynamics
CNC	Computer Numerical Control
CROME	Centennial Restartable Oxygen Methane Engine
cSETR	Center for Space Exploration and Technology Research
DAQ	Data acquisition
EFC	Ethanol Fuel Concentrations
FCV	Fuel Cavitating Venturi
GH_2	Gaseous Hydrogen
GOX	Gaseous Oxygen
H_2O_2	Hydrogen Peroxide
HPGS	High Pressure Gas System
ISRU	In-Situ Resource Utilization
JP-1	Jet Propellant-1
LCH_4	Liquid Methane
LH_2	Liquid Hydrogen
LOX	Liquid Oxygen
MDF	Medium-Density Fibreboard
MMH	Monomethylhydrazine
N_2O_4	Nitrogen Tetraoxide
NASA	National Aeronautics and Space Administration
NI	National Instruments
NO_2	Nitrogen Dioxide
NPT	National Pipe Thread
NTO	Nitrogen Tetraoxide

OCV	Oxidizer Cavitating Venturi
OF Ratio	Oxidizer to Fuel Mass Flow Rate Ratio
PID	Proportional–Integral–Derivative
RP-1	Rocket Propellant-1
UDMH	Unsymmetrical Dimethylhydrazine
USA	United States of America
UTEP	University of Texas at El Paso
VTOL	Vertical Takeoff Vertical Landing

1. INTRODUCTION

Rocket propulsion systems can be mainly divided into two groups, electrical propulsion and chemical propulsion. Electrical propulsion systems use electric energy to generate thrust from the propellants. They can be grouped in three categories: electrothermal, electrostatic and electromagnetic. Ionized propellant is accelerated by static electric field in electrostatic systems. Propellant is heated by electric energy and than accelerated by a nozzle in electrothermal systems. In electromagnetic thrusters, Lorentz force is used to accelerate ionized propellant. Electrical propulsion systems generate lower thrust compared to chemical propulsion systems. However, they use the propellant more effectively because they can accelerate the propellant to much higher velocities. Therefore, they have higher specific impulse. Chemical propulsion systems have specific impulse values between 40 and 450 seconds whereas 1000-3000 seconds can be achieved with electrical propulsion systems [1].

In chemical propulsion, energy released from the chemical reactions is used to accelerate gasses and generate thrust. Mono-propellant, solid propellant, liquid bi-propellant or hybrid systems can be used. Exothermic decomposition of a single propellant is used to generate thrust in mono-propellant systems. Thrust is generated by burning a fuel and an oxidizer in a combustion chamber and then accelerating hot combustion gas by a nozzle in solid propellant, liquid bi-propellant and hybrid systems. Both the fuel and the oxidizer are in solid state in solid propellant engines. They are mixed as grains and they are contained in a metal casing. When the grain mixture is ignited, they release hot gasses and these are accelerated through a nozzle. Solid propellant engines have quite simple design and they can be stored easily. However, they cannot be shut down after they are ignited and they cannot be throttled. Both the fuel and the oxidizer are in liquid state in liquid bi-propellant engines. They are injected into a combustion chamber from an injector and mixed in the combustion chamber before undergoing a chemical reaction. Propellants can be pressurized by an inert gas like helium or turbopump systems can be used for pressurization. Mass flow rate of the

propellants and the generated thrust can be adjusted in liquid bi-propellant engines. Restarting the engine after shut-down is also possible. In hybrid propellant engines, fuel is in solid form and oxidizer is in liquid form. Opposite of this design also exists, where the oxidizer is in solid form and the fuel is in liquid form. Hybrid propellant engines have higher specific impulse than solid propellant engines but they are more complicated. However, they are throttleable and restartable like liquid bi-propellant engines. Also, hybrid motors have lower throttling range and lower specific impulse than liquid bi-propellant engines.

Rocket engines can be classified in two types depending on their propellant supply: pressure fed and pump-fed. In pressure fed systems, several methods can be used for pressurization. Pressurized gas tanks that supply pressurized gas at specified pressure by a pressure regulator to the tanks can be used to pressurize propellants. External pressurizer tanks increase the overall weight of the vehicle in this method. In other method called blow-down, propellant tanks are pre-pressurized and pressure decreases continuously during the engine operation. Injector and combustion chamber should be designed so that they can operate at different pressure levels for the blow-down mode. There is no need for external pressurizer tank for the blow-down mode which decreases the overall mass.

Gas generator cycle, expander cycle and staged combustion cycle are the commonly used methods for pump-fed systems. Tap-off cycle and catalytic decomposition of a mono-propellant are the two other methods that are used less commonly.

Gas generator cycle is an open cycle. Portion of the fuel and portion of the oxidizer are burned in a gas generator, a kind of a small combustion chamber, and hot gas is used in turbine system to generate power for the pump system. Exhaust of the turbine is dumped outside through a secondary nozzle. That is why it is classified as an open cycle. Thrust of this secondary nozzle is much smaller than the main nozzle and dumped propellant can be considered as increased fuel consumption. Since the dumped propellants cannot be used for significant thrust generation, main idea is achieving a

high pressure ratio at the turbine and to use the lowest possible mass flow rate for the turbine. Higher turbine power can be achieved by increasing the pressure ratio at the turbine or increasing the mass flow rate through the turbine. High pressure ratio at the turbine is used for gas generator cycles instead of using higher turbine mass flow rate to decrease dumped propellant mass flow rate. Turbine inlet temperature is limited by the material of the turbine. Moderate combustion chamber pressures, around 130 bar, and large thrust ranges, between 30 kN and 7000 kN, can be achieved with gas generator cycle. Very high combustion chamber pressures cannot be achieved because increased combustion chamber pressure increases the dumped mass flow rate and specific impulse starts decreasing after some point because of the high fuel consumption. In other words, increase in thrust is over-compansated by open cycle losses after a specific combustion chamber pressure in terms of specific impulse. Gas generator cycles are mainly used in boosters, core stages and upper stages.

Another commonly used open cycle system is expander cycle. There is no gas generator in this cycle. Instead, fuel or oxidizer is heated through cooling channels around the nozzle, the throat and the combustion chamber, and then expanded through a turbine. Turbine is used to power the propellant pumps. Expanded propellant is dumped through a secondary nozzle after the turbine just like the gas generator cycle. Therefore, some of the fuel or oxidizer is not used for significant thrust generation and this increases losses. Fraction of the propellant mass flow rate that goes through the turbine can be controlled by adjustable valves according to the desired throttle of the engine. High thrust range and combustion chamber pressure cannot be achieved because high propellant mass flow rate increases the pressure loss at the cooling channels significantly and dumped mass flow rate is increased because of the high pump power need.

Expander cycle can also be used as a closed cycle. If the expanded propellant is not dumped through a secondary nozzle but it is directed to the injector, it becomes closed cycle because all of the propellant goes through the main combustion chamber. Fuel or oxidizer can be used for the turbine flow. Low-to-moderate combustion chamber

pressures, 30 to 80 bar, and low-to-moderate thrust levels, 80 kN to 200 kN, can be achieved with closed expander cycle. High thrust levels and combustion chamber pressures cannot be achieved. High propellant mass flow rates are needed for high thrust and high turbine mass flow rate is needed to satisfy high pump power need for high propellant mass flow rate. However, high fuel or oxidizer mass flow rate at the cooling channels increases the pressure loss at the cooling channels significantly and combustion chamber pressure starts decreasing even if the pump exit pressure is increased further because most of the pump exit pressure is lost at the cooling channels before entering the combustion chamber. Closed expander cycle is mainly used in upper stage engines where the thrust and the combustion chamber pressure are relatively low.

Staged combustion cycle is a closed cycle that is commonly used in boosters, core stages and upper stages. There is a pre-burner in the system to pre-burn the fuel or the oxidizer before entering the injector. All of the fuel and a fraction of the oxidizer or vice versa is pre-burned in a small combustion chamber before entering the turbine. Exhaust flow of the turbine goes into the main combustion chamber instead of being dumped from a secondary nozzle. Therefore, it is called closed cycle. Since the exhaust of the turbine is directed to combustion chamber, high pressure ratio across the turbine is undesired because exit of the turbine should still be at higher pressure than the injector inlet pressure. Low pressure ratio across the turbine is compensated by high turbine mass flow rate because all of the fuel or the oxidizer mass flow rate is passed through the turbine. Turbine inlet temperature is still limited by the turbine material just like the gas generator cycle. High combustion pressures, 130-270 bar, and high thrust levels, 80 kN to 8000 kN, can be achieved because there are no open cycle losses. However, combustion chamber pressure starts decreasing after an optimum pump exit pressure because further increase in pump exit pressure is over-compensated by the turbine pressure drop.

Full flow staged combustion cycle is a special type of staged combustion cycle where two separate pre-burners exist to pre-burn both the fuel and the oxidizer. One of the pre-burner works at fuel rich condition where most of the fuel and small fraction

of the oxidizer is pre-burned and another pre-burner works at oxidizer rich condition where most of the oxidizer and small fraction of the fuel is pre-burned. The exhaust of each of the pre-burners is connected to separate turbines which makes it possible to achieve higher pump power and thus higher combustion chamber pressure. High combustion pressures up to 300 bar can be achieved with full flow staged combustion cycle.

Gas generator cycle makes it possible to develop turbopump and combustion chamber systems seperately because exit of the turbine flow does not go into the combustion chamber. However, turbopump and combustion chamber system should be developed together in staged combustion cycle because combustion chamber pressure is directly affected from the turbine exit pressure. Turbine blade material limits the turbine inlet temperature in both of the systems and the efficiency of both systems can be increased with developments in turbine blade material technology. Schematics of pressure-fed system, gas generator cycle, expander cycle and staged combustion cycle are given in Figure 1.1

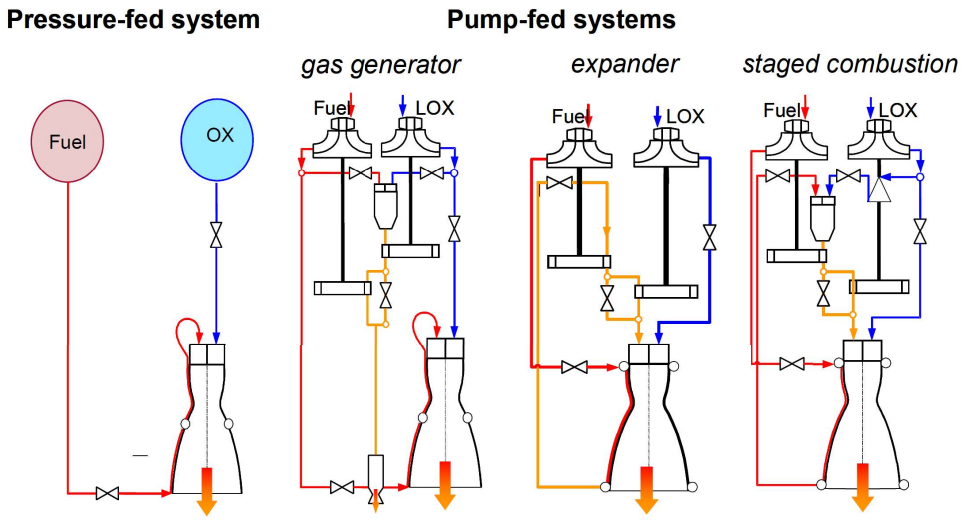

Figure 1.1. Schematics of pressure fed, gas generator cycle, expander cycle and staged combustion cycle systems [2].

Small portion of the exhaust gas is taken from the combustion chamber and routed to the turbine assembly to generate power in tap-off cycle. It is dumped to ambient after the turbine system, therefore it is an open cycle system. Catalytic decomposition of a mono-propellant can be used to generate hot gas to drive turbine system in the gas generator cycle, as well.

In general, pressure fed liquid rocket engine consists of propellant tanks, control valves, injector, combustion chamber and nozzle. Before the firing, propellants are stored in tanks at ambient pressure. They are pressurized by an external pressure cylinder containing an inert gas like helium, argon or nitrogen just before the firing. Propellants flow from the tanks to the injector through the control valves, the venturies and the flow meters by piping. Propellants get into the dome before the injector to achieve an even injection distribution. Injector can be of different types like shower head, double impinging, triple impinging, coaxial or pintle. Oxidizer and fuel mix at the exit of the injector and they start combusting in the combustion chamber. Hot combustion gases are accelerated through the nozzle and they generate thrust while exiting the engine. Since pressurization occurs at the propellant tanks, tanks have to withstand high pressure loads which increases the tank weight significantly.

Pressurization with a turbo-machinery has an advantage of decreased tank weight. Propellant in the propellant tanks stays at low pressure levels, around 1-3 bar, during the whole mission when the turbomachinery is used. Pressurized fluid is present only after the turbo-machinery which decreases the tank weight significantly. However, turbomachinery has its own additional weight and complexity. Rotational speed of the turbomachinery is very high and it increases the probability of the failure.

All of the propulsion systems use some kind of an acceleration system to eject propellant with a high velocity from the engine. When a particle is ejected from the engine with a high velocity, it pushes the engine in other direction. Thrust that is

resulted from the change of the momentum of the propellant can be formulated as

$$\mathbb{T} = \frac{d(mv_e)}{dt} = \dot{m}v_e, \tag{1.1}$$

where $\dot{m}$ is the mass flow rate and v_e is the exit velocity. It is assumed that initial momentum of the propellant is equal to zero, mass flow rate is constant, exit velocity is constant and purely axial, and nozzle exit pressure equals to the ambient pressure in Equation 1.1 [3].

Condition where the nozzle exit pressure equals to the ambient pressure is called adapted nozzle. If the nozzle exit pressure is lower than the ambient pressure, it is called over-expanded nozzle. If the nozzle exit pressure is higher than the ambient pressure, it is called under-expanded nozzle. Thrust equation has an additional term for over-expanded and under-expanded nozzles. This additional terms represents the effect of the difference between the exit and the ambient pressure which can be formulated as

$$\mathbb{T} = \frac{d(mv_e)}{dt} = \dot{m}v_e + (P_e - P_a)A_e. \tag{1.2}$$

When the exit pressure is lower than the ambient pressure, pressure term is negative and this means that thrust is lowered which is an undesirable situation. For a fixed geometry nozzle, exit pressure can be equal to the ambient pressure only at a specific altitude and it works in under-expanded or over-expanded modes at other altitudes. Since the ambient pressure decreases with the increasing altitude, thrust and specific impulse increase while the vehicle gains altitude during the flight.

Total mass of the vehicle changes during the flight since some of the propellant is ejected. Konstantin Tsiolkovsky, a Russian and Soviet rocket scientist, derived a mathematical equation often called “Tsiolkovsky rocket equation” which describes the motion of the rockets. This equation is expressed as

$$\Delta V = v_e \ln \frac{M_o}{M_f}, \tag{1.3}$$

where ΔV represents the maximum achievable increase in velocity while extracting

propellant with the velocity v_e. M_o and M_f are the initial and final masses of the vehicle, respectively. In other words, Equation 1.3 shows how much the velocity of a vehicle can be changed with a certain propellant mass consumption.

Specific impulse is a measure of how effectively the engine creates thrust. It can be formulated as

$$I_{sp} = \frac{\mathbb{T}}{\dot{m} g_0}. \tag{1.4}$$

If the pressure term in thrust equation (Equation 1.2) is assumed to be zero, Equation 1.4 can be represented as

$$I_{sp} = \frac{v_e}{g_0}. \tag{1.5}$$

When v_e term in Equation 1.5 is substituted in Equation 1.3, ΔV can be expressed as

$$\Delta V = I_{sp} g_0 \ln \frac{M_o}{M_f}. \tag{1.6}$$

This equation can be used to calculate maximum achievable velocity increase for a certain propellant mass consumption for a given engine with specified I_{sp}. One of the main outcome of Equation 1.6 is, same ΔV can be achieved with less propellant mass when the I_{sp} of the engine is higher. This becomes very important for an upper stage engine. Main aim of the upper stage engine is to use the fuel as efficient as possible. That is why the upper stage engines have high I_{sp} levels. They attain a higher ΔV than a low I_{sp} engine with the same propellant mass consumption.

As can be seen from Equation 1.1, thrust is the product of the mass flow rate and the exhaust velocity and the exhaust velocity can be calculated from I_{sp} by Equation 1.5. In this way, another equation which relates thrust of the engine to the mass flow rate of the propellants and the I_{sp} of the engine can be formulated as

$$T = \frac{d(m v_e)}{dt} = \dot{m} I_{sp} g_0. \tag{1.7}$$

Main stage engines generally have lower I_{sp} than upper stage engines. Hydrogen is a fuel that has one of the highest I_{sp} among other fuels. However, higher volume fuel tanks are needed and very high mass flow rate cannot be achieved because of its very low density. Turbomachinery needed to pressurize low density hydrogen at very high mass flow rate is very complicated. Even if I_{sp} value of hydrogen is significantly higher than other fuels, very high thrust levels cannot be achieved due to the mass flow rate limitation. Therefore, main stage engines use fuels that have lower I_{sp} at very high mass flow rate to generate very high thrust. In contrast, fuels that have high I_{sp}, like hydrogen, at low mass flow rate are used at upper stage engines for the highest efficiency. Their thrust level is significantly lower than the main stage engines and low hydrogen mass flow rate is sufficient for generating necessary thrust.

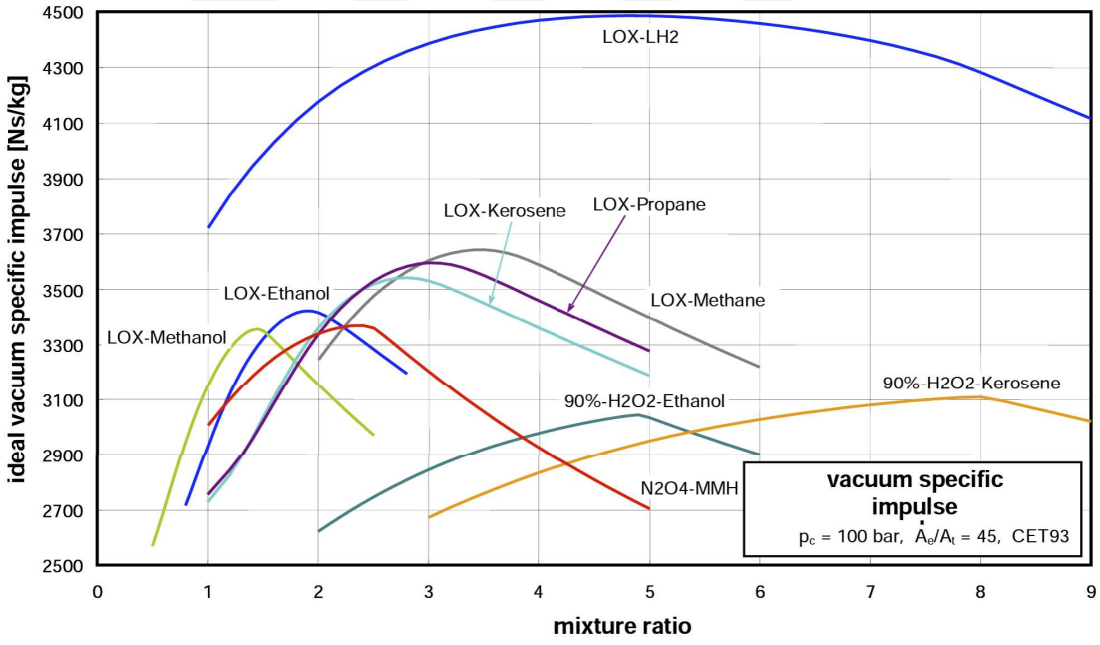

Figure 1.2. Ideal vacuum exit velocity (v_e or $I_{sp}g_0$) values of common propellant combinations for a range of oxidizer to fuel mixture ratios [2].

Ideal vacuum exit velocity (v_e or $I_{sp}g_0$) levels of common propellant combinations can be seen in Figure 1.2. Values are calculated for 100 bar combustion chamber pressure and area ratio (A_e/A_t) of 45. As can be seen from the figure, each fuel

combination has an optimum OF ratio. Vacuum specific impulse decreases further from this optimum value. Also, LOX-LH_2 has significantly higher specific impulse than other propellant combinations.

High combustion temperatures are achieved in liquid rocket engines. Adiabatic flame temperature of the propellants can be as high as 4300 K [4]. It is not feasible to use materials that can withstand such high temperatures. Alternatively, some kind of a cooling method is used to maintain the chamber wall temperature below the melting point of the chamber wall material.

Generally, cooling methods can be classified as transpiration, ablative, radiative, film, and regenerative cooling. A porous combustion wall is used to move the liquid or gas propellant through the wall while both cooling the wall and reducing the heat transfer near the wall in transpiration cooling. A protector material is applied to the combustion chamber wall in ablative cooling. Ablative material vaporizes and it is carried away while engine is working. It is not a continuous method like regenerative or transpiration cooling. It has a specific time of working until all of the ablative material vaporizes. Also, engine wall itself can be used as an ablative material. Radiative cooling can be used in deep space applications, like upper stages of the rockets. Heat is released by radiative heat transfer between the combustion chamber and space. In film cooling, one of the propellants is injected through the holes in the combustion chamber. It creates a thin film of unburned propellant near the wall and reduces the temperature of the wall by reducing heat transfer. In other words, it creates a barrier between the hot combustion gases and the combustion chamber wall. This thin layer diminishes while moving away from the injection holes.

Regenerative cooling is the most common cooling method. One of the propellants is circulated through the channels of the combustion chamber. Flowing propellant cools the combustion chamber walls and its temperature increases while flowing. In some cases, it can change phase and liquid propellant can turn into the gas. This situation may increase the performance of the engine because propellant goes into the combustion

chamber already in a gas phase and evaporation process in the combustion chamber is skipped. A sample regenerative cooling procedure is shown in Figure 1.3. Combustion gasses and coolant fluid flow in opposite directions in Figure 1.3. There are different approaches for regenerative cooling. Inlet position of the coolant and the flow direction can be changed. Film cooling is generally combined with regenerative cooling.

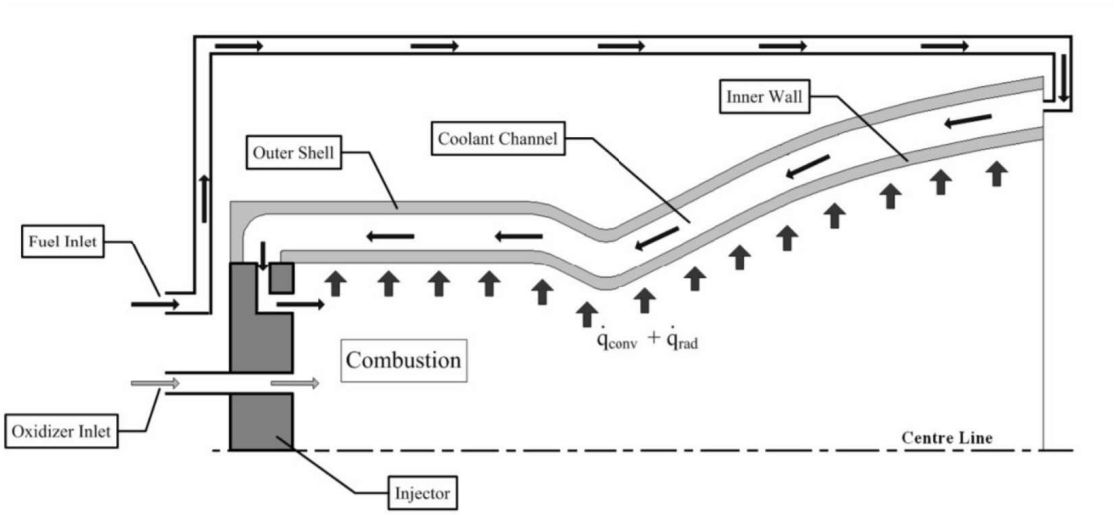

Figure 1.3. Schematic of regenerative cooling in rocket engines [5].

1.1. Literature Review

Liquid propellant rocket engines are studied since the first static test in the history which was accomplished by Robert H. Goddard [6]. They have many usage areas from very small engines that can generate couple of newtons thrust to engines that can generate up to 8000 kN thrust [7]. Some studies that are related with this study are reviewed in this section.

1.1.1. Tecnico Lisboa

A small scale 25 N engine is designed, built and tested at Tecnico Lisboa as a part of a project of the company Omnidea Lda [8]. This company tries to enter the rocket

industry and cooperates with Tecnico Lisboa for the research of their concepts. Efficiency is not the main concern in this study and 15 bar is used as the chamber pressure. First prototype is a pressure fed engine but it is aimed to have a self-pressurisation with a regenerative cooling. Objectives of the project are having a gaseous injection, re-startability and achieving a self-pressurization system by a regenerative cooling. Reducing the weight of the system by not using turbo-pumps or pressurized gas tanks is the main concern.

Gaseous oxygen is used as the oxidizer and different types of fuel are investigated to find the most suitable one. Ethanol is a good choice because it is cheap, easily accessible, its performance is adequate and it has an acceptable cooling capacity. However, its vapor pressure at low temperatures is low which makes it not suitable for self-pressurization. Propane and ammonia are the other candidates. Propane has low critical temperature (369 K) and low critical pressure (42.6 bar). It is desired to work far from the critical conditions. Therefore, propane is not a good choice, also. On the other hand, ethanol and propane does not have compatibility problems with copper, aluminum, stainless steel and nickel super-alloy. However, ammonia has severe incompatibility with copper. Compatibility problem can be overcome by using stainless steel or nickel super-alloy.

Ammonia is chosen as the fuel instead of propane or ethanol after an analytical thermal analysis because it showed a higher cooling capacity. Stainless steel is chosen as the chamber material because of very high cost of nickel super-alloys. Summary of the engine parameters are given in Table 1.1. Even if ammonia is chosen as the fuel, some test are conducted with ethanol to eliminate some kind of stability problems and check the test procedures. Three tests are conducted with externally pressurized ethanol. An old combustion chamber that was manufactured for another project and a simple injector is used in the first test to become familiar with test procedures. Designed combustion chamber and a swirl injector are used in the next two tests. Tests are completed successfully and a stable combustion is achieved. Also, vaporization is achieved in the vaporizer and 25 N thrust is generated.

Table 1.1. Properties of the engine designed at Tecnico Lisboa [8].

ENGINE	OF	1.4
	Total mass flow	9.99 g/s
	I_{sp}	255 s
	Chamber diameter	30 mm
	Throat diameter	3 mm
	Area ratio	3.2
	Chamber pressure	15 bar
	Chamber material	Stainless Steel 304
OXIDIZER	Oxygen	
	Pressure	40 bar
	Temperature	293 K
FUEL	Ammonia	
	Pressure	40 bar
	Temperature	300 K

After the ethanol tests, ammonia is used as a fuel in further tests. It is observed that it is harder to ignite ammonia and glow plug has to be powered for a longer time than the ethanol. Even if there were some issues like OF ratio mismatching, unstable combustion and ignition problems, tests showed that self-pressurization concept is validated. A better working engine can be designed as a further work. Also, it is mentioned that a 300 N self-pressurized engine can be designed with 50 bar chamber pressure.

1.1.2. Minerva Project

Minerva Project is a liquid bi-propellant rocket engine project under the project Perseus [9]. LOX as the oxidizer and ethanol as the fuel are used as propellants in the engine. Several engines are designed under this project which are called MLE5K-S1, MLE5K-S2, MLE5K-S3 and MLE5K-F1. MLE5K stands for MINERVA Lox-Ethanol

5 kN. S1, S2 and S3 designs are for static testing and F1 design is flight demonstrator. Several improvements have been made for each design.



Figure 1.4. MLE5K-S1a design with ablative cooling [9].

Triple impinging injector is used in S1 design. Ablative chamber and calorimetric chamber are tested in S1 design. They can be seen in Figure 1.4 and Figure 1.5. Injector is changed to pintle injector in S2 design. Regenerative cooling is added to the system in S3 design.

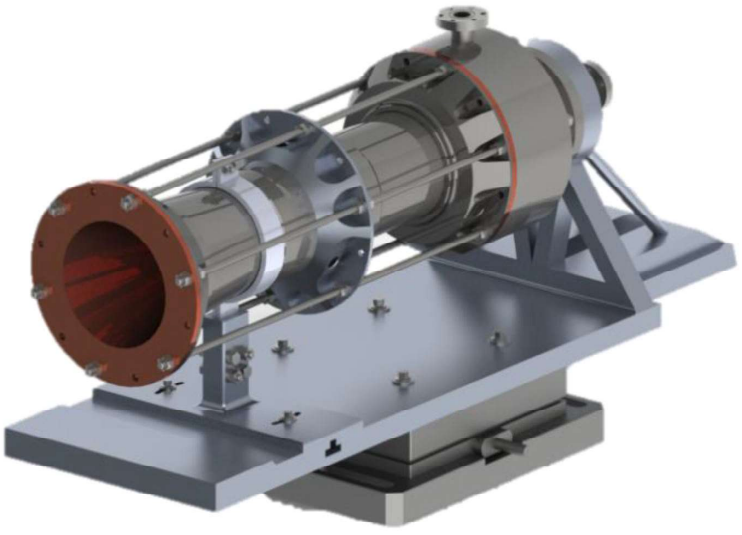

Figure 1.5. MLE5K-S1b design with calorimetric chamber [9].

Impinging injector design is tested with water to check the C_d of the injector. First of all, only a single triplet is tested and result of this test is used to adjust the

rest of the triplets to achieve 10 bar pressure drop at the injector. Figure 1.6 shows the result of the full injector water test. Injector is designed using 0.65 and 0.7 as C_d for LOX and ethanol, respectively. Test results coincide with the design at 10 bar pressure drop.

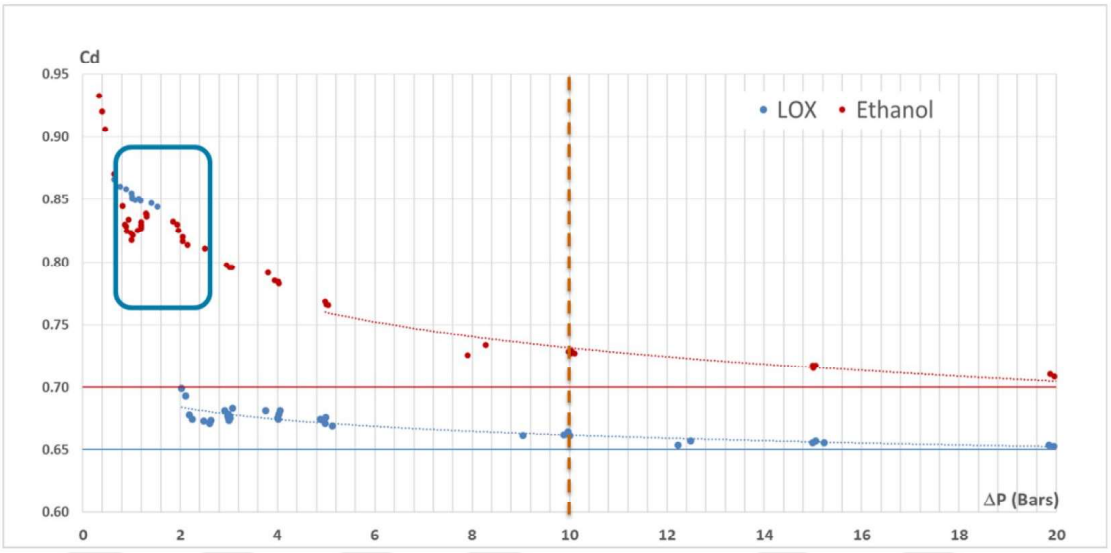

Figure 1.6. Cold flow test results of the impinging injector showing the change of discharge coefficient (C_d) with respect to pressure drop (ΔP) [9].

1.1.3. Lulea University of Technology

A preliminary design of a testing platform for small-scale rocket engines is made by Erik Andersson in Lulea University of Technology [10]. Tested rocket engine is pressure fed and gaseous nitrogen is used as the pressurizer. Gaseous oxygen is used as the oxidizer and ethanol-water mixture is used as the fuel for this engine. They worked on different Ethanol Fuel Concentrations (EFC) for different cases and 70% concentration is chosen. Results of these three cases for chamber pressure of 15 bar are given in Table 1.2. r represents the OF ratio in the table. It is a water-cooled engine and its combustion chamber is made of copper. It can deliver 1000 N thrust. OF ratio of the engine is 1.3 and total mass flow rate is 0.447 kg/s.

Table 1.2. Thrust chamber parameters for three different EFC [10].

	EFC (%)		
	70	**85**	**99.5**
I_{sp} **(s)**	228	235	226
r	1.3	1.45	1.6
c^* **(m/s)**	1645	1675	1710
T_c **(K)**	3030	3120	3200

1.1.4. University of Texas at El Paso

Two liquid methane-liquid oxygen engines are designed at University of Texas at El Paso. One of them has 500 lb (2224 N) thrust and another one has 2000 lb (8896 N) thrust.

Methane is one of the most promising rocket fuel to be used in the Mars missions. It has higher density and it has higher storage temperature than hydrogen. Therefore, it can be stored easier in more compact fuel tanks. One of the most important point is methane can be produced by local sources in Mars. It is called in-situ resource utilization (ISRU). This method allows the needed fuel for the return mission to be produced in Mars instead of carrying it from Earth. It reduces the mission cost significantly. However, methane has lower specific impulse than hyrogen, which reduces rocket performance.

UTEP Center for Space Exploration and Technology Research (cSETR) works as a partner with National Aeronautics and Space Administration (NASA). They work mainly on liquid methane (LCH_4)-liquid oxygen (LOX) rocket engines. Centennial Restartable Oxygen Methane Engine (CROME) is a 500 lb (2224 N) throattable LCH_4-LOX engine that is developed by UTEP cSETR. It will be used as a main engine in a suborbital demonstration vehicle called Daedalus. The main aim of this project is demonstrating the restartability and evaluating the performance of the engine in space

under micro-gravity conditions. Daedalus spacecraft will achieve 90 miles (∼144.8 km) altitude above sea level and stay in sub-orbit around 200 seconds [11].

CROME engine is a pressure fed engine and helium is used as the pressurizer. It is designed to produce 500 lb (2224 N) thrust at sea level and to be throattable 4:1. It has 2.7 OF ratio and 70 to 235 psi (∼4.8 to 16.2 bar) chamber pressure. It is cooled by film cooling which flow rate is the 30% of the fuel flow rate used for the combustion. Inconel 625 is used for the combustion chamber. Its I_{sp} is 227 s at sea level and 336 s in vacuum. Since the engine will be tested at the ambient pressure at sea level, it has a nozzle expansion to be able to work in vacuum. Nozzle extension is used to go from 1.6:1 expansion ratio to 30:1 expansion ratio. Final design of the CROME is given in Figure 1.7.

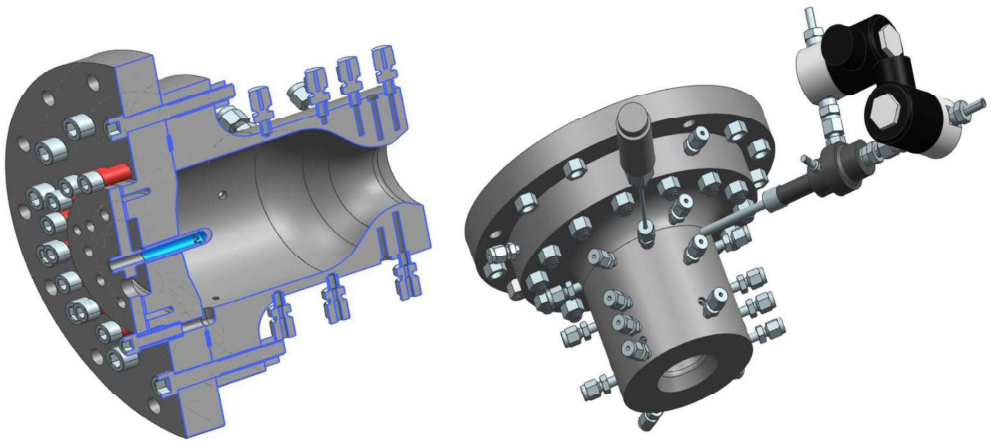

Figure 1.7. Design of the CROME [12].

JANUS is a vertical takeoff vertical landing (VTOL) vehicle developed by cSETR. Methane as a fuel will be tested using this vehicle. It will takeoff from the ground and reach 20 ft (6.1 m) altitude, hover and roll at this altitude and land back vertically. Mission summary can be seen in Figure 1.8.

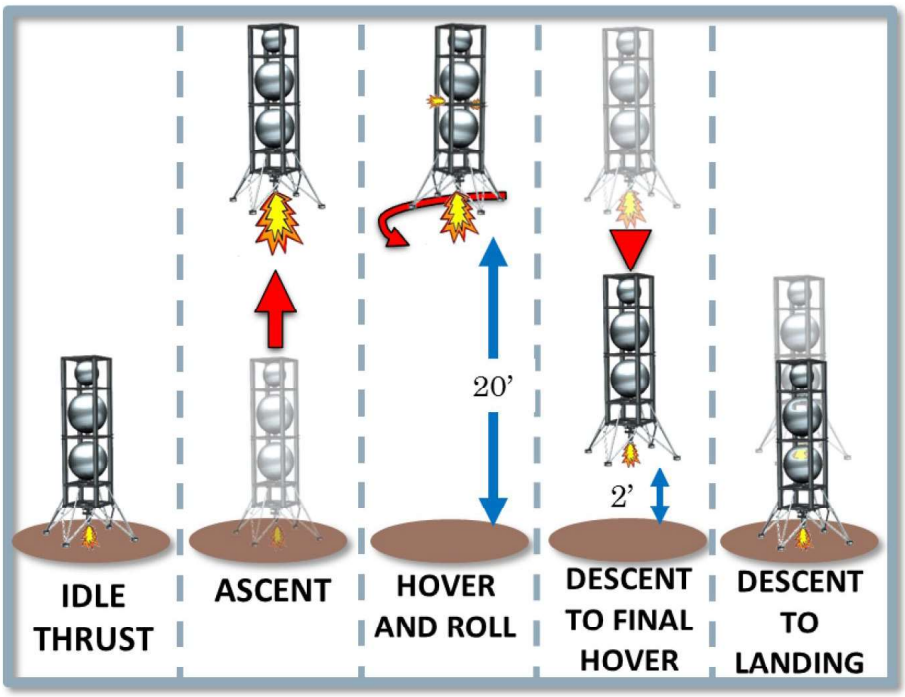

Figure 1.8. Mission summary of the JANUS [13].

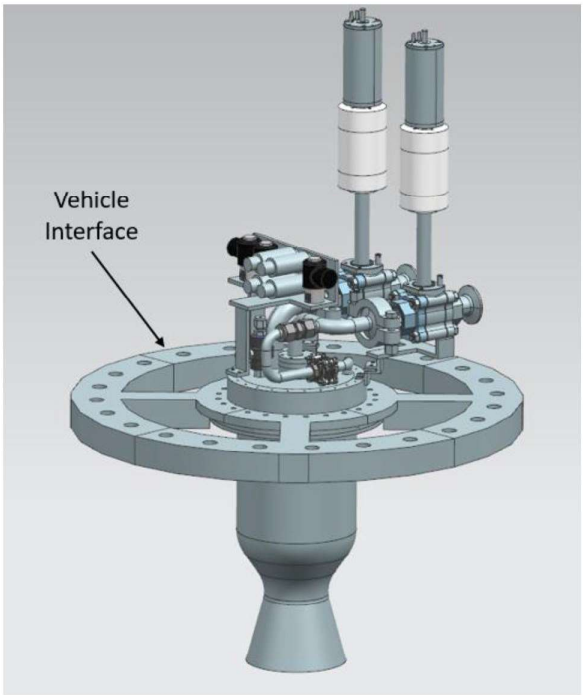

Figure 1.9. CROME-X engine attached to the vehicle interface [13].

Main engine, CROME-X, is mounted on the vehicle by a gymbal. CROME-X is a 2000 lb (8896 N) engine that will be used in project JANUS. It can be throattable between 500-2000 lb (∼2224-8896 N) thrust range to be able to perform vertical takeoff vertical landing mission. It has 75.2-232.8 psi (∼5.2-16.0 bar) chamber pressure, 2.7 OF ratio (1.89 including film cooling) and 2.7 expansion ratio. Combustion chamber is made of Inconel 718 and injector is made of Inconel 625. 316 stainless steel is used for manifolds and lines. CROME-X engine as attached to the vehicle interface is given in Figure 1.9.

1.2. Scope of This Study

The main aim of this study is to design, manufacture and test a 5 kN ethanol-liquid oxygen liquid bi-propellant rocket engine. This thesis mainly focuses on propellant selection, thrust chamber design, cooling, mass flow control and pressurization system for this engine. BUSTLab V1 rocket engine is designed and tested for this purpose.

In Chapter 2, combustion chamber and nozzle sizing are explained by giving required equations. Commonly used propellants in rocket engines are presented and heat transfer in cooling channels is investigated. Design criteria and design procedure for BUSTLab V1 is given in Chapter 3. Injector, combustion chamber, nozzle and cooling channel design parameters are investigated. Propellant feed system including propellant tanks, valves, cavitating venturi and pressure control system are explained in detail in Chapter 4. The main mass flow control device, cavitating venturi, is investigated with water test results in this chapter as well. Test setup and subsystems like cooling water supply system and control table are given in Chapter 5. Each of the components and their manufacturing processes are explained in Chapter 6. Chapter 7 focuses on tests of the individual components and the complete thrust chamber. Injector water tests, cooling channel tests, cold flow test, open fire tests and the complete thrust chamber firing test are discussed in Chapter 8. Finally, conclusion regarding this study are made in Chapter 8. Possible improvements and future work are also discussed in

this chapter. Result of some cavitating venturi tests and technical drawings of the parts are given in APPENDIX A and B.

2. THEORETICAL BACKGROUND

Although the flow in the real nozzle is not adiabatic and isentropic, adiabatic and isentropic flow assumption gives useful results for the preliminary design. It is assumed that there is no wall friction, transient effects, heat transfer and shock waves; flow is one directional, steady and leaves the nozzle completely axially; working gas is homogeneous and perfect gas. Actual performance of the engine is generally %1 to %6 lower than the calculated values with these assumptions [3]. Required equations for the combustion chamber, the throat and the nozzle sizing are explained in this chapter. Also, a background for propellant selection and cooling channel design is given.

A^* is the diameter of the nozzle throat. It is calculated so that given mass flow rate can pass through the throat at choked conditions with the given stagnation temperature and stagnation pressure for the specific propellant combination. Stagnation temperature and stagnation pressure are assumed to be equal to the chamber conditions during the calculations. A^* can be calculated as

$$A^* = \frac{\dot{m}}{P_o}\sqrt{T_o\frac{\mathbb{R}}{\gamma}}\left(1+\frac{\gamma-1}{2}\right)^{\frac{\gamma+1}{2(\gamma-1)}}. \tag{2.1}$$

Throat diameter (D_{throat}) is calculated using the throat area (A^*) as

$$D_{throat} = \sqrt{\frac{4A^*}{\pi}}. \tag{2.2}$$

OF ratio is the ratio of oxidizer mass flow rate to the fuel mass flow rate. It can be expressed as

$$OF = \frac{\dot{m}_o}{\dot{m}_f}. \tag{2.3}$$

Mass flow rates of the fuel and oxidizer (m_f and m_o) can be calculated by the given OF ratio as

$$\dot{m}_f = \frac{\dot{m}}{1+OF}, \tag{2.4}$$

$$\dot{m}_o = \dot{m} - \dot{m}_f. \tag{2.5}$$

Characteristic velocity (c^*) is a measure of the performance of the combustion. It does not have an exact physical meaning and can be calculated as

$$c^* = \frac{P_c A^*}{\dot{m}} = \frac{\sqrt{\gamma \mathbb{R} T_c}}{\gamma \sqrt{[2/(\gamma+1)]^{(\gamma+1)/(\gamma-1)}}}. \tag{2.6}$$

Characteristic velocity depends on the propellant combination and combustion chamber characteristics, and it is independent of the nozzle configuration. It can be used to compare different kind of propellants and combustion chamber configurations.

Theoretically, first and second formulations in Equation 2.6 are equal to each other. However, experimental combustion pressure and mass flow rate are usually different from the theoretical values. Combustion pressure (P_c) and mass flow rate ($\dot{m}$) can be measured during the test and throat area (A^*) is a known value. First formulation can be used to find experimental c^* value. Specific heat ratio (γ), specific gas constant ($\mathbb{R}$) and combustion temperature (T_c) can be theoretically calculated for a desired propellant combination in the second formulation and can be used to find theoretical c^* value. Experimental and theoretical values can be used to calculate c^* efficiency which is the ratio of the experimental c^* value to the theoretical c^* value. c^* efficiency is a measure of the completion of the combustion in the combustion chamber. Typical values are between 92% and 99.5% [3].

Exit Mach number (M_e) can be calculated as

$$M_e = \sqrt{\frac{2\frac{P_e}{P_o}^{\frac{-(\gamma-1)}{\gamma}} - 1}{\gamma - 1}}, \tag{2.7}$$

assuming the exit pressure is equal to the ambient pressure. Ratio of area of any section (A) to the throat area (A^*) can be calculated as

$$\frac{A}{A^*} = \frac{1}{M}\left(\frac{2}{\gamma+1}\left(1 + \frac{\gamma-1}{2}M^2\right)\right)^{\frac{\gamma+1}{2(\gamma-1)}}, \tag{2.8}$$

where A is the area of any section in the nozzle and M is the mach number at that section.

Exit area (A_e) can be found by substituting A_e and M_e instead of A and M in Equation 2.8, respectively. Exit diameter (D_e) is calculated from the exit area (A_e). Formulations for A_e and D_e are given as

$$A_e = \frac{A^*}{M_e}\left(\frac{2}{\gamma+1}\left(1+\frac{\gamma-1}{2}M_e^2\right)\right)^{\frac{\gamma+1}{2(\gamma-1)}}, \tag{2.9}$$

$$D_e = \sqrt{\frac{4A_e}{\pi}}. \tag{2.10}$$

Exit velocity (v_e) can be calculated using the exit mach number and the exit temperature as

$$v_e = M_e\sqrt{\gamma\mathbb{R}T_e} = \sqrt{2\left(\frac{T_o}{\mathbb{M}}\right)\left(\frac{\mathbb{R}_{univ}\gamma}{\gamma-1}\right)\left(1-\frac{P_e}{P_o}^{\frac{\gamma-1}{\gamma}}\right)}. \tag{2.11}$$

Also another formulation, the one on the right side of Equation 2.11, can be used to calculate v_e.

As can be seen from Equation 2.11, exit velocity increases with increasing T_o/M ratio and decreasing P_e/P_o ratio. The highest exit velocity can be achieved when the P_e/P_o ratio reaches zero, which is impossible in practice. I_{sp} of the engine is proportional to the exit velocity by Equation 1.5. Therefore, higher I_{sp} can be achieved with higher T_o/M ratio and lower P_e/P_o ratio.

Thrust of the engine consist of two parts; difference in the momentum of the entering and exiting fluid, and the pressure force effecting on the engine. It can be formulated as

$$\mathbb{T} = \dot{m}v_e + A_e(P_e - P_a). \tag{2.12}$$

Momentum at the inlet can be neglected since the velocity of the fluid is significantly lower than the exit. Also, exit pressure can be taken as equal to the ambient pressure

for an adapted nozzle. Adapted nozzle means that nozzle exit area is designed so that pressure of the flow equals to the ambient pressure while exiting the nozzle. Generally, pressure term is much smaller than the momentum term in Equation 2.12.

Specific impulse (I_{sp}) is a measure of how effectively the engine uses the propellant. From another perspective, specific impulse is the thrust per unit weight of the propellant usage. It highly depends on the propellant combination and the nozzle configuration and can be expressed as

$$I_{sp} = \frac{\mathbb{T}}{\dot{m} g_0}. \tag{2.13}$$

Characteristic chamber length (L^*) can be defined as the length that a chamber of the same volume would have if its cross-sectional area was the nozzle throat area. The effect of L^* is discussed more detail in Section 3.3.2. Characteristic chamber length is formulated as

$$L^* = \frac{V_{chamber}}{A^*}. \tag{2.14}$$

2.1. Propellants

The choice of the propellant for the rocket engine is affected by many factors. Their physical properties and combustion performance are some of these factors. I_{sp} of the engine is directly affected from the propellant combination. Higher combustion temperature and a lower molecular weight of the combustion gases results in higher I_{sp}. For instance, LH_2/LOX combination is a favorable choice in terms of I_{sp}. However, LH_2 has drawbacks due to its low density. There is not a best choice, many factors has to be considered for choosing the propellants. Combustion stability, compatibility with the other hardware, availability, cost, ignition capability and storability are some other factors that need to be considered.

2.1.1. Fuels

Kerosene, liquid methane, liquid hydrogen and ethanol are some of the most commonly used fuels in rocket engines. Main advantages and disadvantages of them are discussed in this section.

2.1.1.1. Liquid Hydrogen. Liquid hydrogen has very low boiling point (20.4 K) and it has lower density (71 kg/m^3) with respect to other fuels. Therefore, it is very hard to store liquid hydrogen and it needs bulky tanks. All common fluids and gases solidify in liquid hydrogen because of its low temperature. Solidified particles may cause problems at the valves, the orifices and the venturies. Also, using liquid hydrogen makes the turbomachinery more complex because of its low density and the large density difference with the oxidizer. However, very high I_{sp} levels can be achieved with LH_2 because of its low molecular weight. I_{sp} levels up to 455 s can be achieved with LH_2/LOX combination [2].

2.1.1.2. Liquid Methane. Liquid methane is another cryogenic fuel that is becoming more and more popular. Companies like SpaceX (Raptor engine) and Blue Origin (BE-4 engine) use liquid methane as the fuel [12]. It can be produced in-site on Mars which can reduce the tank and propellant weight of the space vehicle significantly. Space vehicle can be refuelled using the methane on Mars. Compared to liquid hydrogen, methane has higher density (423 kg/m^3) and higher boiling temperature (111.7 K) but achievable specific impulse is lower (up to 369 s [2]). Also, methane is extremely flammable [10].

2.1.1.3. Kerosene. Kerosene has different types like RP-1, JP-1 and Jet A-1. They have different additives but they are all kerosene based. Kerosene based fuels are easy to handle and they are easily accessible. They can be stored in ambient temperature and they do not need cooling or insulation for storage like cryogenic fuels. Kerosene may form carbon deposits when burned and these deposits may reduce heat transfer

which increases wall temperature of the chamber [3]. Kerosene gives lower specific impulse (358 s) than liquid methane and liquid hydrogen [2].

2.1.1.4. Ethanol. Ethanol has simple handling, storage and low cost. Its I_{sp} is lower than other mentioned fuels but it has relatively low combustion chamber temperature. Also, its combustion temperature can be adjusted by mixing ethanol with water. These properties make ethanol a very good candidate for lab-scale experiments.

2.1.2. Oxidizers

Liquid Oxygen (LOX), Hydrogen Peroxide (H_2O_2), Nitrogen Tetroxide (N_2O_4) and Nitrogen Dioxide (NO_2) are some of the most common oxidizers. Liquid fluorine is the most energetic oxidizer having the highest density and highest specific impulse and it is tried in several rocket engines but is not used anymore because of its hazards [3].

2.1.2.1. Liquid Oxygen (LOX). LOX is one of the most common oxidizer in rocket engines. It can be used with the fuels like alcohols, kerosene based fuels (RP-1), and hydrogen. Atlas V (USA), Soyuz (Russia) and Ariane V (France) use LOX as the oxidizer for instance [3].

It is a cryogenic propellant and it must be stored below 90 K at the standard atmosphere. Generally, LOX is filled in the tanks just before the launch or the test because it evaporates relatively fast. All of the lines, tanks, valves etc. should be well insulated to reduce evaporation losses and be cooled before the engine start. Also, a special cleaning method called "oxygen cleaning" should be used to prevent uncontrolled reactions between the oxygen and the other compounds in the oxidizer line.

2.1.2.2. Hydrogen Peroxide (H_2O_2). Hydrogen peroxide is a clean burning oxidizer. It can also be used as a monopropellant and it produces nontoxic combustion products. It decomposes into water (H_2O) and oxygen (O_2) when it is used as monopropellant.

This decomposition can be accomplished by using a catalyst. Silver screen, liquid permanganate, platinum and iron oxide can be used as catalyst for hydrogen peroxide. Hydrogen Peroxide becomes hypergolic when it is used with hydrazine as the fuel. They start burning as soon as they get in contact with each other without a need for an igniter.

2.1.2.3. Nitrogen Tetroxide (N_2O_4). N_2O_4 (or NTO) is hypergolic with many fuels like hydrazin, monomethylhydrazine (MMH) and unsymmetrical dimethylhydrazine (UDMH). It can be stored in sealed containers made of compatible materials without a time limit. However, it can cause spontaneous ignition with common materials like paper, grease, wood or leather [3]. It is one of the most commonly used oxidizer because of its high storability. Its melting point is -11.2 °C and boiling point is 21.7 °C. Therefore, it can accidentally be frozen or boiled because of the narrow range of the liquid phase. It is often used in small thrusters because of its hypergolic characteristic.

2.1.2.4. Nitrous Oxide (NO_2). Nitrous Oxide is also known as "laughing gas". It is much less toxic than NTO and it can be used as anesthetic, food additive or oxidizer in rocket engines. It is also used as the oxidizer in hybrid motors of SpaceShipOne, the first private manned spaceraft to carry humans to suborbital spaceflight [14]. Its vapor pressure is 5.1 MPa at 20 °C which is very high with respect to other oxidizers. Therefore, its vapor pressure can be used for self-pressurization.

2.2. Heat Transfer in Cooling Channels

Combustion of the propellants in the combustion chamber results in high temperature exhaust gas, up to 4300 K [4]. Therefore, wall of the combustion chamber and the nozzle have to be cooled or designed in a such way that they can withstand high temperatures during the firing of the engine. Regenerative cooling is one of the most common rocket engine cooling methods. Chamber and nozzle walls are cooled by a fluid flow around them. One of the propellants is used as the cooling fluid. Similar

to the regenerative cooling, an external fluid like water can also be used as the cooling fluid for ground tests of the engine. Analytical heat transfer solutions can be used for the preliminary design of the cooling channels for the regenerative cooling.

A sample regenerative cooling schematic is shown in Figure 2.1. Cooling channels can be seen in more detail in Section A-A. There is a hot gas flow inside the chamber and cooling flow around the chamber. Coolant flows between the external and the internal walls and cooling channels are separated by ribs. S_w is the thickness of the internal wall, t_w is the thickness of the ribs, b is the width of the each channel and $\mathbb{L}$ is the height of the each channel in Figure 2.1.

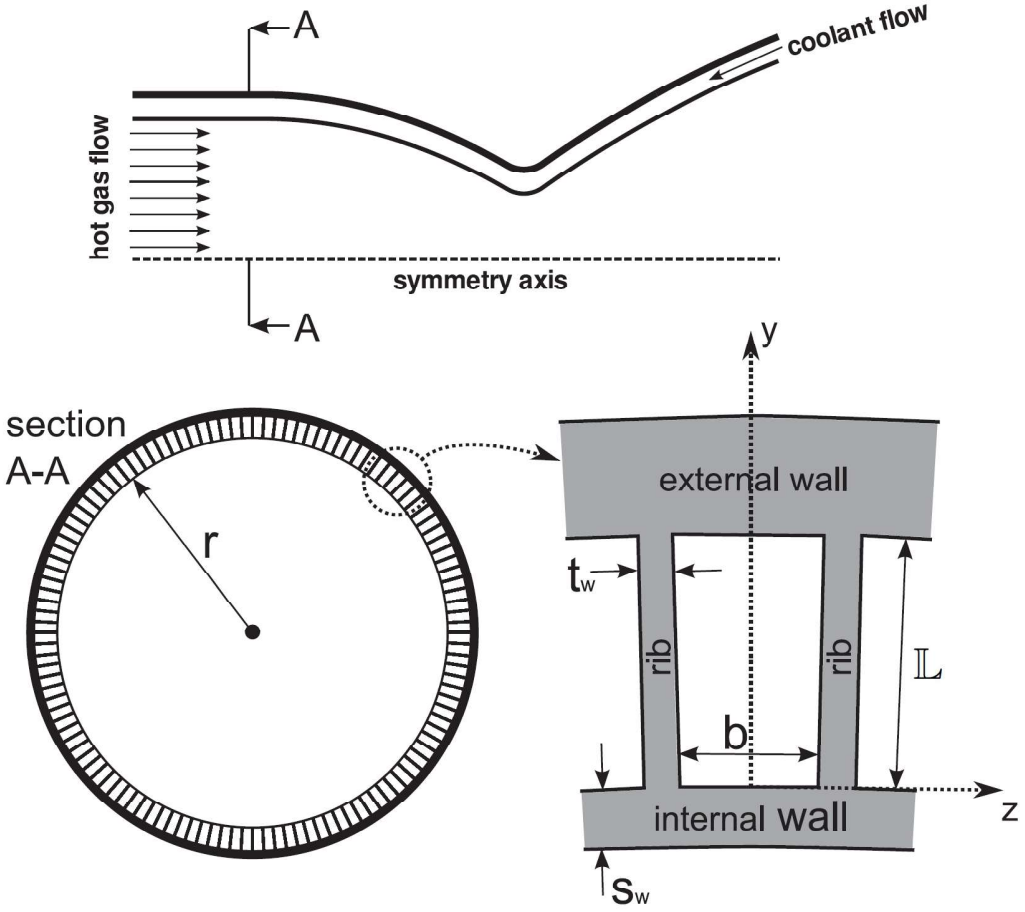

Figure 2.1. Sample schematic of regenerative cooling [15].

Flows in the cooling channels and combustion chamber can assumed to be turbulent and fully developed along the entire length. Reynolds numbers of the coolant flow and the hot gas inside the chamber are calculated to be larger than 2300 [16] for BUSTLab V1 engine. Therefore, flows are modeled as "Turbulent Flow in Circular Tubes" [16]. Even if the cooling channels are not circular tubes, hydraulic diameter method can be used to analyse rectangular sections.

External wall is assumed to be adiabatic and ribs are modeled as extended surfaces or fins. Heat transfer between the coolant and the hot gas can be modeled as "The Counterflow Heat Exchanger" [16] and heat transfer can be calculated as

$$Q = UA\Delta T_{lm}, \tag{2.15}$$

where Q is the heat transfer rate, U is the overall heat transfer coefficient, A is the heat transfer area and ΔT_{lm} is log mean temperature difference. ΔT_{lm} is defined as

$$\Delta T_{lm} = \frac{\Delta T_2 - \Delta T_1}{ln(\Delta T_2/\Delta T_1)}, \tag{2.16}$$

where ΔT_1 and ΔT_2 can be formulated for the counterflow heat exchanger as

$$\begin{aligned} \Delta T_1 &= T_{h,i} - T_{c,o}, \\ \Delta T_2 &= T_{h,o} - T_{c,i}, \end{aligned} \tag{2.17}$$

where $T_{h,i}$ and $T_{h,o}$ are the inlet and the outlet temperature of the hot gas side and $T_{c,i}$ and $T_{c,o}$ are the inlet and the outlet temperatures of the coolant side.

Resistance network method can be used to calculate UA is expressed as term in Equation 2.15. There are three resistances connected in serial in the system: thermal resistance due to the convection at the hot gas side ($R_{conv,h}$), thermal resistance due to the chamber wall ($R_{cond,wall}$) and thermal resistance due to the convection at the coolant side including the fin effect ($R_{conv,c}$). UA is expressed as

$$UA = \frac{1}{R_{conv,c} + R_{cond,wall} + R_{conv,h}}. \tag{2.18}$$

Each of the resistance in Equation 2.18 are formulated separately. $R_{conv,h}$ is expressed as

$$R_{conv,h} = \frac{1}{h_h A}, \tag{2.19}$$

where h_h is the convection heat transfer coefficient at the hot gas side and A is the heat transfer area. $R_{conv,h}$ is calculated as

$$R_{conv,c} = \frac{1}{\eta_o h_c A}, \tag{2.20}$$

where η_o is the overall efficiency of fin array, h_c is the convection heat transfer coefficient at the coolant side and A is the heat transfer area. $R_{cond,wall}$ is formulated as

$$R_{cond,wall} = \frac{ln(\frac{r_2}{r_1})}{2\pi Lk}, \tag{2.21}$$

where r_2 and r_1 are outer and inner radius of the chamber wall, L is the length of the heat transfer area in axial direction and k is the thermal conductivity of the chamber wall.

Overall efficiency of fin array (η_o) in Equation 2.20 represents the performance of the fin array. It can be calculated by using the efficiency of the single fin η_f as

$$\eta_o = 1 - \frac{NA_f}{A_{total}}(1 - \eta_f), \tag{2.22}$$

where N is the number of fins, A_f is the surface area of the fin, A_{total} is the total surface area including exposed area of the base and the total fin area and η_f is the fin efficiency.

Efficiency of the fin with an adiabatic tip and rectangular cross section area can be calculated as

$$\eta_f = \frac{tanh(\mu\mathbb{L})}{\mu\mathbb{L}}, \tag{2.23}$$

where $\mathbb{L}$ is the height of the fin and μ is a quantity which is formulated for this fin configuration as

$$\mu = \left(\frac{2h}{kt_w}\right)^{1/2}, \tag{2.24}$$

where h is the convection heat transfer coefficient, k is the thermal conductivity of the fin and t_w is the thickness of the fin.

Convection heat transfer coefficient at each side of the chamber wall can be calculated as

$$h = \frac{Nu\, k}{D}, \tag{2.25}$$

where D is the diameter of the cross sectional area of the flow. To be able to apply this formulation to the coolant flow, hydraulic diameter concept should be used because the cross sectional area of the coolant flow is rectangular, not circular. Hydraulic diameter of a rectangular cross section can be calculated as

$$D_h = \frac{4A_c}{\mathbb{P}}, \tag{2.26}$$

where A_c is the cross-sectional area of the flow and $\mathbb{P}$ is the wetted perimeter.

Nusselt number can be found for the hot gas and the coolant flows as

$$Nu_D = 0.023 Re_D^{4/5} Pr^n, \tag{2.27}$$

where Nu_D is the local Nusselt number, Re_D is the local Reynolds number, Pr is the Prandtl Number and n equals to 0.4 for heating and equals to 0.3 for cooling of the fluid [16].

Equation 2.27 gives the local Nusselt number for the fully developed turbulent flow. Fully developed turbulent flow in circular tubes can be assumed for (x/D)>10 [16]. It can be said that majority of the flow in the coolant channels is fully developed since the length of the cooling channel is much more greater than 10 times of the hydraulic diameter of the channels. However, the hot gas flow is also assumed to be fully developed for the entire chamber for easier calculations for the preliminary design even if it is not fully developed in most of the chamber.

3. ENGINE DESIGN

Design of the rocket engine starts with determining the requirements for the specific mission. The main target of the BUSTLab rocket project is designing and manufacturing an engine for a lander vehicle. This engine must be throttleable and reignitable in order to achieve a soft landing on the surface. In other words, the goal of the project is to develop a vehicle that can achieve vertical takeoff and vertical landing.

BUSTLab V1 engine is a preliminary design for that purpose. Many engines in the literature and space industry are investigated and 10 kN is chosen as a design thrust considering the available engines in the industry. It can carry almost 1000 kg vehicle which could be a good starting point for further developments. First aim is to lift off the vehicle without any payload. It should be able to carry only the needed parts for the engine, like the propellant tanks, propellants, piping, valves etc. Even if 10 kN is chosen as a initial design, further tests showed that more than 5 kN thrust is not feasible with the available pressurizing and mass flow control systems. Therefore, all the manufactured parts are designed for 10 kN but firing tests are conducted for 5 kN configuration. This change has some drawbacks like over-expansion in the nozzle but also some advantages like reduced required cooling water mass flow rate. These drawbacks and advantages will be investigated further in following chapters.

First design is not needed to be throttleable because main idea is testing the engine itself. Also, it is designed to be cooled with an external water supply. These designs are chosen to reduce the complexity of the engine because it is the first designed liquid propellant rocket engine in BUSTLab and main idea is to prove the concept and see the difficulties. Final lander vehicle must have a throttleable engine to be able to achieve soft landing and compensate the weight lost during the flight. Also, cooling of the final design should have regenerative cooling because external water supply cannot be used for a flying vehicle.

Even if BUSTLab V1 is designed as a constant thrust and externally cooled engine, it is designed so that it can be converted into a regeneratively cooled throttleable engine with minimal changes.

3.1. Propellants

Kerosene and gaseous oxygen (GOX) are chosen as the propellants in the first 10 kN engine design. However, propellant combination is changed along with decrease in thrust level from 10 kN to 5kN, as well. It is found that kerosene is not easy to find propellant for experimental use. Ethanol-water mixture (75%-25%) is used as the fuel and liquid oxygen (LOX) is used as the oxidizer in the engine tests. This combination is chosen because both ethanol and LOX are commercially available and low cost propellants. Ethanol is mixed with water to decrease the combustion chamber temperature.

Ethanol-water mixture (75%-25%) (will be mentioned as ethanol) and LOX will be used as the propellants for the BUSTLab V1 rocket engine because they are easily available, easy to handle and they have low cost. Also, they do not have a significant compatibility problem with stainless steel, brass, copper or aluminum. Adding water into ethanol reduces combustion temperature which makes the cooling of the chamber easier. Change in the combustion temperature with respect to OF ratio, water content and combustion pressure can be seen in Figure 3.1. Data is generated using NASA Chemical Equilibrium with Applications (CEA) software.

As can be seen from Figure 3.1, combustion temperature increases with increasing combustion chamber pressure and ethanol concentration. Also, OF ratio that maximum combustion temperature is achieved moves from 2 at %100 ethanol concentration to 1.5 at %75 ethanol concentration.

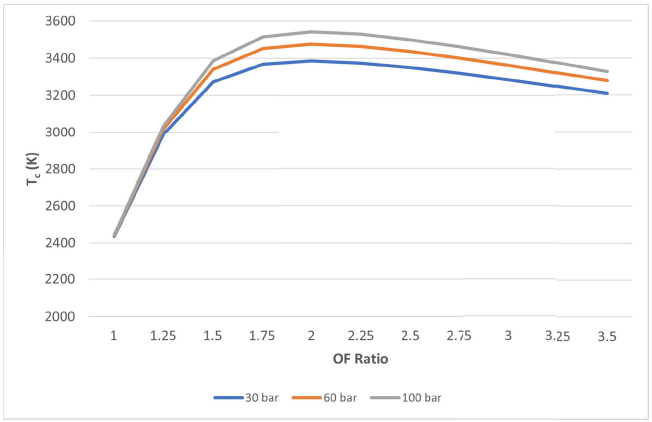

(a)

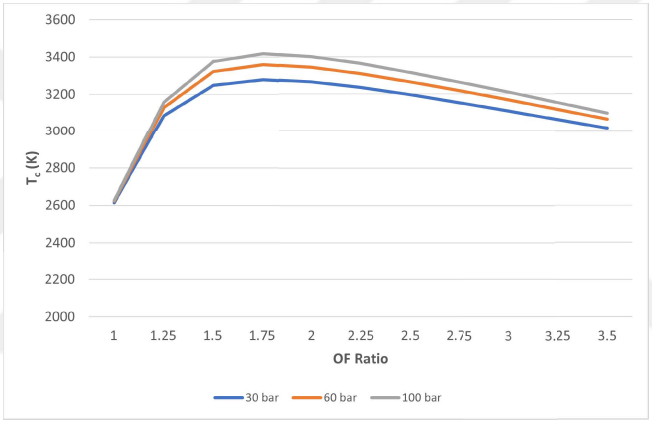

(b)

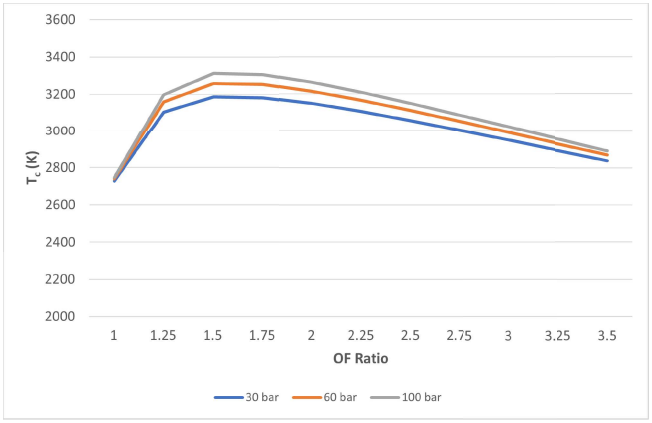

(c)

Figure 3.1. Change of the combustion temperature with the OF ratio for (a) %100-%0 ethanol-water, (b) %85-%15 ethanol-water and (c) %75-%25 ethanol-water concentration.

Figure 3.2 shows the change of I_{sp} with respect to OF ratio at 30 bar chamber pressure using 7.14 expansion ratio for %75 concentrated ethanol and %100 concentrated ethanol. As can bee seen from the figure, optimum OF ratio is different for two curves. Maximum I_{sp} can be achieved at 1.50 OF ratio for %100 concentrated ethanol whereas at 1.25 OF ratio for %75 concentrated ethanol. Also, The maximum I_{sp} of %75 concentrated ethanol is lower than the maximum I_{sp} of %100 concentrated ethanol.

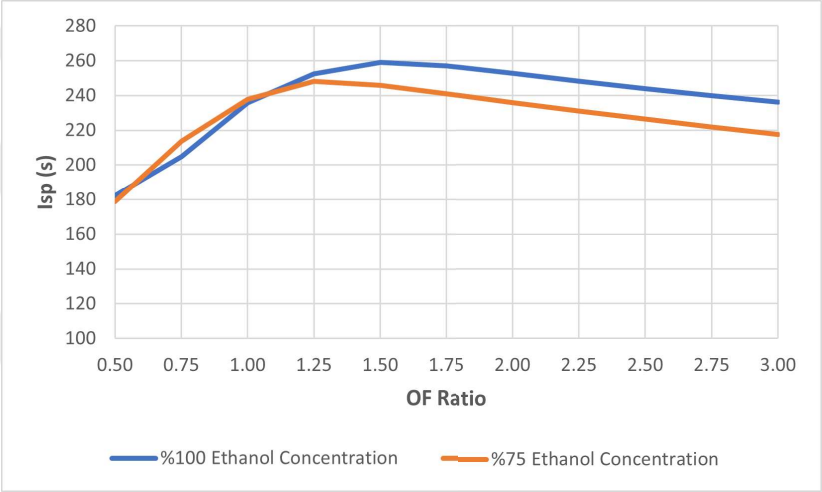

Figure 3.2. Change of the I_{sp} with OF ratio and ethanol concentration.

%75-%25 ethanol-water concentration at 1.25 OF ratio is chosen as a working condition to keep combustion temperature relatively low without a significant loss of I_{sp}. Even if the main aim was reducing the combustion chamber temperature by adding water into the ethanol, it is realized after the tests that combustion temperature at 1.25 OF ratio for %75 concentrated ethanol is higher than %100 concentrated ethanol. This caused from the shift of the optimum OF ratio with the increasing water content.

Combustion chamber pressure is chosen considering the similar engines in the literature, size constraints and I_{sp}. 50 bar combustion pressure is chosen for the initial design. Increasing the combustion pressure decreases the size of the engine for the same thrust level and increases the sea level I_{sp}. As mentioned before, combustion pressure

is decreased to 30 bar for the final design because of the limits of the available test setup. This situation resulted in a decrease in thrust, as well.

In summary, a 10 kN kerosene/GOX engine which works at 50 bar chamber pressure is designed and manufactured as the initial design. However, this design is adjusted and necessary changes are made so that it can work at 30 bar chamber pressure to generate 5 kN thrust with %75 concentrated ethanol/LOX propellant combination. Most of the manufactured engine parts could not be re-manufactured due to the budget and limited time. All of the design choices and changes will be investigated in detail in relevant chapters. In this way, propellants, thrust level and combustion pressure are pre-determined and other engine properties and characteristics are to be calculated using these values.

3.2. Thrust Chamber Characteristics

Properties of the combustion products must be known to be able to determine the combustion chamber and nozzle sizes and mass flow rates of the propellants. Properties of the combustion products are found using NASA CEA software. NASA CEA is a software that calculates the chemical properties and equilibrium compositions of the mixtures and it is published by NASA [17]. Also, it can calculate theoretical rocket performance characteristics. There are more than 2000 species in the software and almost all of the common rocket propellants are available. Combustion pressure, propellants and OF ratio are given as input to the software and it calculates the properties like combustion chamber temperature, molecular mass of the combustion products and specific heat ratio of the combustion products. These results are used with isentropic flow equations to calculate thrust, geometry (combustion chamber, throat and exit area) and Isp of the engine.

A MATLAB code is generated for this purpose. Properties of the combustion products (molecular mass and specific heat ratio for the combustion products), combustion conditions (chamber temperature, chamber pressure and OF ratio), mass flow

rate, characteristic chamber length, ambient pressure and gravity are given as inputs. MATLAB code calculates combustion chamber diameter and length, throat diameter, nozzle exit diameter, theoretical characteristic velocity, exit velocity, thrust and I_{sp} so that the nozzle exit pressure is equal to the ambient pressure. Equations used in the MATLAB code are given in this section. It should be mentioned that combustion chamber and nozzle are designed for the initial 10 kN kerosene/GOX combination and the values in the following equations are given for this initial design. Performance of the engine when ethanol/LOX combination is used instead of kerosene/GOX combination is given at the end of this section.

First of all, throat area (A^*) is calculated from the given mass flow rate, the chamber pressure and the chamber temperature for the chosen propellant combination as

$$A^* = \frac{\dot{m}}{P_o}\sqrt{T_o\frac{\mathbb{R}}{\gamma}}\left(1+\frac{\gamma-1}{2}\right)^{\frac{\gamma+1}{2(\gamma-1)}}, \tag{3.1}$$

where T_o is 3564 K, P_o is 50 bar, $\mathbb{R}$ is 380.2 J/(kg.K) and γ is 1.148. Stagnation temperature and stagnation pressure are assumed to be equal to the chamber conditions.

Throat diameter (D_{throat}) is calculated using the throat area (A^*) as

$$D_{throat} = \sqrt{\frac{4A^*}{\pi}}, \tag{3.2}$$

where A^* is 0.0013 m^2.

Mass flow rate and OF ratio are given as inputs to the MATLAB code and the mass flow rate of each propellant is calculated as

$$\dot{m}_f = \frac{\dot{m}}{1+OF}, \tag{3.3}$$

$$\dot{m}_o = \dot{m} - \dot{m}_f. \tag{3.4}$$

where OF ratio is 2.25.

Total mass flow rate is chosen as an iterative process. An initial total mass flow rate is given as an input to the MATLAB code and resulting thrust is calculated. Total mass flow rate is changed until the desired thrust is reached. If the achieved thrust is lower than the desired, mass flow rate is increased.

Characteristic velocity (c^*) can be calculated theoretically as

$$c^* = \frac{P_o A^*}{\dot{m}} = \frac{\sqrt{\gamma \mathbb{R} T_c}}{\gamma \sqrt{[2/(\gamma+1)]^{(\gamma+1)/(\gamma-1)}}}, \tag{3.5}$$

where T_c is 3564 K, $\mathbb{R}$ is 380.2 J/(kg.K) and γ is 1.148. As mentioned before, formulation on the right side can be used for theoretical calculation and the one on the left side for experimental calculation.

Exit mach Number (M_e), exit area (A_e), exit diameter (D_e) and exit velocity (v_e) are calculated as

$$M_e = \sqrt{\frac{2\frac{P_e}{P_o}^{\frac{-(\gamma-1)}{\gamma}} - 1}{\gamma - 1}}, \tag{3.6}$$

$$A_e = \frac{A^*}{M_e}\left(\frac{2}{\gamma+1}\left(1 + \frac{\gamma-1}{2}M_e^2\right)\right)^{\frac{\gamma+1}{2(\gamma-1)}}, \tag{3.7}$$

$$D_e = \sqrt{\frac{4A_e}{\pi}}, \tag{3.8}$$

$$v_e = \sqrt{2\left(\frac{T_c}{M}\right)\left(\frac{\mathbb{R}_{univ}\gamma}{\gamma-1}\right)\left(1 - \frac{P_e}{P_o}^{\frac{\gamma-1}{\gamma}}\right)}. \tag{3.9}$$

where P_e is 1 bar, P_o is 50 bar, γ is 1.148, A^* is is 0.0013 m^2, M_e is 2.96, A_e is 0.009 m^2, T_c is 3564 K, M is 21.87 kg/kmol and $\mathbb{R}_{univ}$ is 8.314 J/(K.mol).

Thrust of the engine is calculated as

$$\mathbb{T} = \dot{m} v_e + A_e(P_e - P_a). \tag{3.10}$$

where P_e and P_a are pre-defined, which are taken equal to each other, and $\dot{m}$ is firstly given as an estimation. A_e and v_e are calculated from Equation 3.7 and Equation 3.9.

Obtained thrust value is compared with the desired thrust value. Mass flow rate is changed accordingly and all of the calculations are done again until the desired value is achieved as a result of Equation 3.10.

Theoretical specific impulse (I_{sp}) of the engine is calculated as

$$I_{sp} = \frac{\mathbb{T}}{\dot{m}g}, \tag{3.11}$$

using the determined mass flow rate and the calculated thrust.

Characteristic chamber length (c^*) is chosen from the literature for kerosene-LOX combination for the initial design as 1.27 [3]. Value for kerosene-GOX combination could not be found in the literature and value given for the LOX is used. Characteristic chamber length is different for ethanol/LOX combination but combustion chamber is manufactured for initial kerosene/GOX combination. Meaning of the characteristic chamber length and the effects of using the value for kerosene-LOX combination are discussed in Section 3.3.2.

Combustion chamber volume is calculated as

$$V_{chamber} = L^* A^*. \tag{3.12}$$

Chamber cross sectional area is formulated as

$$A_{chamber} = A^* \left(8(D_{throat} * 100)^{-0.6} + 1.25\right). \tag{3.13}$$

Length of the combustion chamber ($L_{chamber}$) and the combustion chamber diameter ($D_{chamber}$) are calculated directly from the geometric relations of a cylinder as

$$L_{chamber} = \frac{V_{chamber}}{A_{chamber}}, \tag{3.14}$$

$$D_{chamber} = \sqrt{\frac{4A_{chamber}}{\pi}}. \tag{3.15}$$

Nozzle length can be calculated for 80% bell contour nozzle as [3]

$$L_{nozzle} = \frac{6.45 D_{throat}}{2}. \tag{3.16}$$

All of the needed sizing parameters and engine performance parameters are determined thus far and important results are given in Table 3.1. Table 3.1 is created for the initial propellant combination of kerosene/GOX. Table 3.2 shows the parameters when ethanol-water/LOX combination is used to generate 5 kN thrust for the manufactured chamber and the nozzle. It can be seen that exit pressure is not equal to the ambient pressure anymore and over-expansion is observed. Also, I_{sp} is lower. This section is a summary of the rocket engine design procedure. Following sections concentrate on the each of the engine section in more detail.

Table 3.1. Summary of the initial 10 kN design with Kerosene-GOX propellant combination.

Propellant	Kerosene-GOX
Thrust	9942 N at sea level
Chamber Pressure	50 bar
Exit Pressure	1 bar
Chamber Temperature	3564 K
OF Ratio	2.25
Mass Flow Rate	3.45 kg/s
Expansion Ratio (Ae/At)	7.14
Isp	294 (Theoretical Sea Level)
Propellant Feed System	Pressure Fed
Chamber Cooling	Water cooling with cooling channels

3.3. Thrust Chamber

Thrust chamber consists of the injector, the combustion chamber and the nozzle. It is where the propellants are injected, combusted and accelerated to generate thrust. Each of these are investigated separately in the following sections.

Table 3.2. Summary of the final 5kN design with ethanol-LOX propellant combination.

Propellant	Ethanol-water (75%-25%) and LOX
Thrust	5647 N at sea level
Chamber Pressure	30 bar
Exit Pressure	0.58 bar (over-expansion)
Chamber Temperature	3057 K
OF Ratio	1.25
Mass Flow Rate	2.27 kg/s
Expansion Ratio (Ae/At)	7.14
Isp	254 (Theoretical Sea Level)
Propellant Feed System	Pressure Fed
Chamber Cooling	Water cooling with cooling channels

3.3.1. Injector

There are different kinds of injectors that are used in rocket engines. Shower head, impinging, pintle, swirl and shear coaxial injectors are the most widely used types.

Shower head is the most simple one. Fluid comes out of the injector axially and mixing is achieved by turbulance and diffusion.

Propellants directly interact with each other in an impinging injector. There are doublet, triplet, quadlet and pentad types which represents how many jets are impinging. Impinging jests can be classified as like on like (fuel on fuel or oxidizer on oxidizer) or unlike (fuel on oxidizer) according the types of impinging jets. There might be instabilities caused from the misaligned impingement position caused from the manufacturing defects. Difference between shower head and impinging injectors can be seen in Figure 3.3.

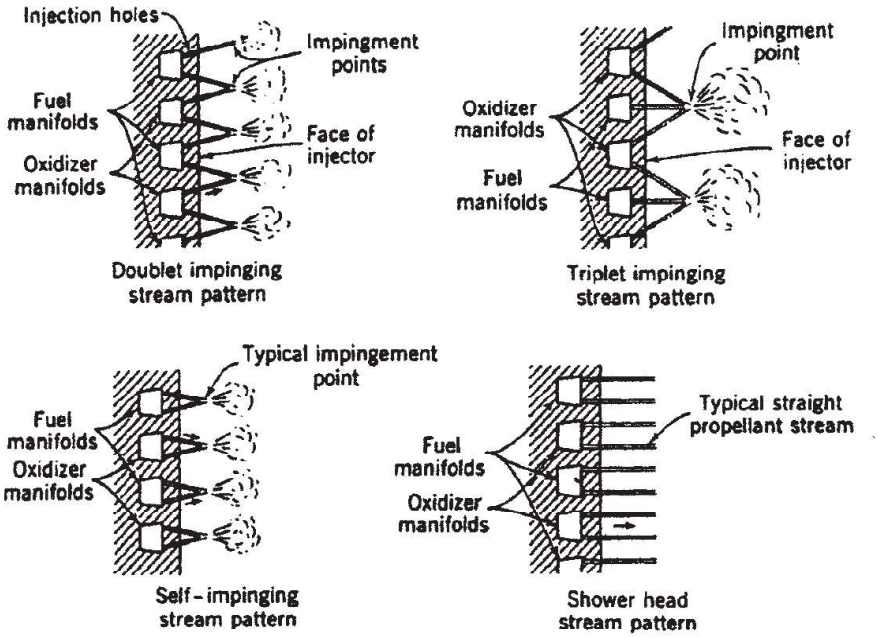

Figure 3.3. Representations of impinging and shower head injectors [3].

Pintle injector is a special kind of a impinging injector. One of its advantage is ease of changing the injector area to achieve throttleability. A sample pintle injector can be seen in Figure 3.4. Fuel flows radially outwards and oxidizer flows axially in this design. They imping and mix near the pintle tip wall.

Swirl injector introduces a swirling motion to the fluid which increases the mixing and atomization of the propellants. Oxidizer or fuel can be used in swirling section. Figure 3.5 shows a swirl injector where the oxidizer has a swirl and fuel flows axially. They collide just at the exit of the swirl tube.

Shear coaxial injector uses shear force between the fluids to increase mixing and atomization. It is most suitable for the propellants with large density ratio, like liquid-gas. Figure 3.6 shows a typical shear coaxial injector where the gas jet flows around the liquid jet and shear forces mix the two fluid.

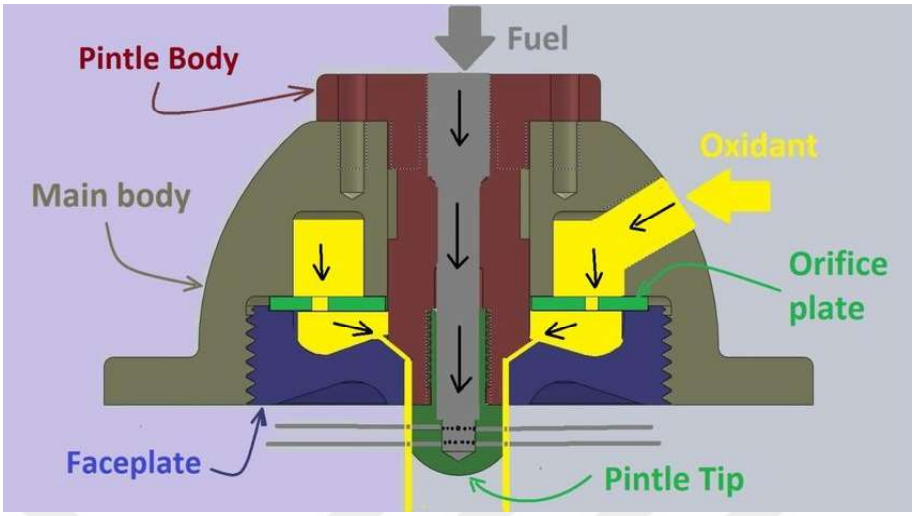

Figure 3.4. A sample pintle injector [18].

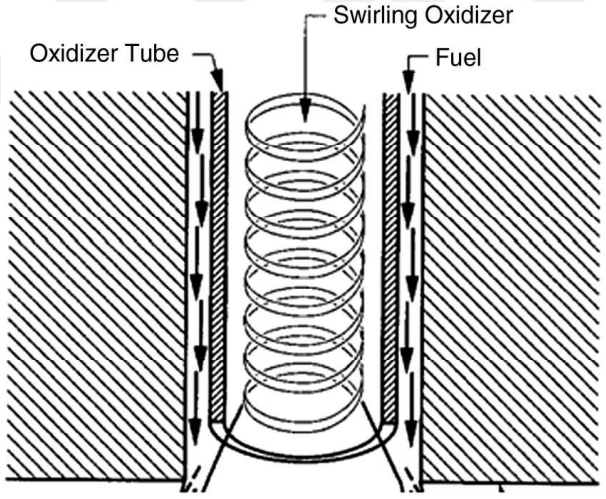

Figure 3.5. Schematic of a swirl injector [19].

A triplet impinging injector is chosen for the design of BUSTLab V1 engine. Oxidizer flows from the outer two holes and fuel flows from the center hole. This design is chosen because it has good mixing capabilities and manufacturing is not so complicated.

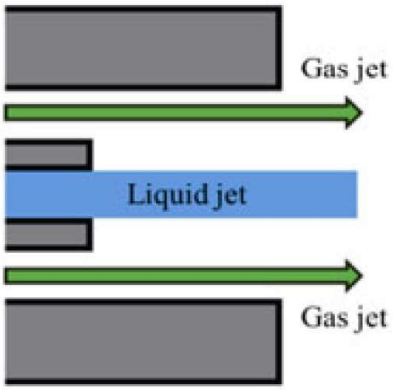

Figure 3.6. Schematic of a shear coaxial injector [20].

3.3.2. Combustion Chamber

Combustion chamber is the portion of the thrust chamber where the propellants are mixed and combusted. There are some critical points in the design of a combustion chamber.

- Volume of the combustion chamber should be large enough to achive adequate mixing and complete combustion. Performance of the engine decreases if the propellant do not mix enough and combustion is incomplete. Smaller chamber volumes can be achieved with better mixing injectors and higher chamber pressures.
- Volume of the combustion chamber affects cooling of the chamber because higher combustion chamber diameter means lower combustion gas velocity and larger surface area.

Characteristic chamber length can be defined as the length that a chamber of the same volume would have if its cross-sectional are was the nozzle throat area. It can be formulated as

$$L^* = V_{chamber}/A^*. \tag{3.17}$$

Table 3.3. Typical L* values for the rocket engines.

Propellant Combination	**L* (m)**
LOX/GH_2	0.6-0.7
LOX/LH_2	0.7-1.0
LOX/Kerosene	1.0-1.3
NTO/N_2H_4	0.8-1.0
NTO/UDMH	1.2
NTO/Aerozine	0.9

Characteristic chamber length changes between 0.8 and 3.0 m for most of the common engines. It is determined by the used propellants [3]. Typical values for characteristic chamber length are given in Table 3.3. A sufficient residence time is needed to obtain full combustion in the combustion chamber. Increased reaction rates decreasee the needed residence time. For example, L^* for LH_2 is higher than the L^* for gaseous H_2 because more time is needed for the full combustion of LH_2. LH_2 temperature increases and vaporizes when it enters the combustion chamber. These heating and vaporization steps increase the needed residence time for LH_2 and results in higher L^*. L^* of kerosene/LOX combination is significantly higher than LH_2/LOX combination because combustion reaction chain of kerosene is more complicated than LH_2 and it needs more time.

L^* depends also on injection system. More efficient injection system can decrease the L^*. L^* of BUSTLab V1 engine is 1.27 because kerosene-LOX propellant combination was used as a reference for the initial design. Even if the initial propellants were kerosene and GOX, no such combination was found in the literature and reference data for the LOX is used. 1.27 is quite high for ethanol/LOX combination but it ensures that full combustion is reached at the end of the combustion chamber. It could not be changed because the combustion chamber was already manufactured for kerosene/GOX combination.

3.3.3. Nozzle

Nozzle is the part of the engine where the fluid is accelerated and exhaust gas is expelled to the atmosphere to generate thrust. Nozzle has a converging part, a throat and a diverging part. Calculation of the throat diameter is mentioned in Section 3.2. It is designed so that choked flow condition is achieved at the throat. Flow is accelerated further at the diverging section. Nozzle exit diameter determines the exit velocity and exit pressure of the flow.

As can be seen from Equation 3.10, increased exhaust velocity results in higher thrust. However, for the same combustion chamber conditions like the same pressure and the same temperature, increased exhaust velocity results in decreased exhaust pressure. When the exit pressure of the nozzle decreases below the ambient pressure, ambient pressure compresses the exhaust gas and flow separates from the nozzle wall. This is called over-expansion. There is a lower limit for the exhaust gas pressure because too much pressure difference between the ambient and the nozzle exit causes a phenomena called "flow separation". After a certain P_e/P_a ratio, flow separation becomes uneven and uncontrolled so that it generates lateral forces on the nozzle wall and causes structural damage. Summerfield criterion gives a preliminary design value for the ratio of exit pressure to ambient pressure for flow seperation [21]. This criteria is expressed as

$$\frac{P_e}{P_a} \approx 0.35 - 0.4. \tag{3.18}$$

If the exit pressure of the exhaust gas is higher than the ambient pressure, under-expansion occurs. Exhaust gas continues expanding after the nozzle until its pressure reaches the ambient pressure. Under-expansion does not cause significant structural loads on the nozzle but it decreases the engine performance.

Figure 3.7 shows under-expansion and over-expansion behaviours for three different nozzle configurations. First nozzle configuration is designed to work at sea level and low altitudes as a booster or first stage. Second and third configurations are used

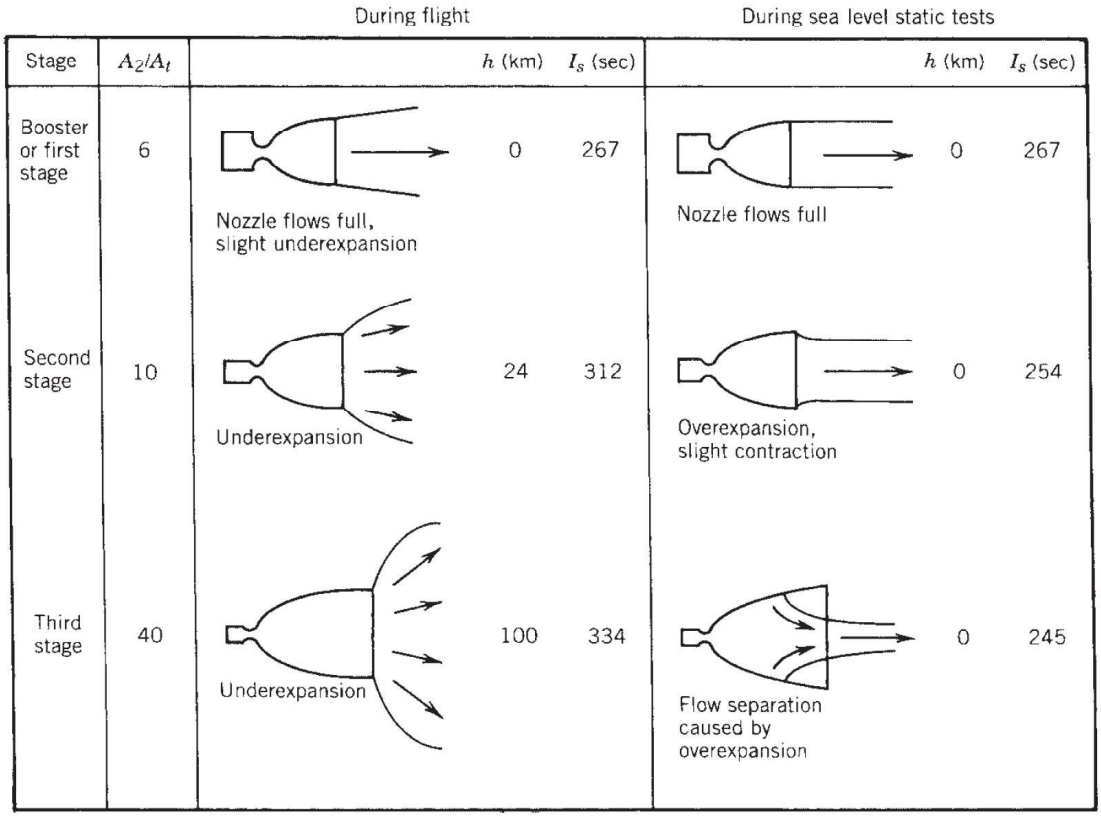

Figure 3.7. Exhaust gas behaviour for three different nozzle configurations for sea level test and flight conditions [3].

for higher altitudes as second and third stages. First configuration is designed so that exit pressure matches with the ambient pressure at the sea level. Second configuration is designed to match a lower ambient pressure at a higher altitude. Therefore, over-expansion occurs when this nozzle is tested at the sea level. This over-expansion is acceptable since it is not too severe to cause structural damage. Even if this nozzle is designed to match the ambient pressure at a certain altitude, under-expansion occurs with the further increase in the altitude because of the decreasing pressure. Third stage nozzle is designed to work at very high altitudes where the ambient pressure is almost zero. Exit area of this nozzle has to be very large in order to equate the exit pressure to the ambient pressure. However, increased exit area means longer nozzle but then, nozzle becomes too heavy and structural problems occur. Therefore, third stage nozzle

is generally designed to work in under-expansion mode. When this nozzle is tested at sea level, over-expansion becomes so significant that uncontrolled flow separation occurs. Therefore, it is not preferred to test high area ratio nozzles at sea level [3].

3.3.4. Cooling Channels

In this section; the effect of the chamber material selection, water channel geometry and number, wall thickness of the combustion chamber and mass flow rate of the water used for cooling are investigated. A MATLAB code is generated and proper heat transfer equations are used. The approach to the problem is as following: There are two flows in the rocket engine, water flow and combustion gas flow. They are investigated separately to calculate their convective heat transfer coefficients and then, they are combined to calculate heat transfer.

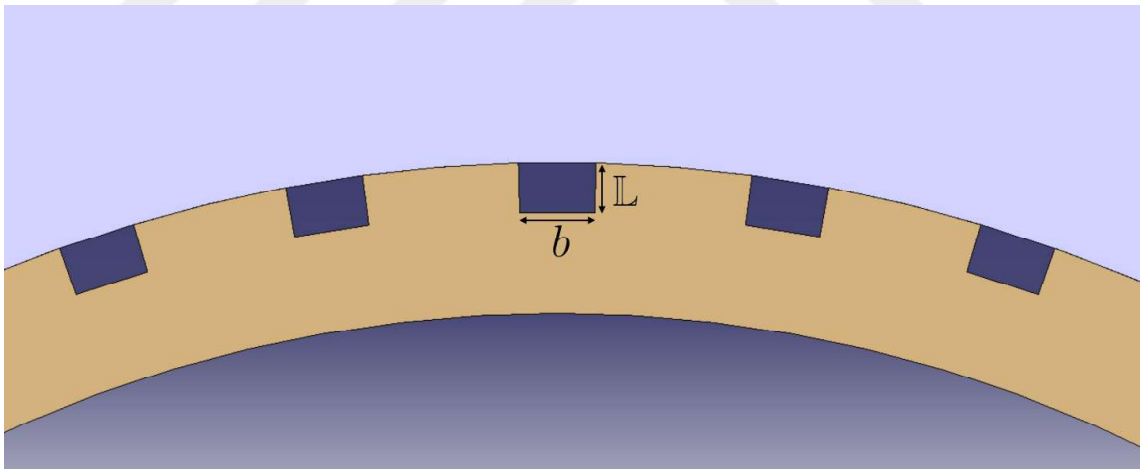

Figure 3.8. Closer look at the cooling water channels.

Figure 3.8 shows the water channels and their dimension that are used in the MATLAB code. These channels are assumed to be rectangular with "b (width of the channel)" and "$\mathbb{L}$ (height of the channel)" dimensions. Walls of the water channels act like the extended surface with an adiabatic tip. Surface between the jacket surrounding the combustion chamber and the combustion chamber is assumed to be adiabatic.

3.3.4.1. Calculating Convective Heat Transfer Coefficients. As mentioned before, water flow in the cooling channels and hot gas flow in the combustion chamber are assumed to be fully developed turbulent flow. First of all, Nusselt number and convection heat transfer coefficients are calculated for water and hot gas flows using Equation 2.27 and Equation 2.25.

Values for heat capacity, dynamic viscosity, conductivity, Prandtl number and density of the combustion products are taken from NASA CEA. Temperatures at the combustion chamber, the throat and the nozzle exit sections are obtained from NASA CEA, as well. NASA CEA gives the temperatures and fluid properties of the combustion gasses at each of the combustion chamber, the throat and the nozzle exit sections.

Problem is divided into three sections: Combustion chamber, converging nozzle section and diverging nozzle section. Combustion gas properties at combustion chamber, throat and nozzle exit are obtained from NASA CEA. Water properties are obtained from the "Thermophysical Properties of Water" tables at initially guessed temperatures.

Flow area of one channel, mass flow rate at one channel, flow velocity, Reynolds number, Nusselt number, and convective heat transfer coefficient are calculated at the combustion chamber, the throat and the nozzle exit sections. Heat transfer area is calculated as cylindrical area, conical frustum and conical frustum at the combustion chamber, the converging section and the diverging section, respectively. Convective heat transfer coefficient at the converging and the diverging sections are calculated as the average of combustion chamber-throat and throat-nozzle exit convective heat transfer coefficients, respectively. This can be seen in Figure 3.9. For example, heat transfer coefficient for the L(2) part is calculated as (h1+h2)/2.

Walls between the cooling channels are analyzed as extended surfaces (fins). Fins are assumed to be straight fin of uniform cross section and with an adiabatic tip. Fin efficiency and overall surface efficiency are calculated by Equation 2.23 and Equation

2.22. Thermal resistance is calculated by Equation 2.20 for the water and by Equation 2.19 for the hot gas.

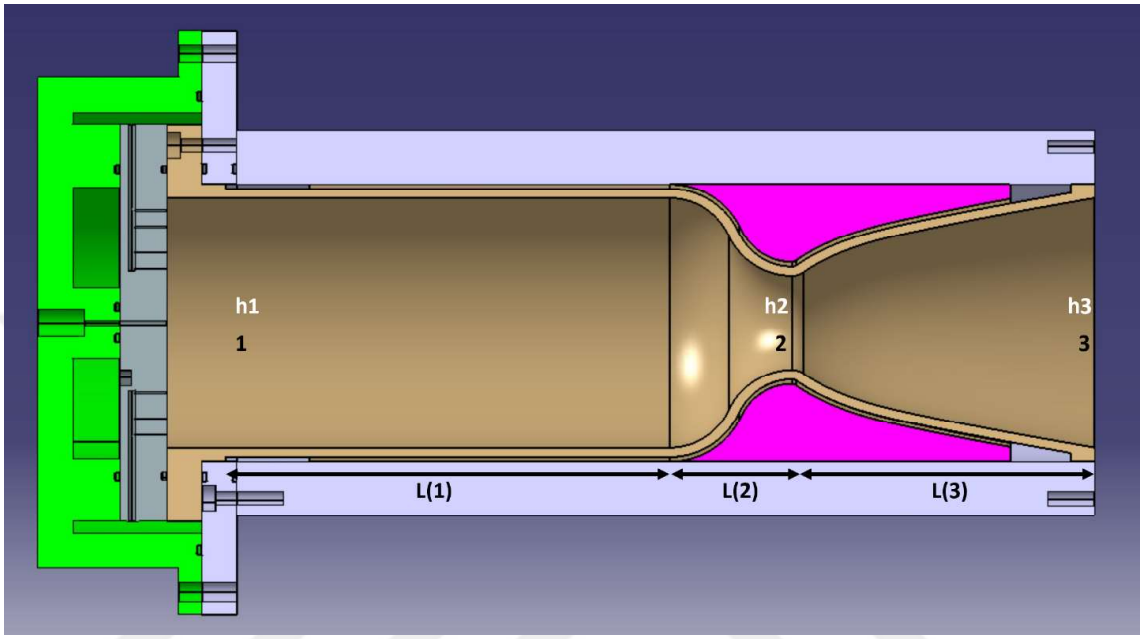

Figure 3.9. Longitutional cross-section of the rocket engine showing the sections 1,2 and 3 used in the heat transfer calculations (L(1) =0.27 m, L(2) = 0.05 m and L(3) = 0.13 m).

Wall resistance of the combustion chamber wall is calculated for a hollow cylinder by Equation 2.21. For converging and diverging sections, wall resistances are calculated as the average of the combustion chamber-throat and throat-nozzle exit wall resistances. The product of the overall heat transfer coefficient and the heat transfer area (UA) is calculated at each section from the thermal resistances.

Iterations are made for calculating water temperature at different sections as follows:

(i) Heat transfer at each section is calculated using the product of the overall heat transfer coefficient and the heat transfer area (UA), and the log mean temperature

difference at the inlet, the throat and the outlet sections as

$$Q = UA\Delta T_{lm}. \tag{3.19}$$

(ii) Total heat transfer is calculated by summing heat transfer at each section as

$$Q_{total} = Q_1 + Q_2 + Q_3. \tag{3.20}$$

(iii) Corrected water outlet temperature is calculated from the total heat transfer as

$$T_{water,corrected} = \frac{Q_{total}}{\dot{m}_{water} c_{p,water}} + T_{water,3}. \tag{3.21}$$

(iv) Water temperature at the throat is calculated by taking the average of the inlet and outlet water temperatures as

$$T_{water,2} = \frac{T_{water,1} + T_{water,3}}{2}. \tag{3.22}$$

This process is repeated until the water temperatures converge. After that, thermal resistance per unit area (R") is calculated for the water, the chamber wall and the hot gas at each section. Thermal resistance per unit area (R") is calculated by multiplying the thermal resistance (R) with the heat transfer area (A). Heat transfer per unit area (Q") at each section is calculated using thermal resistance method as

$$Q'' = (T_1 - T_2)R'', \tag{3.23}$$

where T_1 and T_2 are the temperatures at the inner and outer surfaces of the combustion chamber wall. Inside and outside temperatures of the chamber wall can be calculated using this equation. During the calculations, it is assumed that temperature of the combustion gas is constant within each section. However, temperature of the combustion gas is different for each section which is obtained from NASA CEA software.

For BUSTLab V1 rocket engine, water channel width is chosen to be 3 mm, 2.2 mm and 3 mm at the combustion chamber, throat and nozzle sections, respectively. 2.2 mm is chosen as the minimum width to make the manufacturing easier. Water channel height is chosen to be 3 mm.

3.4. Igniter

There are different kind of igniters that are used for igniting the rocket engines. Igniter is used to provide enough heat to mixed propellants to start combustion. Igniter can be placed at the forward or aft end of the engine; it can be fixed on the engine or it can be used externally. The most commonly used types are pyrotechnic, pyrogen and spark igniters [3]. Pyrotechnic igniter uses an energetic material like solid explosives to generate heat. Generally, they have short burning times and heat is transferred mainly by radiation. Electric signal can be used to initiate ignition in this type. Pyrogenic igniter is basically a very small rocket motor which is not designed to generate thrust. It may have subsonic or supersonic nozzle. Heat is transferred from pyrogen gas to the main propellants by convective heat transfer. Pyrogenic igniter can be placed on large motors externally so that hot pyrogen gas is directed towards large motor nozzle. Spark igniter is a type of igniter that uses high voltage to generate spark between two surfaces. It is mainly used for small scale experimental rocket engines.

Spark igniter is chosen as a ignition method for the BUSTLab V1 rocket engine because it has low cost, it is commercially available and reusable. A commercially available spark plug that is used in gas heated aluminum melting furnaces is chosen. It consists of two metal rods which have ceramic holders for mounting and a high voltage source. Distance between the two rods can be adjusted manually. Several tests are made to find optimum distance between the rods. If the distance is too large, there is no spark. If the rods are too close to each other, spark is too small to start ignition.

Igniter is connected to a pneumatic linear actuator that moves up and down and placed externally in front of the engine nozzle. It is moved up before the engine test to align with the nozzle and moved down when the propellants ignite to protect igniter from the hot exhaust gas.

4. PROPELLANT FEED SYSTEM

Propellants are kept in propellants tanks before the firing of the engine. They are delivered to the engine through the pipes, valves, sensors, flow meters etc. Pressure of the working fluid changes in each section of this delivery system. All of the pressure losses should be considered in the design of a propellant feed system. Overview of the pressures in the system is given in Figure 4.1. It should be mentioned that this figure is not created using the test results of the components. It is showing the expected pressures in the system and these pressure are used to design the cavitating venturies and the injector.

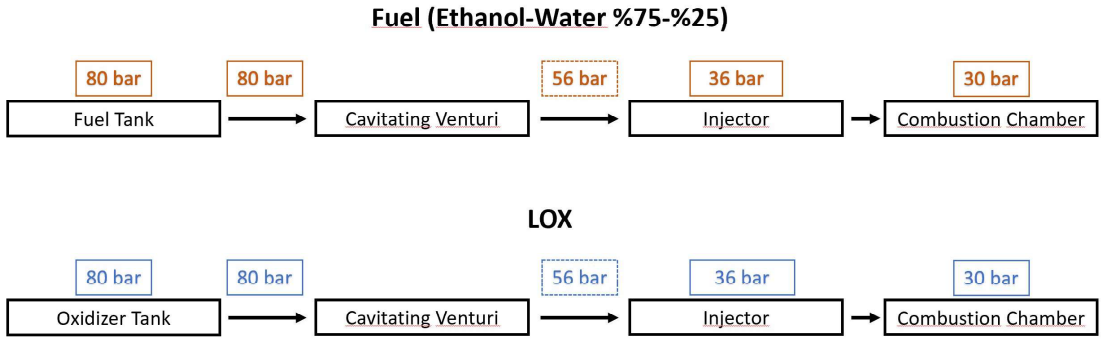

Figure 4.1. Overview of the predicted pressures in the system.

Propellant tanks are at 80 bar. It is assumed that there is no pressure loss between the tanks and the cavitating venturies and upstream pressures of the cavitating venturies are 80 bar, as well. 56 bar shown inside the dashed rectangle between the cavitating venturies and the injectors represents the minimum downstream pressure that the cavitating venturi can work in cavitating mode which will be explained in more detail in Section 4.3.

At first, external pressure cylinders (nitrogen or argon) are used with a spring-loaded pressure regulator to pressurize the propellant tanks. The pressure regulator is

placed at the exit of the high pressure cylinders and it reduces the 235 bar pressure in the high pressure cylinder to 80 bar. 235 bar pressure in the high pressure cylinder decreases during the test and this results in decreased pressure at the exit of the regulator, lower than 80 bar. Remote controlled pressure regulators or actively PID controlled pressure regulators can be used to prevent this situation. Otherwise, pressure in the propellant tanks decreases during the test which results in decreasing mass flow rate. OF ratio can also be affected from that change in tank pressures. Later on, this pressurization is with bang ang control system which will be explained in detail in following sections.

Cavitating venturies are used to determine the mass flow rates in the system. Cavitating venturies are explained in more detail in section 4.3. Cavitating venturies are designed to pass desired mass flow rates at 80 bar upstream pressure. Pressure ratio between the downstream and the upstream of the cavitating venturi should not exceed 0.7 for venturi to be able to work properly. So, pressure at the downstream of the cavitating venturi should not be higher than 56 bar.

There should be around 15-20% pressure drop at the injector to achieve good atomization and mixing [3]. Injector is designed considering this criteria. Injector is designed to achieve 6 bar pressure drop. If 6 bar pressure drop is achieved, upstream pressure of the injector becomes 36 bar for 30 bar combustion chamber pressure. However, injector tests showed that pressure drop at the injector for the desired mass flow rates are different from 6 bar. Using 80 bar tank pressure, pressure drop at the injector is measured to be 6.5 bar and 4 bar at the cold flow tests (Section 7.2.1) for the fuel side and the oxidizer side, respectively. This will be discussed again in Section 7.2.1.

Actually, there are two important sections where the mass flow rate of the working fluid can be limited: the cavitating venturi and the throat section of the nozzle. Mass flow rate is determined by the upstream pressure at these sections regardless of the downstream pressure.

When the upstream pressure of the cavitating venturies are 80 bar, total mass flow rate is 2.26 kg/s. Mass flow rates of the fuel and the oxidizer are 1.01 kg/s and 1.25 kg/s, respectively. Until the downstream pressure of the cavitating venturi is below the 70% of the upstream pressure of the venturi, in other words below 56 bar, mass flow rate at the cavitating venturi is constant regardless of the rest of the system.

Another section where the mass flow rate is restricted by the upstream conditions is the nozzle throat section. Geometry of the nozzle is determined. Mass flow rate at the nozzle throat is constant for specific combustion product gases at the specified temperature and the pressure. Nozzle throat diameter is 40 mm in BUSTLab V1 and mass flow rate at the throat is calculated as 2.27 kg/s for 3057 K chamber temperature and 30 bar chamber pressure. As mentioned, cavitating venturies pass 2.27 kg/s total mass flow rate at 80 bar tank pressure. For this reason, chamber regulates its pressure itself to reach 30 bar to be able to pass 2.27 kg/s. Chamber pressure is determined in this way, just by controlling mass flow rate at the cavitating venturi by controlling upstream pressure of the cavitating venturi.

Actually, this method can be used to make the engine throttleable. Mass flow rate, chamber pressure and thrust can be controlled by changing the upstream pressure of the cavitating venturi as long as the downstream pressure of the cavitating venturi is lower than 70% of the upstream pressure.

4.1. Propellant Tanks

There are two propellant tanks, one for the fuel and one for the oxidizer. Fuel tank has 100 L capacity and its working pressure is 60 bar but it is tested at 90 bar by the manufacturer. P460 steel is used for this tank and it is not stainless steel. So, it cannot be used with LOX.

Another tank for LOX is made of 316 stainless steel. It is suitable for LOX usage. It has a 100 L capacity and its working pressure is 60 bar, too. It can be used up to

90 bar for short time periods. LOX tank is insulated with 15 cm polyurethane foam to decrease evaporation loss. Manufactured oxidizer tank before and after the insulation process can be seen in Figure 4.2. A steel structure is constructed around the tank for easy transportation.



(a) (b)

Figure 4.2. Oxidizer tank (a) before and (b) after the insulation.

Tank capacity is determined from the required propellant mass. Estimated firing duration is 20 seconds. Required fuel and oxidizer mass are 20.2 kg and 25 kg respectively. Also, some of the oxidizer will be used for chilling the oxidizer line. 100 L tanks are chosen which is a readily available size for commercial use.

4.2. Valves

Pneumatic valves are used to control the valves remotely. Pneumatic valves are used with solenoid valves to be able to control them with electric signal. Most of the pneumatic valves are chosen as normally closed configuration. In this way, they will be automatically closed if a power loss or a signal loss occurs. Purge valves are selected

as normally open configuration to purge the lines in case of a power or signal loss. Pressurized air (6 bar) is connected to the solenoid valve and when the signal is sent to the solenoid valve, it sends pressurized air to the pneumatic valve which opens the pneumatic valve. All of the valves can be controlled remotely in this way.

Standard ball valves are used in the fuel line. In the LOX line, cryogenic ball valves are used as the remotely controlled valves and cryogenic globe valves are used as the manual valves.

Cryogenic valves are designed so that none of the materials inside them lose their function at cryogenic temperatures. Also, they have some holes inside them to allow the stuck fluid inside them to escape when the valve is closed. Otherwise, cryogenic fluid vaporizes and increases pressure inside the valve because it cannot escape and this increased pressure can cause the valve to blow up.

4.3. Cavitating Venturi

Active or passive flow controllers are used to control mass flow rate in the rocket engines. A precise and accurate mass flow control is essential for a stable combustion and fine thrust control of the engine. Position controlled valves can be used for an active mass flow control but they are heavy, expensive and mass flow rate through the valve is affected by downstream flow conditions. Unstable combustion can disturb the mass flow rate through the valves. An orifice or a venturi can be used as a passive mass flow control device. Passive flow control devices are lightweight, less complex and they have lower cost. However, mass flow rate cannot be adjusted easily like an active flow controller. Therefore, combustion instabilities and mass flow rate deviations from the design values during the test cannot be compensated.

Orifice is a simple flow control device and consists of a hole in a flat plate. Mass flow rate is determined by the size of the hole. It is one of the most simple passive flow control device and it is very easy to manufacture. Also, it has a very small size.

However, this simple flow control device produces swirl and eddy flow structures in the flow and these cause unrecoverable pressure losses. These losses can be reduced by using a baffle plate with multiple holes or using a nozzle instead of a flat plate [22].

Venturi is a passive flow rate controller which has a conical shape inlet and outlet sections and a throat between them. Main difference between a venturi and an orifice is the gradual expansion or contraction of the flow. This prevents swirl creation and flow separation. However, frictional pressure losses increase due to the large surface area. Even so, it still provides a much lower pressure loss when compared with an orifice so they are generally preferred for the applications where large pressure losses must be avoided. On the other hand, its size is larger, it is heavier and it has a higher cost with respect to the orifice.

When a liquid experiences a pressure drop below its saturated vapour pressure at constant temperature, rupture occurs and it is characterized by bubble formation. This phenomena is called cavitation [23]. Main difference between cavitation and boiling is cavitation is driven by a decrease in pressure at constant temperature whereas boiling is driven by an increase in temperature at constant pressure. As its name states, cavitating venturi uses cavitation phenomena to control the mass flow rate.

Cavitating venturi is a passive flow rate controller where the flow is accelerated gradually through converging conical section, passed through a throat and decelerated through a diverging conical section. Flow is accelerated at the inlet section so that static pressure drops below the saturation pressure of the liquid that causes cavitation and cavitation bubbles are formed. These bubbles disappear at the diverging section due to the decelerated flow and increased static pressure.

Choked nozzle is the equivalent of cavitating venturi for gas substances. Calculation of sonic velocity for homogeneous gas substance is relatively easy. However, speed of sound calculation is troublesome for heterogeneous multi-phase flows. Figure 4.3 shows the relation between sonic velocity and air volume fraction for homogeneous

water/bubble mixture. There are layers at different volume fractions in a cavitating venturi. Air volume fraction is close to zero one the throat wall and zero at the middle portion of the flow.

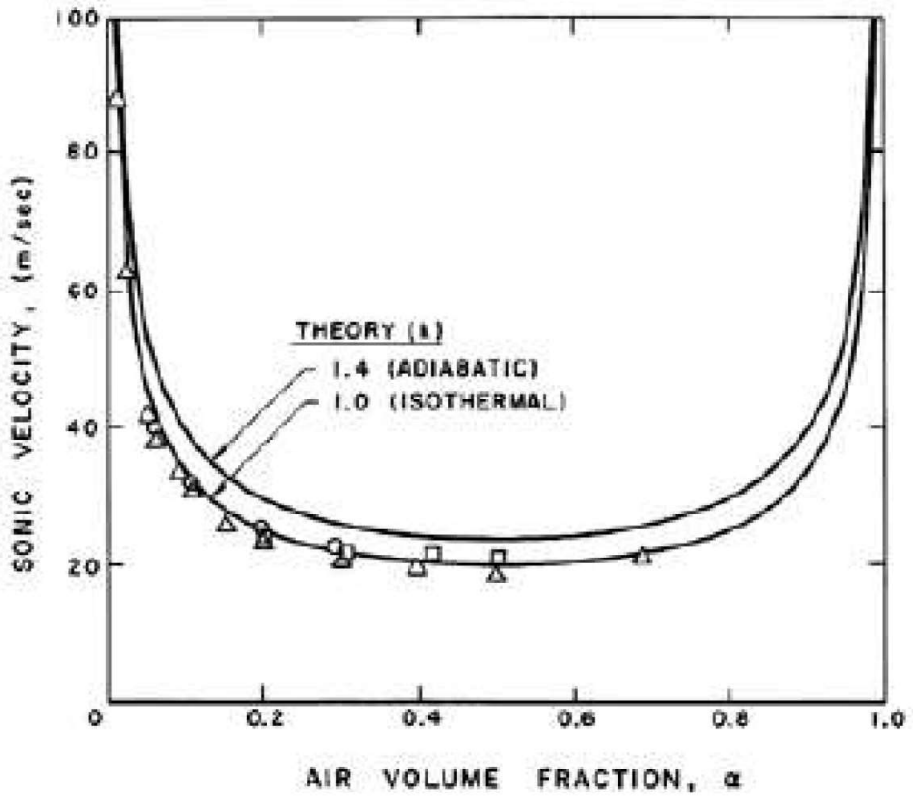

Figure 4.3. Change of sonic velocity with respect to air volume fraction for water/bubble homogeneous mixture [23].

Flow rate through the venturi can be controlled by changing upstream and downstream pressures. Cavitating venturi has two modes, cavitating mode and non-cavitating mode. Mass flow rate through the cavitating venturi is not affected by the downstream pressure in the cavitating mode and it is constant for a specified upstream pressure. In other words, controlling the growth of the cavitation nuclei is the aim for cavitating mode and this can be achieved by changing the upstream conditions. Cavitating mode is reached when the ratio of the downstream pressure to the upstream pressure (P_{ratio}) is below 60-80%. It acts like a typical venturi in the non-cavitating

mode and mass flow rate depends both on the upstream pressure and downstream pressure.

4.3.1. Design of the Venturi

Sizing of the cavitating venturies are done using both the analytical relations and CFD analyses. First designs are done using a study in the literature. CFD analyses are conducted and compared with this study. Further designs are done using the results of this initial design. Design of the cavitating venturies, final cavitating venturi dimensions and used methods are explained step by step throughout this section.

In the non-cavitating mode, flow rate through the venturi can be calculated as

$$C_d = \frac{\dot{m}}{A_{flow}\sqrt{2\rho(P_{up} - P_{down})}}, \tag{4.1}$$

where P_{up} and P_{down} are the upstream and the downstream pressures of the cavitating venturi. Pressure difference is important in this equation. C_d may change with the pressure. It can be found by computational fluid dynamics (CFD) analysis or by a flow rate test.

If the pressure ratio (downstream pressure/upstream pressure) drops below a certain point, about 0.6-0.8, venturi changes operation mode. After that point, the effect of the downstream pressure disappears.

In the cavitating mode, pressure difference does not affect the mass flow rate. Mass flow rate changes with the upstream pressure. Changing downstream pressure does not change mass flow rate. This can be used to control the mass flow rate in a rocket engine. The mass flow rate is not affected by the pressure changes in the combustion chamber and flow rate is always constant. Mass flow rate through the venturi in cavitating mode can be found as

$$C_d = \frac{\dot{m}}{A_{flow}\sqrt{2\rho(P_{up} - P_{vap})}}, \tag{4.2}$$

where P_{vap} is the vapour pressure of the fluid. Difference between Equation 4.1 and 4.2 is the P_{down} term. P_{down} term in the non-cavitating mode changes to P_{vap} (vapor pressure of the fluid) term in the cavitating mode and the mass flow rate formula does not have a downstream conditions dependent term anymore. Instead, mass flow rate depends on the vapor pressure of the fluid.

4.3.1.1. CFD Benchmark Study. First of all, a benchmark study is done to verify CFD analysis setup using the studies of Kang et. al. [24]. Kang et. al. designed two cavitaing venturies for kerosene and LOX. Their mass flow rates are in the same range as the initial kerosene/GOX BUSTLab V1 engine. Fuel mass flow rate is 4.1 kg/s and LOX mass flow rate is 1.2 kg/s for 64.5 bar upstream pressure for the venturies that are used by Kang et. al.. These designs are used as references for the first cavitating venturi CFD analysis and the CFD results are compared with Kang et. al. results.

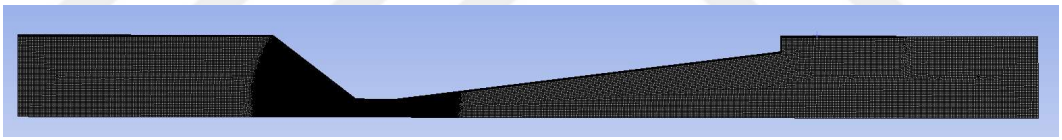

(a)

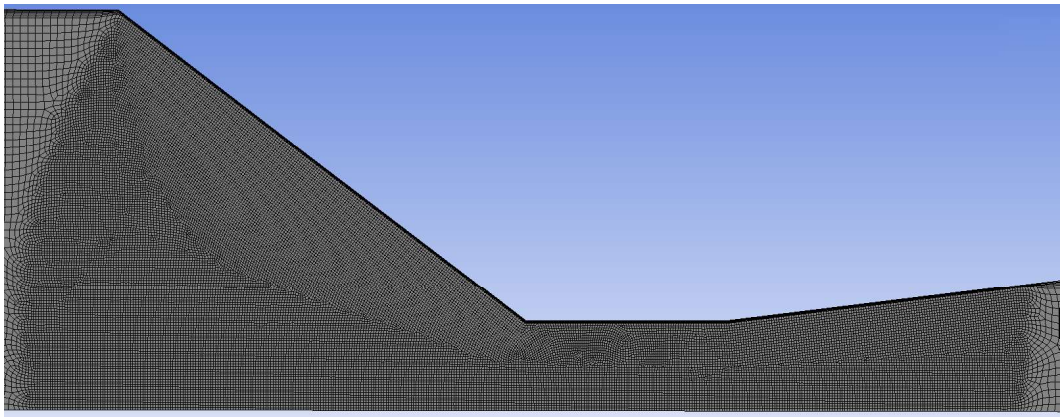

(b)

Figure 4.4. Used quadrilateral mesh in the benchmark study. (a) shows the full model and (b) shows critical region which has a denser mesh.

The same geometry as Kang et. al. design is created in Ansys Fluent and CFD analyses are conducted. A 2D axisymmetric model and quadrilateral mesh are used. Used geometry and mesh in the benchmark study are given in Figure 4.4. Throat section is the most critical region in this model where the cavitation occurs. Therefore, density of the mesh is higher in this area. "Sphere of Influence" method is used to generate this high density mesh region.

Liquid phase volume fraction contours for two downstream pressures 44 bar and 55 bar are given in Figure 4.5. Beginning of formation of the cavitation bubble can be seen in Figure 4.5 (a). Cavitation bubble is bigger in Figure 4.5 (b) because of the lower downstream pressure.

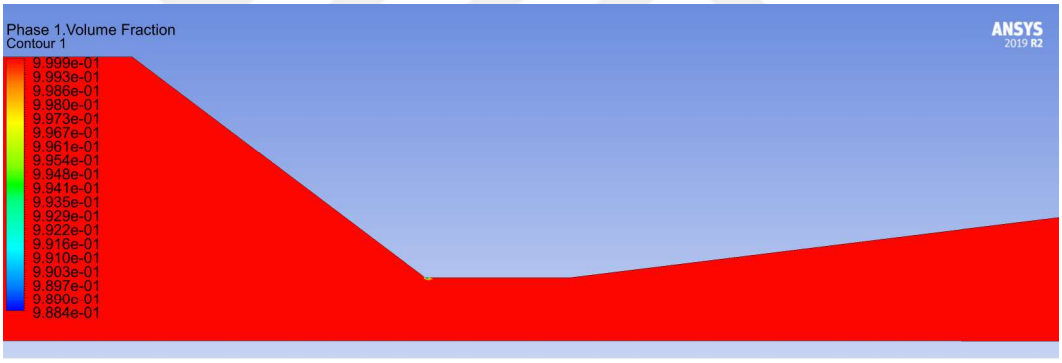

(a)

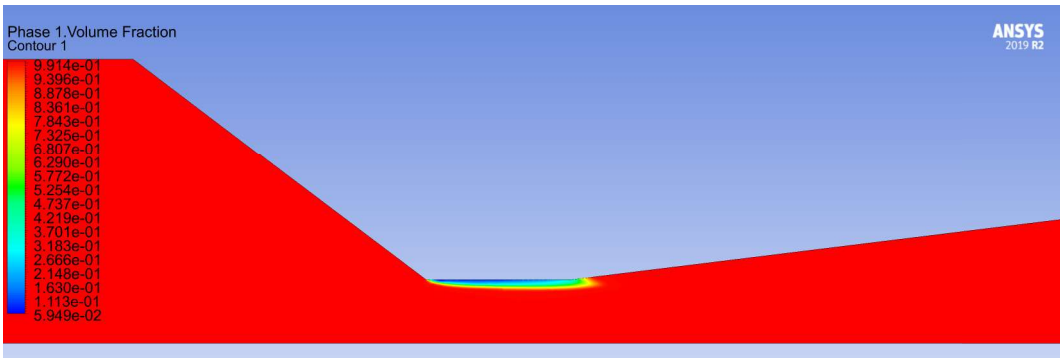

(b)

Figure 4.5. Liquid phase volume fraction contours (a) for 44 bar downstream pressure and (b) for 55 bar downstream pressure.

As can be seen from Figure 4.6, CFD results coincides with the results of Kang et. al.. Around 4.1 kg/s mass flow rate for the LOX cavitating venturi and around 1.2 kg/s mass flow rate for the kerosene cavitating venturi are achieved at 64.5 bar upstream pressure for the cavitating modes of the venturies. There is small difference between the results in the non-cavitating mode, P_{ratio} below 0.85, but the pressure ratio where the cavitating mode starts and the mass flow rate at the cavitating mode are almost the same. In summary, a CFD benchmark study is done and it is found that results are satisfactory. These CFD model is used for the sizing of the future venturi designs.

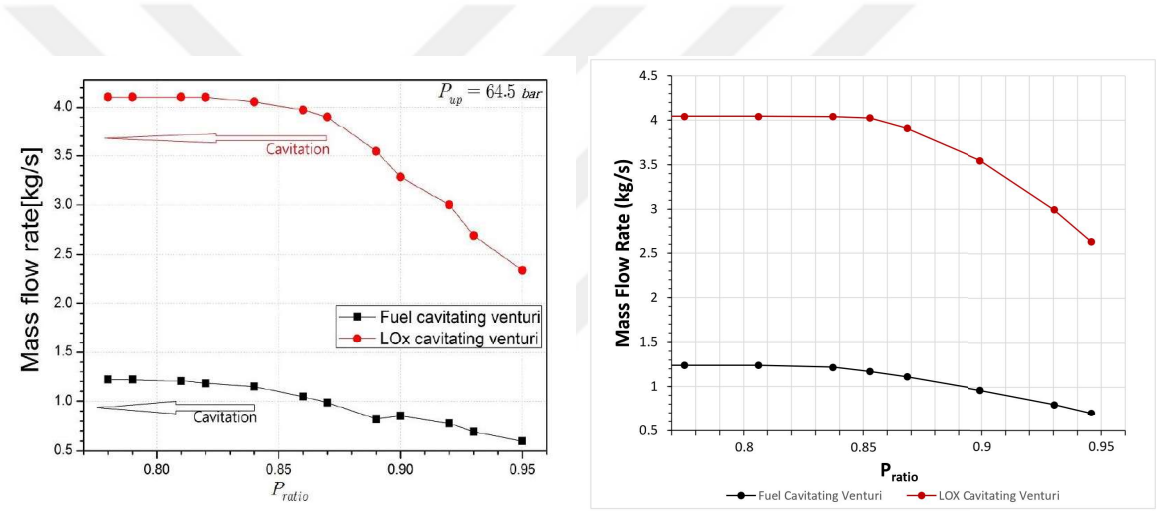

(a) (b)

Figure 4.6. Results of the benchmark study. (a) shows the results of Kang et. al. [24] and (b) shows the results of CFD analysis conducted for benchmark study.

4.3.1.2. Sizing of the venturies. CFD analyses are conducted with ANSYS Fluent to be able to observe cavitating ventury behaviour under different working conditions. Analyses are conducted for different upstream pressures, pressure ratios and throat areas. Critical pressure ratio and mass flow rate-upstream pressure relationships are derived from these results.

After the benchmark study is done, analyses are made with kerosene, LOX and water for different working conditions. First cavitating venturies are designed for

kerosene and LOX because kerosene was used as the fuel in the initial design of the BUSTLab V1 rocket engine. A LOX cavitating venturi is designed for the same mass flow rate of the GOX in case LOX is used instead of GOX. These venturies are manufactured and used to test the venturies experimentally and to compare the results with the CFD data. Water is also used in the analyses because testing the venturies with water is so much easier than testing with LOX and less costly than using kerosene. Results of the water CFD analyses are compared with the water tests of the venturies.

Design that was used in the benchmark study is scaled to required size to achieve desired mass flow rates. Fuel cavitating venturi (FCV-V0) is designed for 1.06 kg/s kerosene mass flow rate at 100 bar upstream pressure and oxidizer cavitating venturi (OCV-V0) is designed for 2.39 kg/s LOX mass flow rate at 70 bar upstream pressure.

70 bar upstream pressure for the LOX venturi was chosen wrongly because of a calculation error but cavitating venturi was already manufactured when this mistake was noticed. These cavitating venturies used to validate the CFD results with the experimental tests. In order to be able to conduct experimental tests with water and compare the results with CFD, CFD analyses are conducted for water instead of kerosene and LOX as well. CFD results for initial designs at different pressure levels are given in Figure 4.7 and Figure 4.8. "Kerosen" and "LOX" lines show results for kerosene flow in fuel venturi and LOX flow in oxidizer venturi, respectively. "Water in Kerosene CV" shows results for water flow in fuel venturi. 5 bar and 30 bar are chosen for the tests but 30 bar could not be achieved with the available pressurization system at the time of tests.

The first important result of the CFD analysis is the pressure ratio where the cavitating mode starts. As can be seen from Figure 4.7 and Figure 4.8, the critical pressure ratio is about 0.8 and it is almost independent from the substance. Also, mass flow rate of the water is slightly higher than the kerosene in the fuel venturi for the same upstream and downstream pressures. Mass flow rate increases with increasing upstream pressure as expected. Figure 4.9 shows the change of mass flow rate through

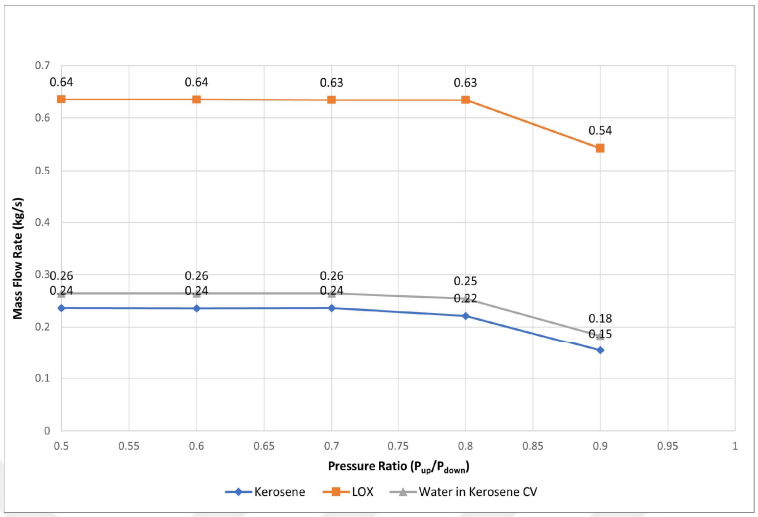

Figure 4.7. CFD results for 5 bar upstream pressure.

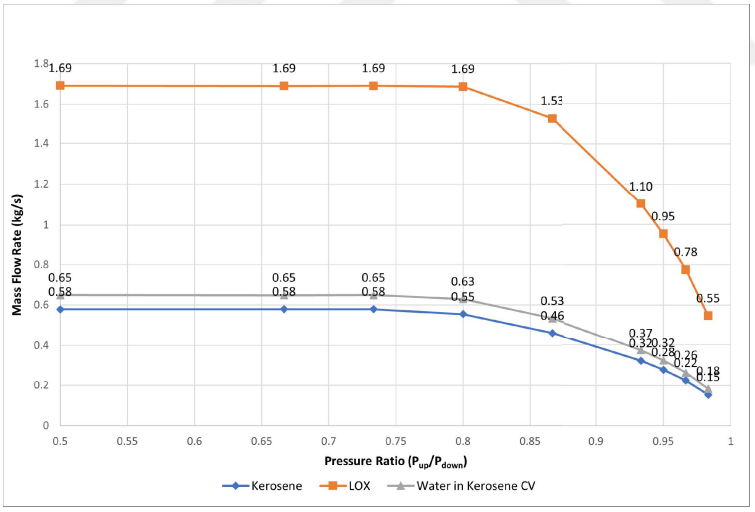

Figure 4.8. CFD results for 30 bar upstream pressure.

the cavitating venturies with changing upstream pressure. As stated before, "Kerosene" and "Water in Kerosene CV" lines are for kerosene and water flow through fuel venturi, respectively. "LOX" line is for LOX flow through the oxidizer venturi.

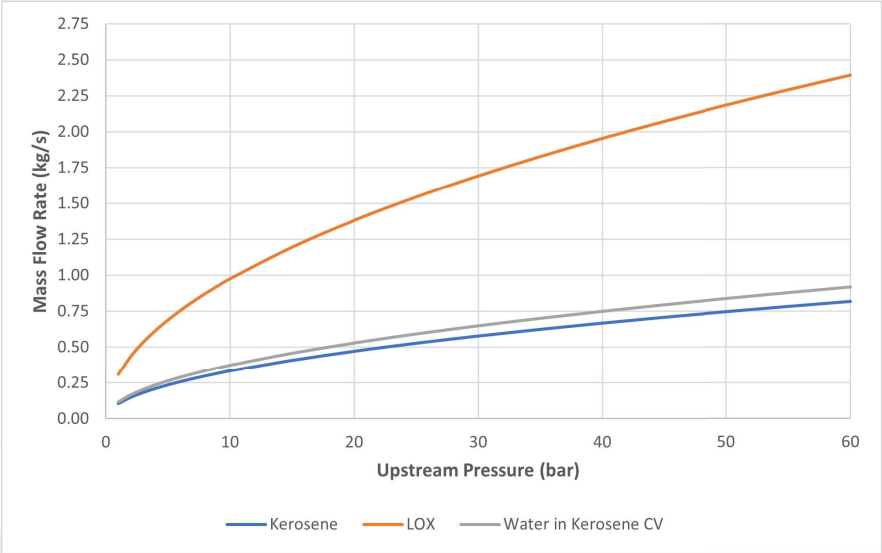

Figure 4.9. Change of mass flow rate for different upstream pressures in cavitating mode.

Figure 4.9 is created using different upstream pressures to check if C_d changes significantly with the upstream pressure. It is seen that C_d almost does not change with the upstream pressure and the expected results from Equation 4.2 are obtained. In Equation 4.2, P_{vap} is significantly smaller than P_{up} for all of the substances and C_d does not change notably with the upstream pressure. Therefore, it can be said that mass flow rate for a given substance is almost proportional to the square root of the upstream pressure.

Cavitating venturi will be used to control the mass flow rate that goes into the combustion chamber of the rocket engine. Therefore, its behaviour under different conditions should be well characterized. After sizing and designing the cavitating venturi with analytical calculations with the help of available literature, CFD analyses are conducted to verify the design and final modifications are made. These results are compared with the experimental test results after manufacturing the venturies. A turbine mass flow meter is used to measure the mass flow rate. However, data from the turbine mass flow meter has some noise. Therefore, moving average method is used

to reduce the noise for the tests. Average of specified number of data is taken in this method. When new data is measured, the first data is removed and the last data is added to the data set in which the average is taken.

The cavitating venturi test system consists of a pressurized water tank, a pneumatic ball valve, a turbine flow meter, a cavitating venturi and two pressure sensors. The manual ball valve is placed downstream of the cavitating venturi to control the downstream pressure by changing the opening of the ball valve. One of the pressure sensors is placed before the cavitating venturi. The second pressure sensor is placed after the cavitating venturi and before the manual ball valve.

Upstream pressure of the cavitating venturi cannot be actively controlled since the pressure in the pressurized water tank cannot be actively controlled. Pressure in the tank decreases slowly during the test because we cannot supply enough gas to the tank. This problem is solved with a bang bang control for the actual engine tests which will be explained in detail in Section 4.4.

If there was no manual ball valve after the venturi, downstream pressure of the venturi would be at the atmospheric pressure, around 1 bar. So, pressure ratio would stay almost constant during the test and it would be too low to observe the non-cavitating case because cavitation occurs when the pressure ratio is above 0.6-0.8. Manuel ball valve is used to control the downstream pressure of the cavitating venturi. In this way, pressure ratio between the two sides of the cavitating venturi can be controlled manually, and both cavitating and non-cavitating modes of the venturi can be observed.

As mentioned, mass flow rate is proportional to the square root of the upstream pressure in the cavitating mode. It is not so easy to achieve the same upstream pressure with the CFD analyses in the test because there is not an active pressure controller in the test system and the pressure drops when the test is started. Therefore, initial tank pressure should be determined by trial and error.

Figure 4.10 shows the water test results of FCV-V0. Upstream pressure is 9 bar at the beginning of the test but decreases significantly when the test starts. The reason is pressure regulator cannot supply enough pressurizer gas to the water tank. However, upstream pressure is almost constant at 6.4 bar between the 102th and 115th seconds. Pressure ratio changes from 0.2 to 0.88 during this period. So, both modes of the cavitating venturi can be observed in this section of the test.

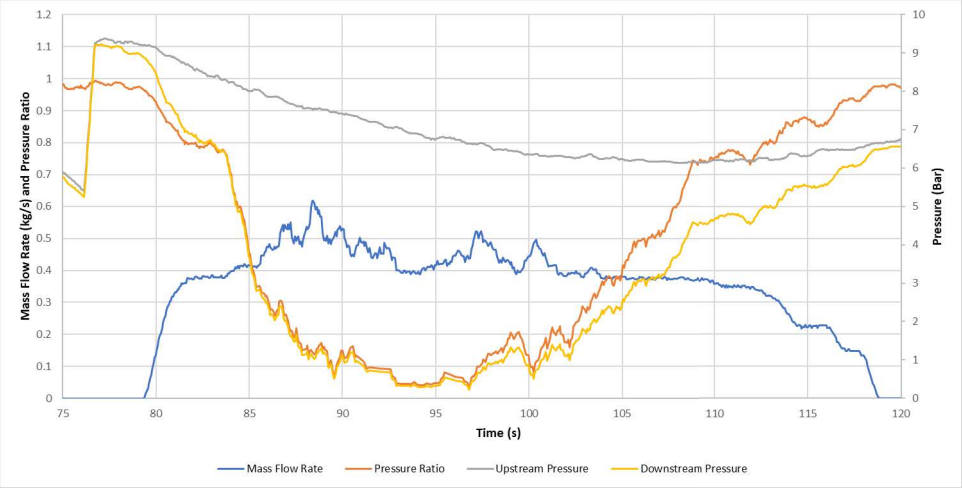

Figure 4.10. Test results of the fuel cavitating venturi FCV-V0 for the upstream pressure of 6 to 9 bar.

Mass flow rate stays constant at 0.38 kg/s at 6.20 bar upstream pressure until pressure ratio reaches 0.76. After that point, mass flow rate starts decreasing with the increasing pressure ratio even if the upstream pressure is constant. It shows that the critical pressure ratio is 0.76 for FCV-V0. However, mass flow rate at cavitating mode is higher than the expected at 6.2 bar. Mass flow rate for 6.2 bar upstream pressure is 0.29 kg/s in CFD results whereas measured mass flow rate is 0.38 kg/s which is %31 higher than the expected. Further investigation of the venturi showed that throat diameter is larger than the design value.

Oxidizer cavitating venturi, OCV-V0, is designed for 2.39 kg/s LOX mass flow rate at 70 bar upstream pressure. It is tested after the tests of FCV-V0. Results of

water test for 4 to 7 bar upstream pressure, OCV-V0 - Test 1, are given in Figure 4.11. Another water test for OCV-V0, OCV-V0 - Test 2 (Figure A.1), is given in APPENDIX A.1.

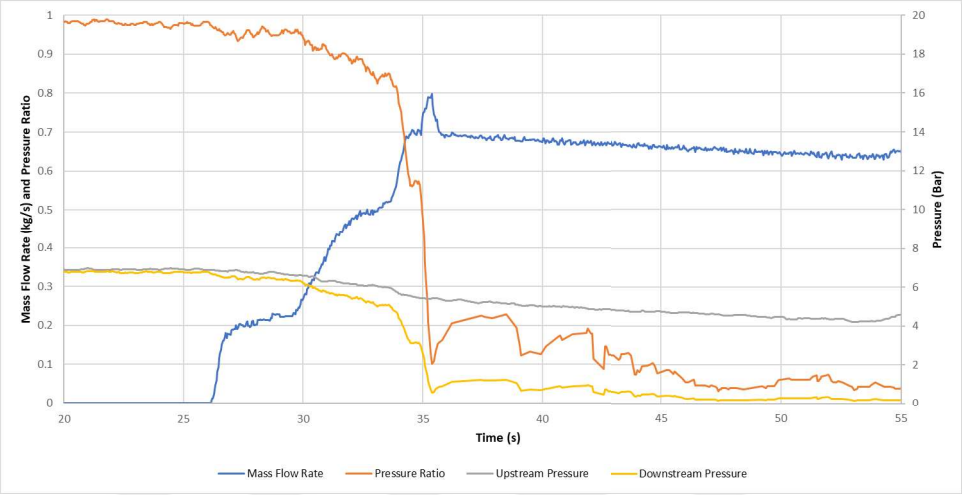

Figure 4.11. Water test results of the oxidizer cavitating venturi OCV-V0 for the upstream pressure of 4 to 7 bar (OCV-V0 - Test 1).

Upstream pressure is set to 7 bar in the "OCV-V1 - Test 1" before the test which can be seen in Figure 4.11. It changes from 7 bar to 4.25 bar during the test. Mass flow rate decreases from 0.7 kg/s to 0.64 kg/s during the test between 36th and 55th seconds. Also, it can be observed from the graph that cavitating mode starts when the pressure ratio reaches 0.7 and mass flow rate is 0.64 kg/s at 4.25 bar upstream pressure. CFD analysis gives 0.60 kg/s mass flow rate for 4.25 bar upstream pressure.

Change of the mass flow rate with respect to the pressure ratio for 4.25 bar upstream pressure is given in Figure 4.12. This figure is created using the data of OCV-V0 - Test 1 in Figure 4.11. As can be seen in Figure 4.12, it can be said that critical pressure ratio is around 0.7. Mass flow rate starts decreasing for the same upstream pressure after this point.

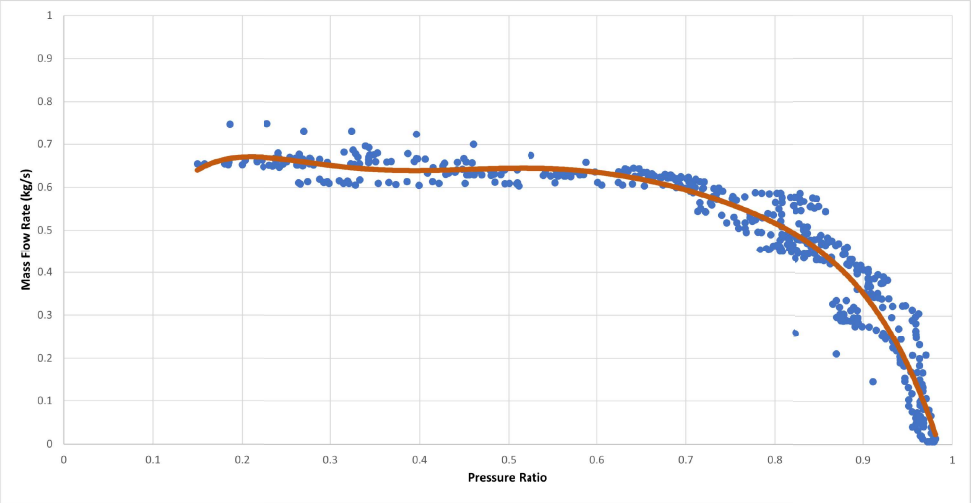

Figure 4.12. Change of mass flow rate with the pressure ratio for OCV-V0 - Test 1.

Summary of the designs and the test results of FCV-V0 and OCV-V0 are given in Table 4.1. "Designed $\dot{m}_{water}$" and "Measured $\dot{m}_{water}$" columns represent the results of the CFD analyses and the experimental tests for the given upstream pressures, respectively. The upstream pressure and the mass flow rate that will be used for the actual working conditions may be different from the tested conditions in Table 4.1. Water tests are conducted with the available pressurization system at the time venturies are manufactured and actual working conditions could not be achieved with the available water test setup.

Table 4.1 shows that designed mass flow rate is almost the same as the measured mass flow rate for OCV-V0 but measured mass flow rate for FCV-V0 is significantly higher than the design value. As mentioned, it is noticed that the difference between the designed and measured mass flow rate is caused from the manufacturing error at the throat of the FCV-V0. Test results of the FCV-V0 and OCV-V0 are used to design new venturies to be used for ethanol/LOX propellant combination. FCV-V1 and OCV-V1 are designed so that 1.01 kg/s ethanol mass flow rate and 1.26 kg/s LOX mass flow rate can be achieved with 80 bar upstream pressure.

Table 4.1. Test results for the cavitating venturies FCV-V0 and OCV-V0.

Venturi Type	**Throat Diameter (mm)**	**Test Upstream Pressure (bar)**	**Designed $\dot{m}_{water}$ (kg/s)**	**Measured $\dot{m}_{water}$ (kg/s)**
FCV-V0	3.52	6.20	0.29	0.38
OCV-V0	5.6	4.25	0.60	0.64

Results of the water test for FCV-V1 is given in Figure 4.13. 24 to 28.5 bar upstream pressure is used in this test. Water tank pressure is set to 28.5 bar, initially. Upstream pressure decreases from 28.5 bar to 24.5 bar gradually when the test starts. Cavitating mode can be observed between 95th and 103th seconds where the pressure ratio is below 0.1. Mass flow rate is measured as 0.59 kg/s for 24.5 bar upstream pressure. There are some errors in the mass flow rate measurements where the downstream ball valve is gradually opened before 95th second and gradually closed after 103th second. Mass flow rate spikes during these periods can be seen in Figure 4.13. Also, a whizzling sound was coming from the cavitating venturi during this period of the test. It is guessed that partial opening of the manual ball valve causes a distortion in the flow and causes a measurement error in the turbine flow meter.

Results of another two water tests for FCV-V1 are given in APPENDIX A.2. Data between the 41th and 70th seconds in Figure A.2 can be used to generate a pressure ratio vs. mass flow rate graph because upstream pressure is almost constant at 14 bar during this period. Resulting graph can be seen in Figure 4.14. The results of the CFD analysis for mass flow rate at 14 bar upstream pressure is also shown in Figure 4.14 with a grey line. Water test results agrees with the CFD analysis results for cavitating mode. However, critical pressure ratio is 0.8 in CFD analyses but it is around 0.7 in the experimental data.

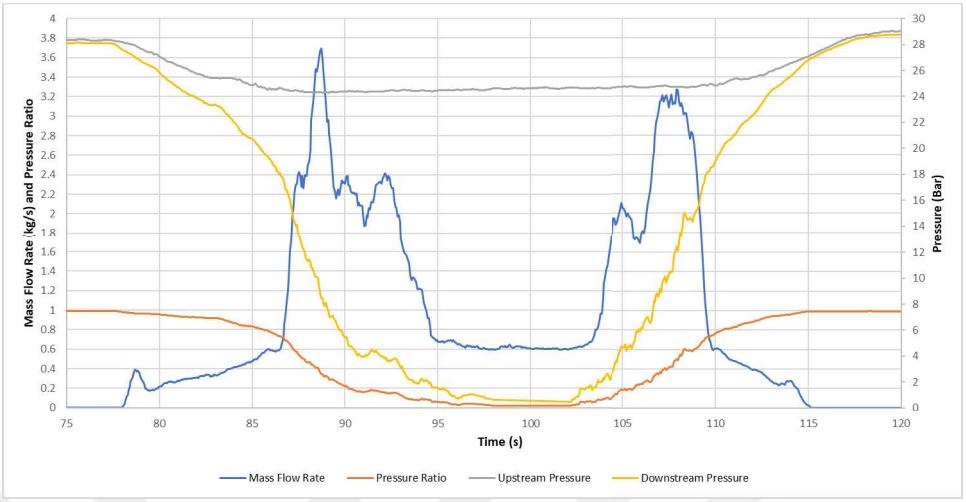

Figure 4.13. Test results of the fuel cavitating venturi FCV-V1 for the upstream pressure of 24.5 bar (FCV-V1 - Test 1).

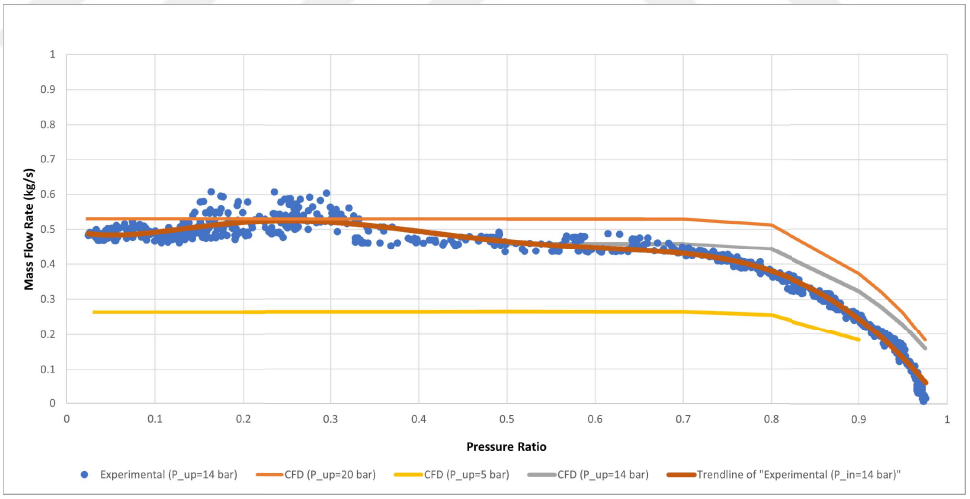

Figure 4.14. Change of mass flow rate with respect to pressure ratio for FCV-V1 at 14 bar upstream pressure.

OCV-V1 water test is conducted with 80 bar upstream pressure. A new pressurization system was set up before the OCV-V1 water test and this pressurization system made it possible to test OCV-V1 at 80 bar upstream pressure. However, there was a problem with the turbine flow meter and mass flow rate is calculated using the change

of the water tank mass. Mass flow rate through OCV-V1 is measured as 1.08 kg/s for 80 bar upstream pressure during the 15 seconds test.

Table 4.2. Test results for the cavitating venturies FCV-V1 and OCV-V1.

Venturi Type	**Throat Diameter (mm)**	**Test Upstream Pressure (bar)**	**Designed $\dot{m}_{water}$ (kg/s)**	**Measured $\dot{m}_{water}$ (kg/s)**
FCV-V1	3.52	24.5	0.59	0.60
OCV-V1	3.72	80.0	1.18	1.08

Summary of the test results for FCV-V1 and OCV-V1 are given in Table 4.2. In conclusion, results of the CFD analyses coincide with the water tests of FCV-V1 and OCV-V1 for different pressure levels. Therefore, venturies can be used for cold flow tests with the actual propellants. It can be said that CFD analyses give satisfactory results and designed mass flow rates could be achieved in water tests with FCV-V1 and OCV-V1. Tests of the venturies with ethanol and LOX are also conducted and results of these tests are discussed in Section 7.2.

4.3.2. Manufacturing

At first, FCV-V0 and OCV-V0 are designed and they are manufactured. These cavitating venturies are used just to justify analytical calculations and CFD results. Water tests of FCV-V0 and further visual investigation showed that there was a manufacturing error at the throat of FCV-V0 and it was manufactured to be larger than the design. FCV-V1 and OCV-V1 are manufactured after the tests of FCV-V0 and OCV-V0. In OCV-V1, surface finish of the converging section was too rough. However, it did not show any significant negative effect in the water tests and the results were as expected.

All of the cavitating venturies are made of stainless steel since it has low cost and it is easy to machine. Converging and diverging sections of the venturies are manufactured by wire erosion. Only exception is the OCV-V1. Its converging and diverging sections are machined by a CNC lathe and its surface is more rough compared to wire erosion. 3/4" NPT threads are opened to the two sides of the cavitating venturies by CNC machining. There were some defects at the NPT threads of the venturies FCV-V1 and OCV-V1. However, tests showed that they do not have a leakage problem. Technical drawings of FCV-V1 and OCV-V1 are given in APPENDIX B.1 and B.2.

4.4. Pressure Control

Mass flow rates of the fuel and the oxidizer in the system are controlled directly by the tank pressures. Therefore, tank pressure should be determined carefully and should be maintained at the same level during the test. There are different approaches for the pressure control.

Blowdown system can be used for the simplest control. The ullage volume of the propellant tanks are filled with a high pressure gas and the pressure in the tank decreases during the test. Pressure decrease during the test depends on the ullage volume and the test duration. Bigger ullage volume can be used for lower pressure decrease but this results in lower test time because of the limited propellant mass for the same total tank volume. Also, mass flow rates of the propellants decrease during the test because of the decrease in the tank pressures.

Propellant tanks can be pressurised by another high pressure gas system (HPGS) during the test. High pressure gas supply can be controlled actively or exit pressure of the high pressure gas supply can be pre-determined by a pressure regulating valve.

A standard spring-loaded pressure regulating valve can be set to desired tank pressure before the test and tanks can be pressurized to the desired pressure level. However, set pressure cannot be maintained when the test starts with the standard

pressure regulating valves and tank pressure decreases up to a certain pressure level and stays at that level as long as the high pressure gas supply pressure does not change significantly. Pressure regulator can be set to a higher level than the desired pressure before the test and desired tank pressure can be achieved when the test starts. Pressure regulator set pressure can be determined by trial and error. Difference between the set pressure and the achieved pressure when the test starts can be decreased by using a valve with a higher flow coefficient (C_v) value. However, HPGS pressure may decrease significantly when the test duration is long.

Another way of maintaining a constant tank pressure or controlling it during the test is using an actively controlled pressure regulating valve. This valve may consist of a dome type pressure regulator and an electropneumatic actuator like TESCOM ER5000. This actuator uses a PID control to maintain set pressure even if the flow conditions change. This method needs a proper selection of the dome pressure regulator for the desired flow rates. TESCOM ER5000 is used to control the cooling water tank pressure during the test. Even if it can be actively controlled and tank pressure can be changed remotely, it is used just to keep constant water tank pressure with changing HPGS pressure.

A simpler and less costly way of an active pressure control is a bang-bang control. HPGS is connected to the propellant tank by a remotely controlled on/off or adjustable valve. Valve is controlled by a algorithm that opens the valve when the tank pressure decreases below to a certain level and closes when a certain pressure level is achieved. Pressure can be controlled more smoothly by using an adjustable valve. Valve can be opened and closed gradually with the magnitude of difference of pressure between the actual and the desired pressure. Also, a depressurizer valve can be added to the system to lower the tank pressure if pressure reaches to a critical level because of the self-pressurization of the cryogenic liquid, if the tank pressure is desired to be lowered during the test or in an emergency situation. Bang-bang control is used for propellant tank pressurization at the BUSTLab V1 cold flow tests, the open fire tests and the complete thrust chamber firing test because of its low cost and it is easier to implement

to the system. On/off valves are used in the system and they resulted in small pressure fluctuations, pressure peaks when the valve is opened, and quite powerful tank wobbles.

5. TEST SETUP

The final test setup consists of five sub-systems: high pressure gas system (HPGS) which consist of two sets of 15 pieces pressurized nitrogen cylinders and 2 pressurized nitrogen cylinders that are used for purge and pneumatic system; control table where most of the pipes, most of the valves, cavitating venturies, bang bang control and NI controllers are placed; fuel and oxidizer tanks which are placed on load cell structures; cooling water system; engine and thrust stand. Each of the sub-systems are explained in detail in the following sections.

5.1. High Pressure Gas System

Each of the propellant tanks are pressurized by separate high pressure nitrogen bundles. Each bundle consists of 15 nitrogen cylinders at 235 bar. There are two outlets on each bundle which are parallel connected. Only one of them is used in the tests. A pressure regulator is placed at the exit of the bundle to reduce the pressure to 150 bar for the bang bang control system. Nitrogen bundles are connected to the bang bang control system on the control table by flexible high pressure hoses.

A single pressurized nitrogen cylinder is used for the purge line. Another pressurized nitrogen cylinder is used to pressurize some of the pneumatic controllers. Cryogenic pneumatic controlled ball valves needed higher pneumatic supply pressure than standard ball valves for smooth operation. Therefore, these pneumatic valves are pressurized by an external pressurized nitrogen cylinder. Standard pneumatic valves are pressurized by a compressor which can supply 6 bar.

5.2. Control Table

A control table is built by aluminum profiles. Top surface and one of the side surface are covered with MDF boards to be able to fix pipes, valves and other parts.

Cavitating venturies, turbine flow meter, bang bang pressure control valves, NI multi-function DAQ devices and electronic control card are mounted on the MDF boards. Later on, these boards are changed with steel plates to enhance the durability of the control table. Bang bang pressure control is placed on the top surface. NI DAQ devices and electronic control card are mounted on the thrust stand side of the top surface. Cavitating venturies, pressure sensors before and after the cavitating venturies and turbine flow meter are mounted on the side of the control table. Control table has four wheels to be able to be transferred easily. Wheels are locked with brake before the tests.

5.3. Propellant Tank Systems

Since there is no cryogenic flow meter in the system and turbine flow meter that is used for measuring the fuel mass flow rate may give erroneous measurements sometimes, mass of the propellant tanks are recorded using load cells to calculate the mass flow rate using the change of the masses of the tanks. Each of the propellant tanks are placed on industrial weighing scales. These scales do not have mounted screens where the mass of the tanks can be read. Instead, there are analog outputs directly from the load cells. These output signals are amplified by commercially available load cell amplifiers because raw output signal is too low, in mV range, to be measured by NI USB 6008. Mass data is recorded during the test and mass flow rate can be calculated using time vs. tank mass data when turbine flow meter does not work.

An analog pressure gauge and a pressure sensor are connected on the one of the ports on the top side of the oxidizer tank. A relief valve and a manual ball valve are placed on the second outlet line on the top side of the tank. Relief valve is set to 85 bar and manual valve is used to depressurize the tank manually. This line is used also for pressurization and filling of the tank. There is another port at the bottom side of the tank. A manual cryogenic globe valve and a pneumatic controlled cryogenic ball valve are placed on this port. This line is used for oxidizer flow to the engine.

There are 5 ports on the top side and 1 port on the bottom side of the fuel tank. A analog pressure guide is mounted on the one port, a pressure sensor is mounted on second port and relief valve which is set to 85 bar is mounted on the third port on the top side. Fourth port is used for filling the tank with fuel and the last one on the top side is used for pressurization. The one on the bottom side is used for fuel flow. There is a manual ball valve and pneumatic controlled ball valve is connected to the bottom line. Bottom ports of both of the tanks are connected to the pipelines on the control table.

5.4. Cooling Water System

As mentioned before, engine is cooled by an external water supply. This system consists of a pressurized nitrogen cylinder for pressurization of the water, a water tank made of steel and TESCOM ER5000 pressure regulator which is an active pressure controller. TESCOM ER5000 is used to keep water tank pressure at 15 bar (which is 1 bar below the maximum operational pressure of the tank) even if the pressure on the pressurized nitrogen cylinder changes. It is an actively controlled pressure regulator. Desired pressure is set on a computer program and it uses a PID controller to keep outlet pressure at desired level regardless from the inlet pressure.

A commercially available pressurized air tank is used as the water tank. It is not made of stainless material but since it will be used for short time, it can be said that oxidation would not be a problem for that short of a time period. Mass flow rate of the cooling water is directly determined by the water tank pressure. Therefore, tank is used at its maximum operational pressure to obtain highest mass flow rate that can be achieved. A relief valve that is set to 16 bar is used to guarantee that maximum operational pressure is not exceeded. Exit port at the bottom side of the tank is connected to the inlet of the cooling channel in the engine by a flexible hose.

5.5. Engine and Thrust Stand

Engine is mounted on the thrust stand by a rail system to be able to measure thrust during the test. Engine can slide freely on the rails when the load cell is not connected. An S-type load cell is connected to the engine by a load plate structure. Thrust stand is manufactured by square steel profiles. Stand is fixed on the concrete floor by four sleeve anchor bolts. Thrust load cell gives an analog voltage output which needs to be amplified by a commercial load cell amplifier to be measured by National NI USB 6008 DAQ device.

Thruster is connected to the propellant feed lines on the control table by high pressure flexible hoses. There are pneumatic controlled ball valves that are acting as main valves just before the fuel and oxidizer dome inlets. There are by-pass lines just before these main valves. LOX by-pass line is used to cool the LOX feed system before the firing. Fuel by-pass line is used to fill the fuel line with ethanol and vent the air in the line before the firing. Purge line in connected to the fuel line just after the fuel main valve. Test stand and load cell connection can be seen in Figure 5.1. Main fuel valve, main oxidizer valve, fuel bleed valve and oxidizer bleed valve are also also presented in this figure.

5.6. Flow Diagram

Schematic of all the fluid systems can be seen in Figure 5.2.There are two nitrogen bundles consists of 15 tanks cylinders each. Nitrogen tanks are at 235 bar initially. They are connected parallel to each other in this bundle and there are two exit ports. Only one exit port is used in the tests. There is a 235 bar to 150-0 bar pressure regulator connected to the exit port of the bundle. This pressure regulator is used to reduce the pressure that can be used for bang bang control. If the pressure in the bang bang control valve is above 150 bar, there might be leakages at the ball valves. Bang bang control valves are placed on the control table.

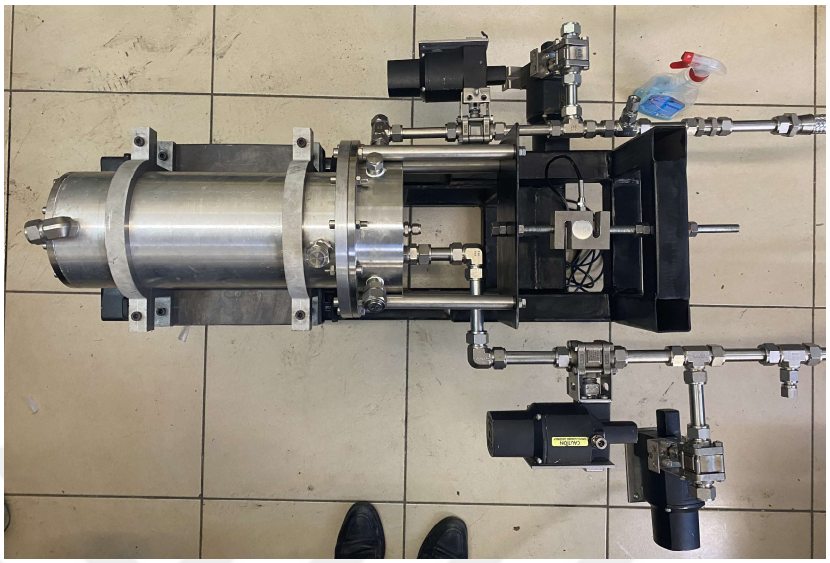

(a)

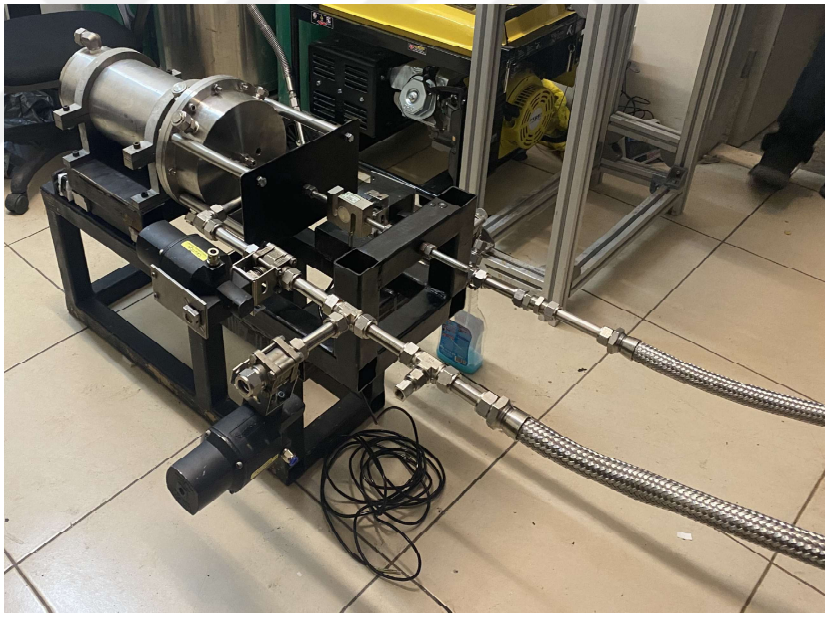

(b)

Figure 5.1. Test stand and load cell connection from (a) upper view and (b) side view.

All of the pneumatic valves, except cryogenic valves, are pressurized by an external compressor which can supply 8 bar pressure. Bang bang control valves are connected to one port of the compressor and the rest of the valves are connected to the second port of the compressor. Otherwise, sudden changes in the pressurizer line

due to the continuous working of the bang bang control valves may effect other valves, too. Cryogenic valves are pressurized by an external nitrogen cylinder because they need higher pressure than the standard ball valves to work smoothly.

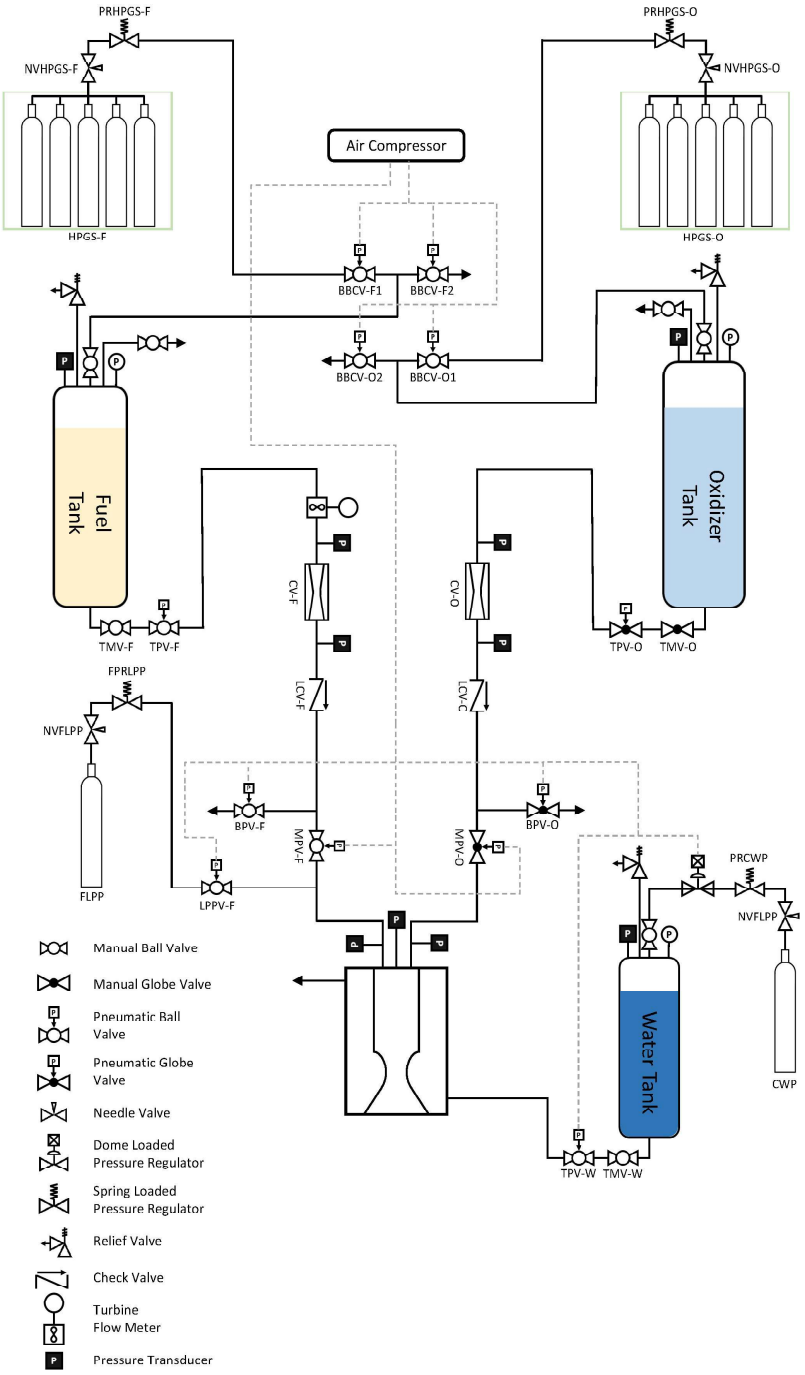

Figure 5.2. Diagram of the propellant feed systems and the cooling water system.

As mentioned before, pressure in the fuel and oxidizer tanks are controlled by bang bang control valves; BBCV-F1, BBCV-F2, BBCV-O1, BBCV-O2. There are two pneumatic ball valves for each line in the bang bang control system. First valve, BBCV-F1 or BBCV-O1, is used for pressurization. When it is opened, pressurizer gas flows into the tank. Second valve, BBCV-F2 or BBCV-O2, is used for depressurization. If the first valve is closed and the second valve is opened, tank pressure drops very quickly. It can be used for full depressurization in an emergency situation or for small pressure adjustments.

There is a manual ball valve (TMV-F) and pneumatic ball valve (TPV-F) at the exit of the fuel tank. Manuel valve is placed for safety before the test and to fully close the fuel tank when it is not used for a long time. After the pneumatic ball valve (TPV-F), fuel line is connected to the control table by a flexible hose. There is a turbine flow meter at the beginning of the fuel line on the control table. Turbine flow meter had some electronic connection problems and sometimes, it was not working properly. Fuel enters the cavitating venturi (CV-F) after the turbine flow meter. There are two pressure sensors before and after the cavitating venturi. These pressure sensors are used to measure pressure ratio at the cavitating venturi. A check valve (LCV-F) is placed at the end of the fuel line on the control table. It is used to prevent flow in the reverse direction in case any problem occurs in the engine. Reverse flow is harmful for the turbine flow meter. Also, there might be hot gas flowing to the fuel tank which is very dangerous.

Fuel main pneumatic valve, MPV-F, and fuel pneumatic bleed valve, BPV-F, are placed between the control table and the engine. MPV-F is used as a main valve during the tests. BPV-F is used to discharge the air inside the fuel line and fill the line with fuel before the tests. In this way, fuel is injected into the injector almost immediately when the main valve is opened without any delay caused from the filling of the lines.

A pressurized nitrogen cylinder (FLPP) is used to purge the fuel line (after the MPV-F) at the end of the tests or in an emergency situation. Its exit pressure is set

to 60 bar, which is higher than the fuel dome pressure. When the fuel line purge valve (LPPV-F) is opened, excess fuel in the fuel dome and injector is injected rapidly through the injector and combustion is ended. MPV-F is closed before opening the LPPV-F to prevent fuel flow in the reverse direction in the fuel line. Also, LCV-F works as a back-up safety device which prevents reverse flow in case LPPV-F is opened without closing MPV-F. Fuel directly goes into the fuel dome after the MPV-F.

Standard valves may have problems with cryogenic fluid. Therefore, standard ball valves are used in all of the fuel lines but cryogenic valves are used at critical points in oxidizer line. A manual cryogenic globe valve and after that, a pneumatic cryogenic ball valve are placed at the exit of the oxidizer tank. These are chosen as cryogenic valves because these are the two valves that are exposed to cryogenic fluid the most.

Oxidizer goes into the line of control table through a flexible hose after the oxidizer tank manual valve (TMV-O) and the oxidizer tank pneumatic valve (TPV-O). There are two pressure sensors at each side of the oxidizer cavitating venturi (CV-O), just like the fuel line. Pressure sensors are placed 25 cm away from the main 3/4" oxidizer line by 1/4" tubes. The reason is, pressure sensors are standard sensors and they cannot be used at cryogenic temperatures. 25 cm 1/4" tube is enough for cryogenic fluid to heat up and prevent damage in the pressure sensor. Cryogenic fluid boils because of high heat transfer at 1/4" stainless steel line and do not directly come in contact with the pressure sensor. Oxidizer line check valve (LCV-O) is placed after the CV-O.

Even if the standard ball valve may have leakage problems with cryogenic fluid, they can be used when they are not exposed to cryogenic fluid for a long time. Not all of the valves in the oxidizer line are cryogenic valves because the cost of the cryogenic valves are significantly higher than the standard valves. Therefore, standard ball valves are used as oxidizer fill valve and oxidizer tank manual depressurization valve.

Oxidizer bleed pneumatic valve (BPV-O) is used to cool the oxidizer line and fill the line with LOX before the test. Otherwise, LOX boils immediately when it gets in contact with room temperature steel pipes at the beginning of the test. Oxidizer directly gets into the oxidizer dome and injector through flexible hose after the MPV-O. Flexible hoses are used to connect lines on the control table to the engine because engine is not fixed and there would be a sliding motion at the engine when the test starts. There is no purge system in the oxidizer line because stopping the fuel flow automatically stops the combustion.

Cooling water system is pressurized by its own nitrogen cylinder, CWP. A 235 bar to 0-40 bar pressure regulator is used before the TESCOM ER5000 to reduce pressure to the working pressure range of TESCOM ER5000. TESCOM ER5000 is used to maintain 15 bar water tank pressure during the test. It actively uses PID control to maintain 15 bar outlet pressure independent from the changing inlet pressure and the gas flow rate. A relief valve is placed on the top side of the water tank and its critical pressure is set to 16 bar because water tank has a 16 bar working pressure limit. Water tank manual valve (TMV-W) and water tank pneumatic valve (TPV-W) are place at the exit of the tank. Exit of the TPV-W is connected to the inlet of the cooling channel on the engine by a flexible hose.

Water temperature in the cooling channel is aimed to be kept below 100°C. Actually, cooling water temperature can be higher than 100°C at a high working pressure. For example, boiling point of the water is 152°C at 5 bar. Outlet water can be discharged directly to the open air far from the engine because water tank capacity is enough for the expected 20 s test duration.

6. COMPONENTS AND MATERIAL SELECTION

In this section, all the components of the liquid rocket engine and their manufacturing processes are investigated. Design choices are explained. Differences between designed and manufactured parts are mentioned. Every part of the engine can be seen in Figure 6.1 which is an exploded CAD view of the engine. Assembled engine can be seen in Figure 6.2.

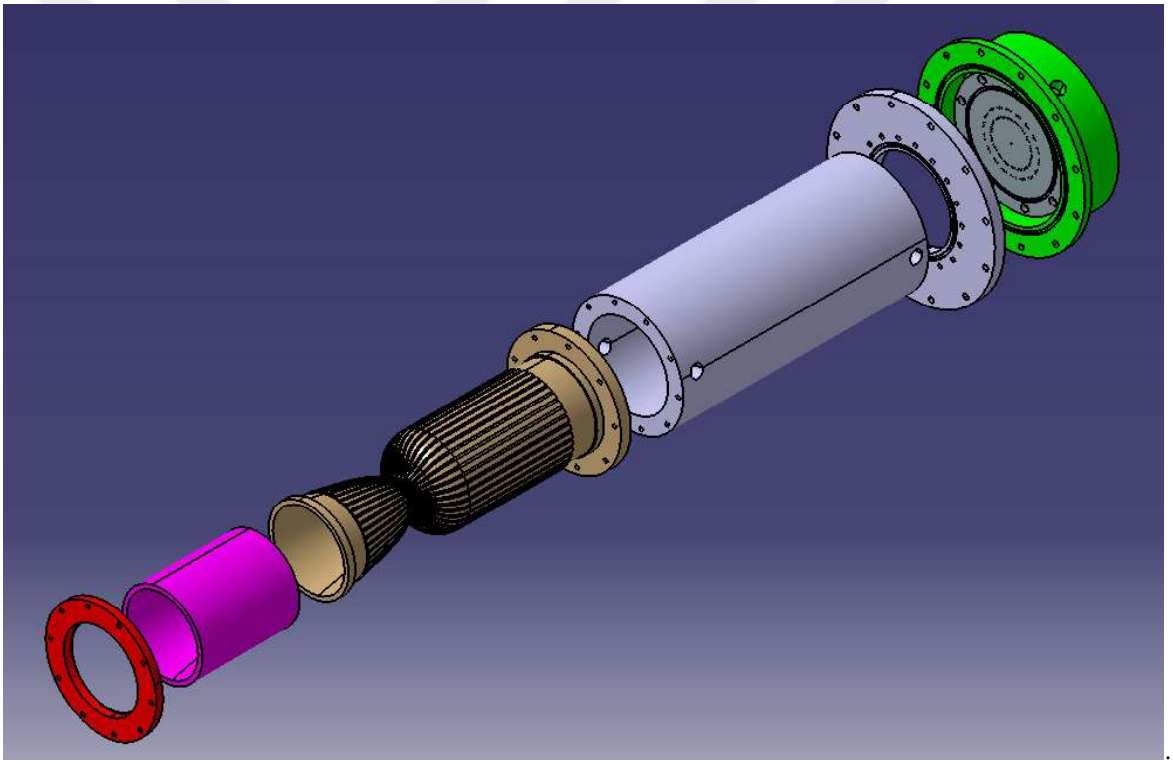

Figure 6.1. Exploded CAD view of the engine.

6.1. Combustion Chamber and Nozzle

Combustion chamber is the part that separates combustion gas from the cooling fluid. It is exposed to the hot gas flow at temperatures as high as 3500 K in BUSTLab V1 engine. It should withstand high temperature and be a good heat conductor for

good cooling. Copper is chosen as combustion chamber material because of its high heat conductivity. It does not have to have very high mechanical strength because jacket surrounds the combustion chamber from all sides and supports the chamber. CAD models of the combustion chamber and cooling channels are given in Figure 6.3.

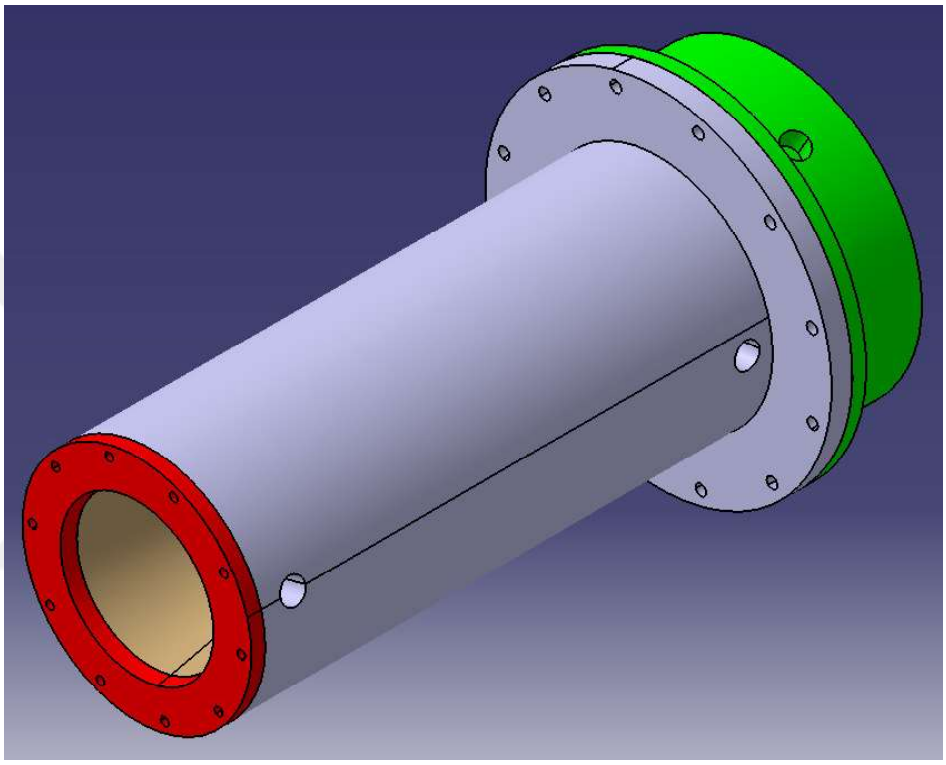

Figure 6.2. Assembled CAD view of the engine.

Combustion chamber is manufactured in two steps from a copper billet; first by a CNC lathe and then by a CNC milling. Contour of the chamber is machined by CNC lathe. Its inner surface is quite wavy because it could not be fixed properly during machining since it has a thin wall and it is quite long and vibration caused a wavy surface finish. Inner profile of the combustion chamber comes from 1D isentropic flow analysis. Wall thickness is 4 mm all over the contour. Thinner wall is better for cooling but it cannot be too thin because it can warp during machining. There is a flange at the one side of the combustion chamber. Combustion chamber is bolted to the jacket part using this flange.

Afterwards, water channels are machined by CNC milling along the contour of the chamber. There are 40 water channels on the outer surface of the combustion chamber surface. Water channel geometry and the size of the channels are investigated in more detail in Section 3.3.4.

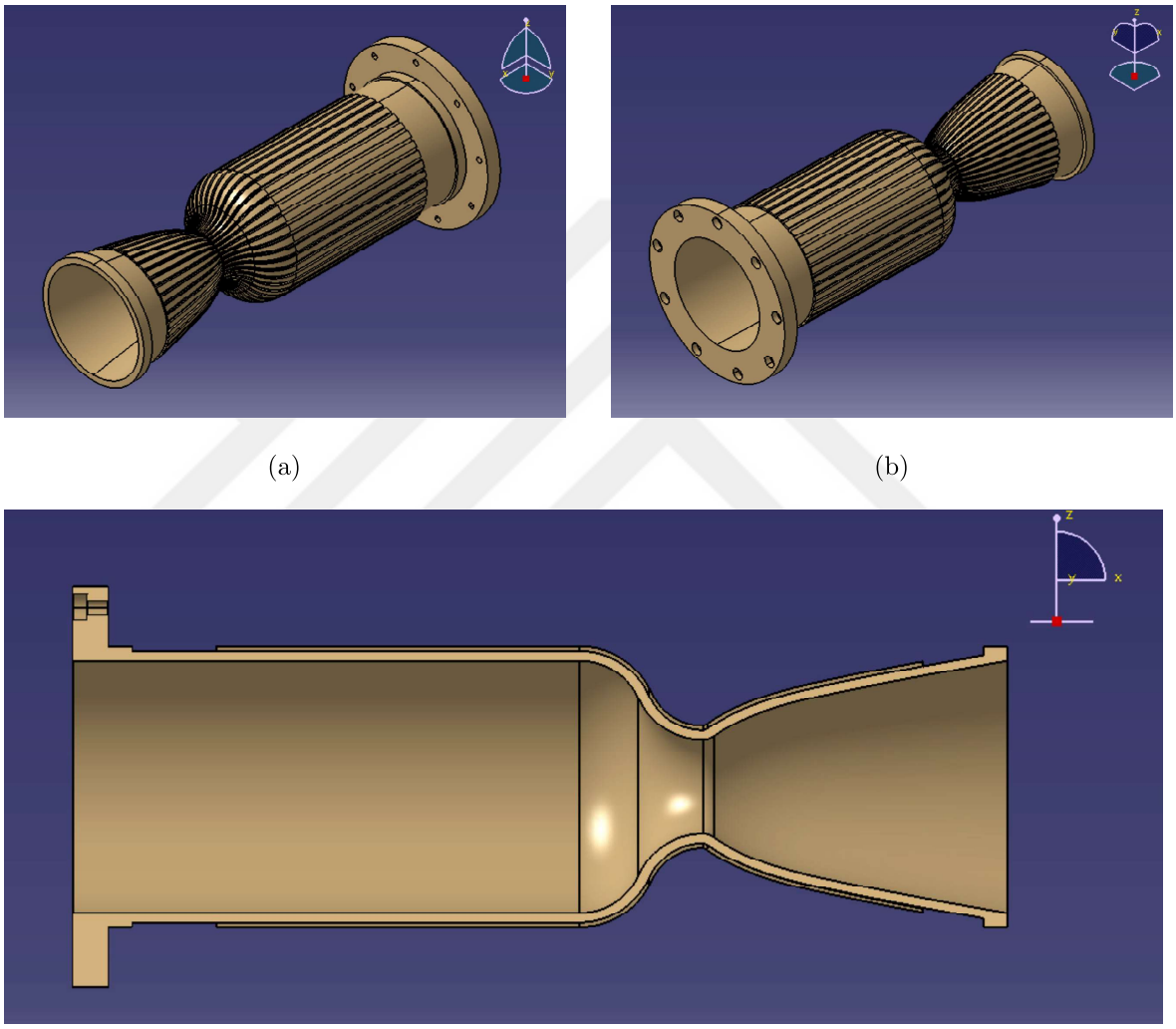

(a) (b)

(c)

Figure 6.3. Designed combustion chamber from (a) front, (b) back and (c) cut views.

In the original CAD model; water channel width was 3 mm, 2.2 mm and 3 mm at the combustion chamber, throat and nozzle sections, respectively. 2.2 mm was chosen as the minimum width to make the manufacturing easier, so that the channels can be milled with a 2 mm milling bit. However, all the channels widths are machined to be

2.2 mm in the manufactured part due to a manufacturing mistake. Effect of this fault is investigated by experimental cooling channels test to decide whether the mass flow rate is sufficient or not.

Copper oxidizes very fast in the ambient air and it gets dark. This is a problem for the heat transfer and it should be cleaned before the firing test. A special chemical solution is used to clean oxidized layer before the firing of the engine.

Manufactured combustion chamber is given in Figure 6.4. Wavy inner surface, oxidized outer and inner surfaces and cooling channels of constant width can be seen from the photograph. Technical drawing of the combustion chamber is given in APPENDIX B.3.



(a) (b)

Figure 6.4. Manufactured combustion chamber showing (a) the side of the chamber and (b) the inner surface of the chamber.

6.2. Injector

Two injectors, Injector V1 and Injector V2, are manufactured. After the water tests of the Injector V1, it was noticed that oxidizer injection area is too large and the desired pressure drop could not be achieved at the injector. Therefore, a new injector (Injector V2) is designed and manufactured.

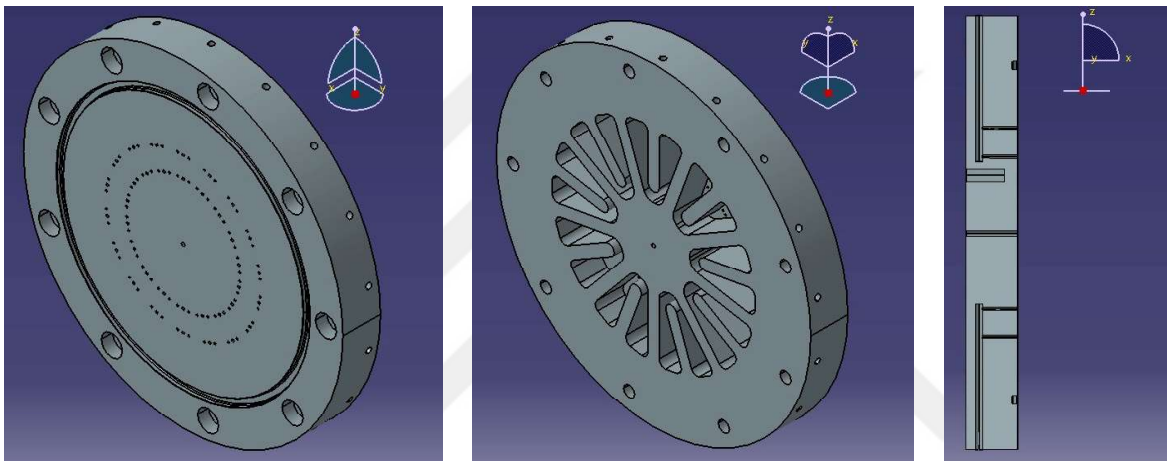

(a) (b) (c)

Figure 6.5. Designed Injector 2 from (a) front, (b) back and (c) cut views.

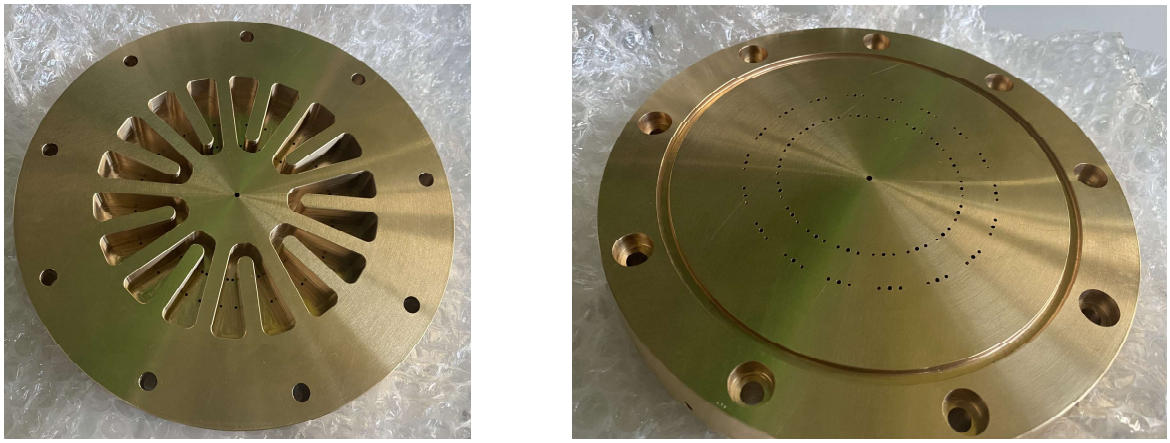

(a) (b)

Figure 6.6. (a) Dome side and (b) chamber side of the manufactured injector.

Final design shown in Figure 6.5 could be manufactured with 3 axes CNC milling machine. There is a o-ring groove at the combustion chamber side of the injector. It squeezes between the injector and combustion chamber to provide sealing between the fuel and the combustion gasses. Injector is made of brass because of its low cost and ease of manufacturing. Manufactured injector can also be seen in Figure 6.6. The hole at the center of the injector is to measure the pressure inside the combustion chamber.

6.3. Dome

Dome is made of stainless steel because its low cost and ease of manufacture. There is no special cooling or strength needs for the dome. It must be compatible with ethanol and LOX and stainless steel is a good choice for this purpose. It is used both as oxidizer and fuel dome. When the injector is assembled to the dome, oxidizer and fuel do not mix. There is a hole at the center of it that is connected to the hole at the center of the injector to measure the pressure in the combustion chamber.

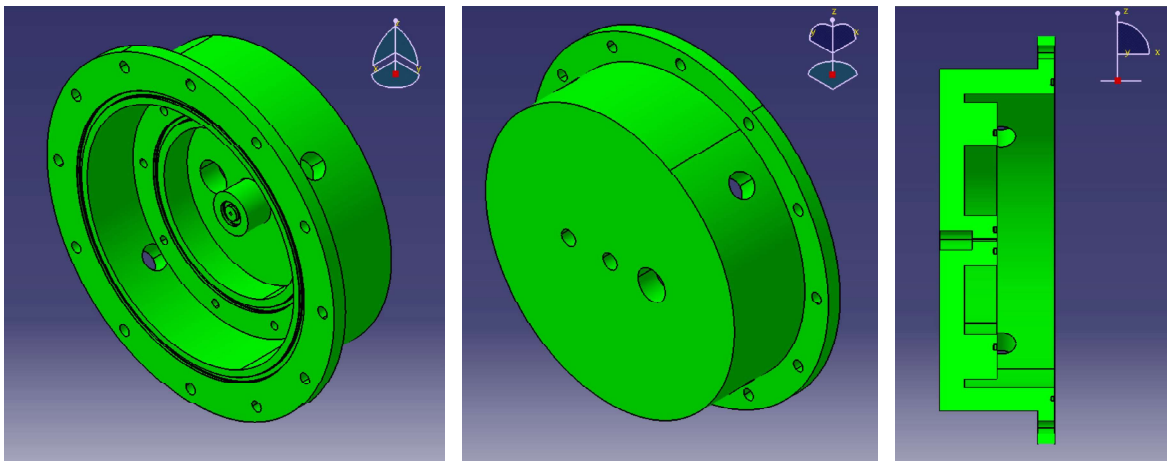

(a) (b) (c)

Figure 6.7. Designed dome from (a) front, (b) back and (c) cut views.

There are four 1/2” NPT holes around it as fuel inlets. Four holes are placed on it because fuel dome has a quite small volume and four inlets provides more equal

flow distribution than one inlet. Four holes provide equal flow to each fuel hole in the injector. 3/4" NPT hole on the upper side of the dome is LOX inlet and 1/4" BSPP hole is used to connect a pressure sensor for measuring the pressure in the LOX dome. Oxygen inlet is not centered and it may cause uneven LOX flow through the injector. Tests showed that its effect can be neglected. CAD model and manufactured dome part can be seen in Figure 6.7 and Figure 6.8. Technical drawing of the dome is given in APPENDIX B.4.

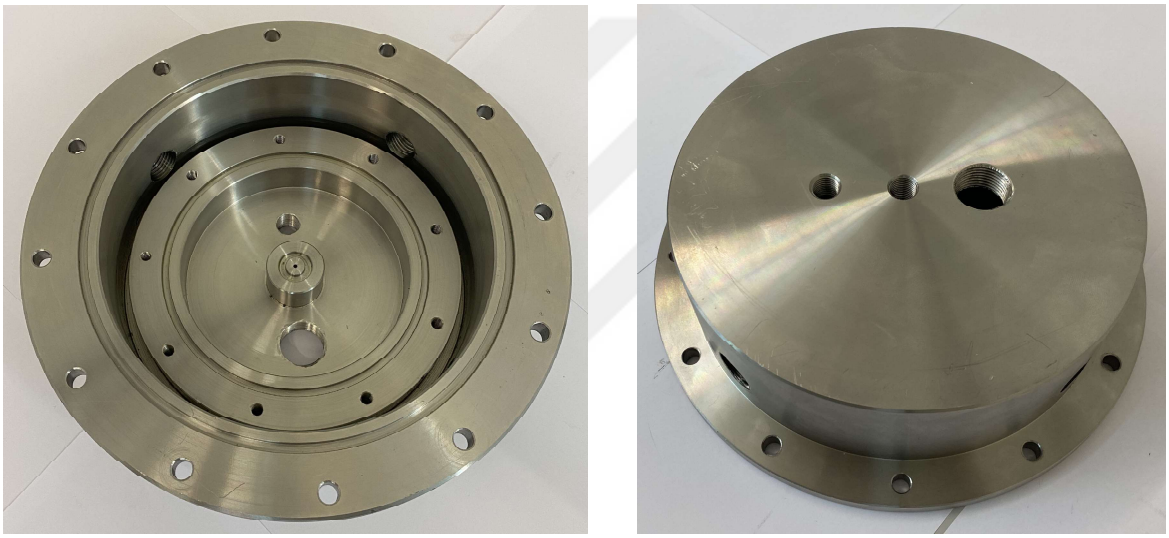

(a) (b)

Figure 6.8. (a) Injector side and (b) outer side of the manufactured dome.

Three o-rings are squeezed at the same time when the injector is screwed to the dome. Two of them between the dome and the injector and one of them between the dome and the jacket flange. This can cause improper squeezing and leakage. Therefore, it should be tested before the firing. No problems encountered during the leakage tests. However, temperature difference between the two sides of the injector may cause uneven elongation-shrinkage during the firing and o-rings may have problems. Besides, it is noticed that there is a leakage at the innermost o-ring during the firing tests.

Another problematic case is 1/2" NPT holes around the dome. Tap is blocked during the tapping operation by the extruded part where the injector is assembled, and it cannot go full depth. Therefore, NPT fittings can be screwed only a few threads. This may cause leakage and they are checked before firing by a leakage test.

6.4. Jacket

As mentioned before, water flows between the combustion chamber and the jacket. Aluminum is used for the jacket because it makes the part lighter with respect to stainless steel.

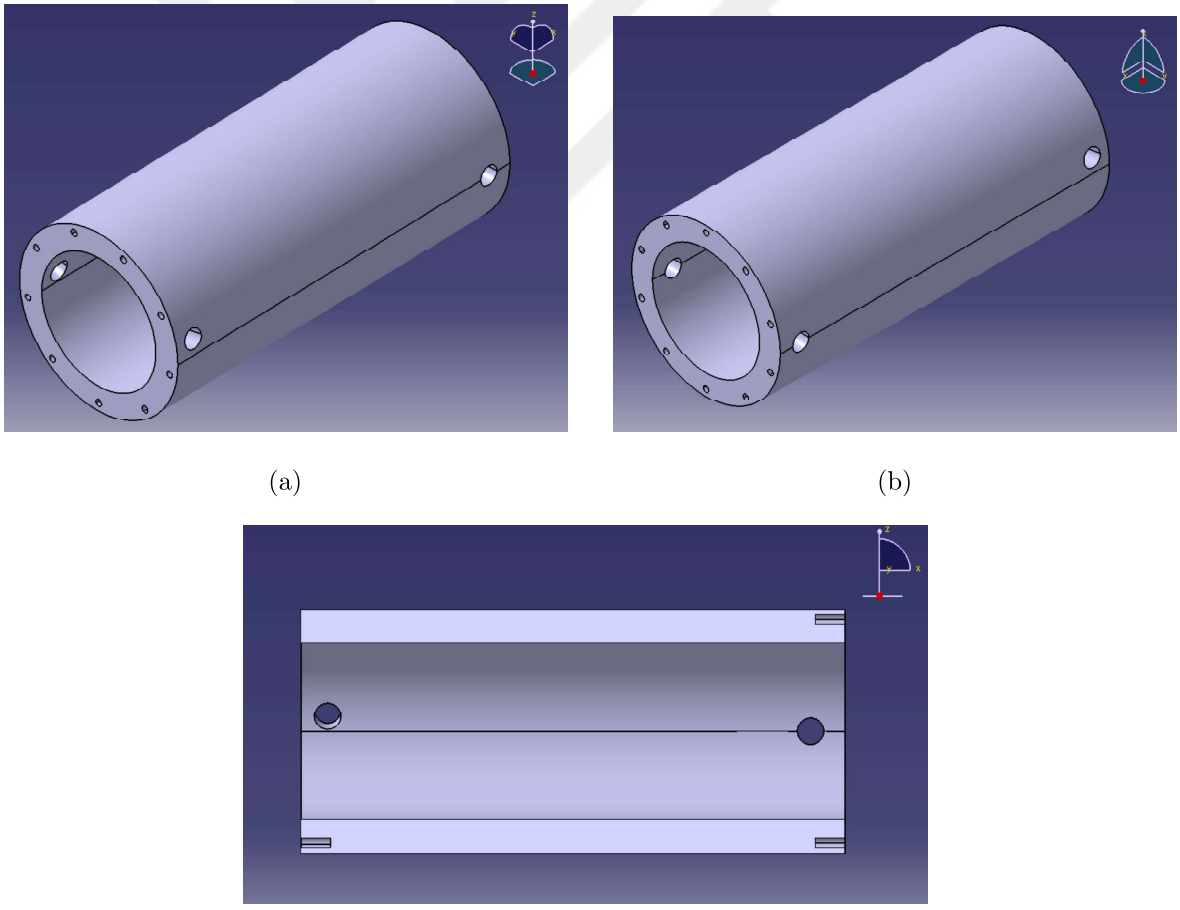

(a) (b)

(c)

Figure 6.9. Designed jacket from (a) front, (b) back and (c) cut views.

Jacket is designed as a straight hollow cylinder. This reduces the manufacturing cost because it can be bought as hollow cylinder instead of a solid billet. Machining process is required only for adjusting the inner and outer diameters. Both machining and raw material costs are reduced in this way.

Two NPT holes are drilled on each side of the jacket for cooling water inlet and cooling water outlet. Inlet and outlet NPT holes are not aligned with each other because there are different number of screw holes at the cylindrical sides of the jacket, 9 at one end and 10 at the other end. NPT holes overlaps with screw holes if the outlet and inlet NPT holes are aligned with each other. CAD model and manufactured part can be seen in Figure 6.9 and Figure 6.10 from different view angles.

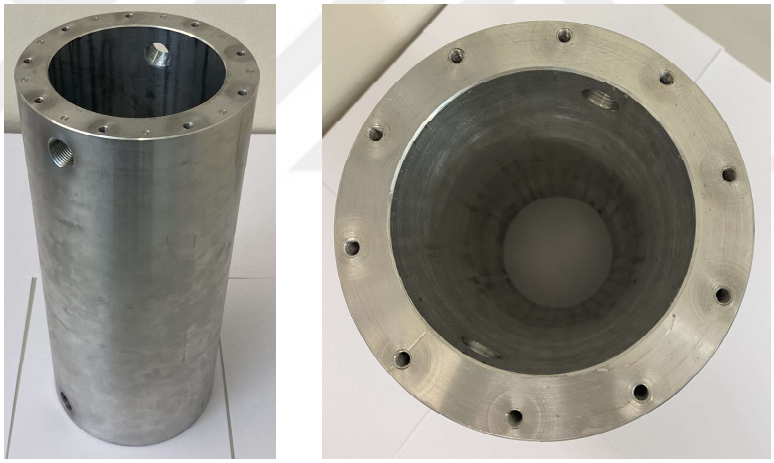

(a) (b)

Figure 6.10. (a) Outside and (b) inside of the manufactured jacket.

6.5. Jacket Flange

Jacket flange is designed as a separate part from the jacket to reduce the scrap and machining costs. Otherwise, a billet with larger diameter would have to be used for manufacturing jacket and flange as a single part. Jacket flange is is made of aluminum. Designed part can be seen in Figure 6.11. There are 12 holes at the flange for fixing it to the dome and 9 holes to fix the flange to the jacket. Final manufactured part

is given in Figure 6.12. O-ring at the one side of the jacket flange is used to prevent cooling water leakage and the one at the another side is between the fuel dome and the water channels.

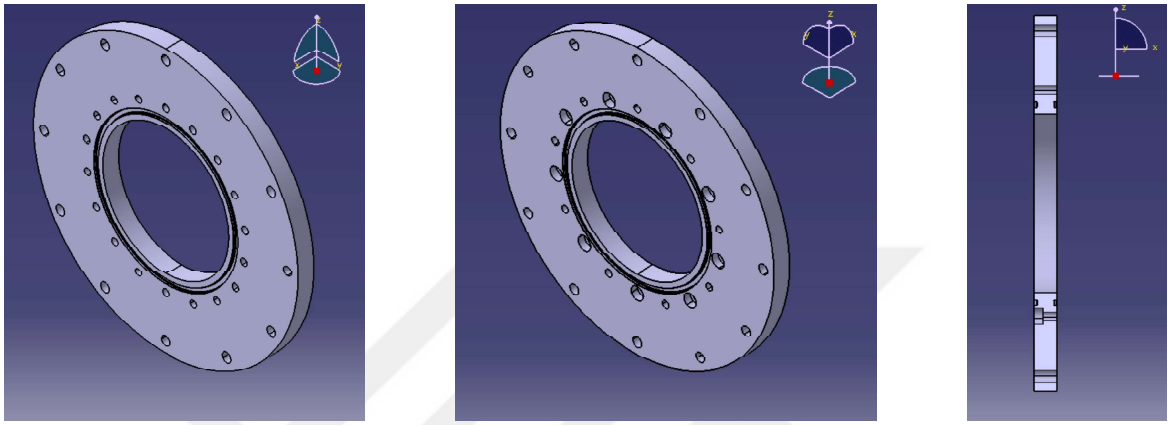

(a) (b) (c)

Figure 6.11. Designed jacket flange from (a) front, (b) back and (c) cut views.

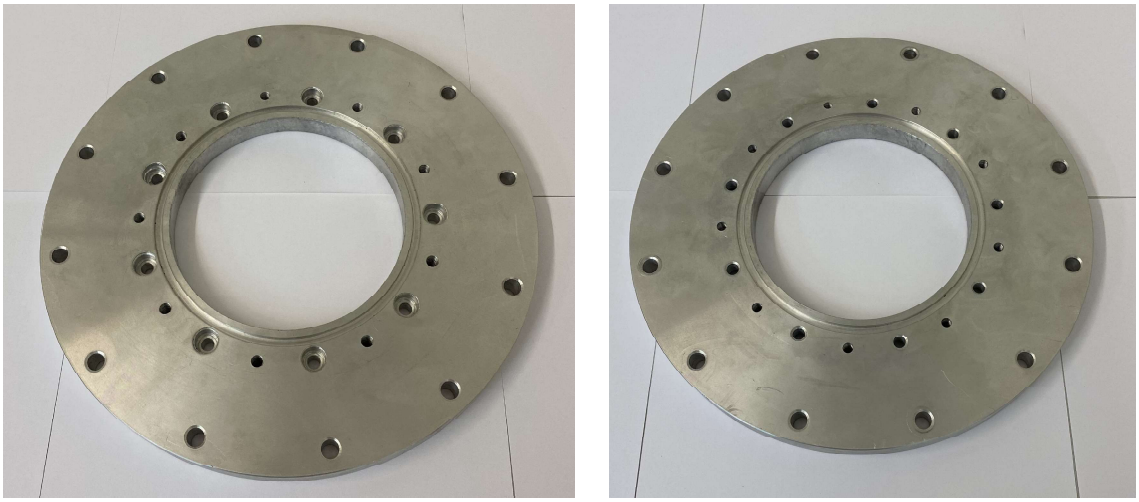

(a) (b)

Figure 6.12. (a) Dome side and (b) combustion chamber side of the manufactured jacket flange.

6.6. Saddle

Saddle is machined from an aluminum billet. It is designed to maintain same water channel cross sectional area in all sections by covering the outside contour of the combustion chamber.

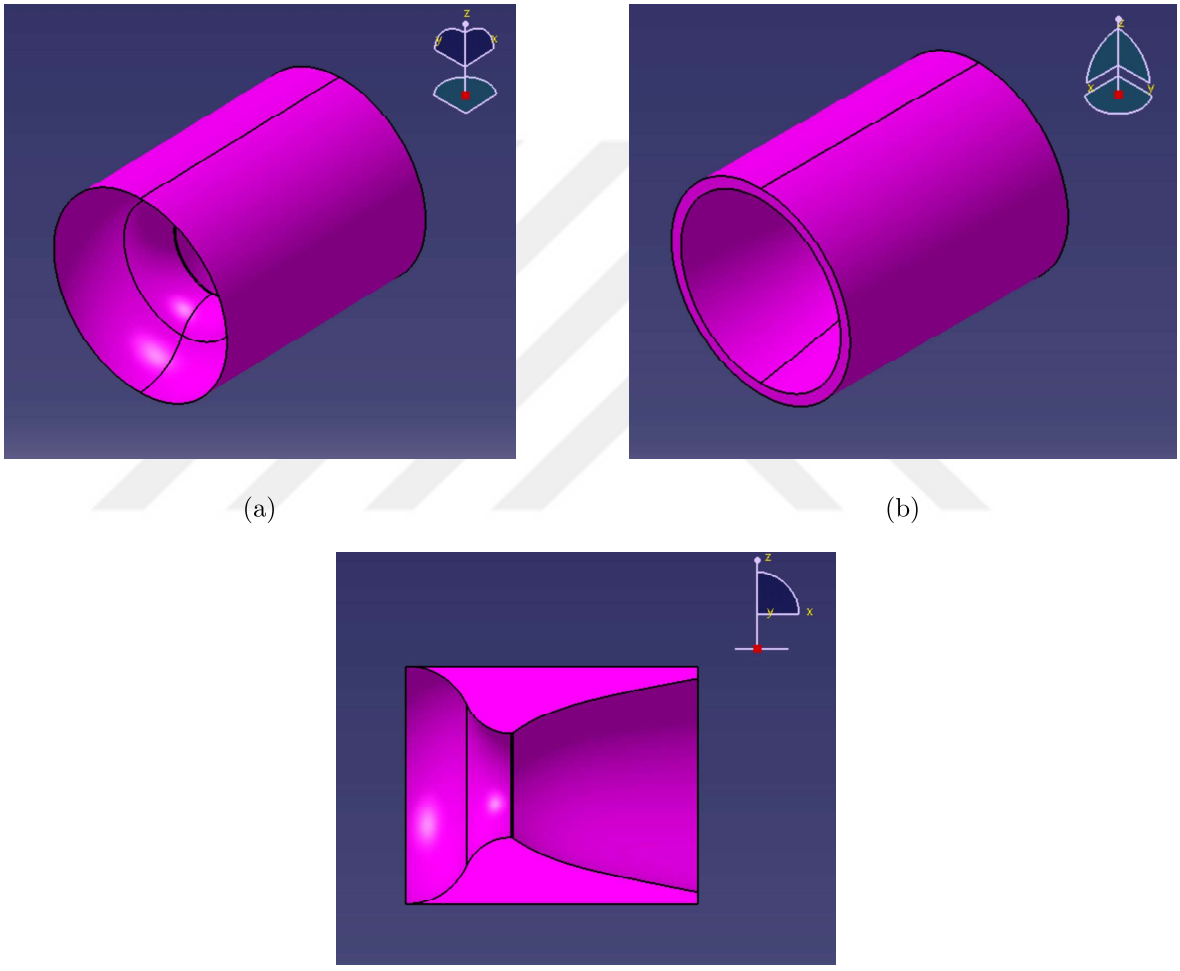

(a) (b)

(c)

Figure 6.13. Designed saddle from (a) front, (b) back and (c) cut views.

Water flows between the saddle and the combustion chamber. Saddle has the same inside profile as the outer profile of the combustion chamber. It is manufactured as a one piece and then cut in half with the wire erosion. These two pieces are placed around the throat section of the combustion chamber.



(a) (b)

Figure 6.14. (a) Outer and (b) inner side of the manufactured saddle.



Figure 6.15. Saddle and combustion chamber assembly.

It is observed that one side of the saddle is too thin and it warps during assembly. It should be improved in the next design. Also, tolerances should be taken into account more carefully because there is a gap between the two pieces and there is not a

perfect match with the combustion chamber profile when assembled. CAD model and manufactured saddle can be seen in Figure 6.13 and Figure 6.14.

Saddle placed on the combustion chamber and placing process of the saddle-combustion chamber assembly into the jacket can be seen in Figure 6.15. The gap between the two parts of the saddle can be seen in Figure 6.15 (b).

6.7. Cover

Cover is placed at the end of the combustion chamber (nozzle side) to prevent water leakage. An alternative design was to use a radial o-ring between the combustion chamber and the jacket. However, it was not chosen because of the lack of experience with radial o-ring.

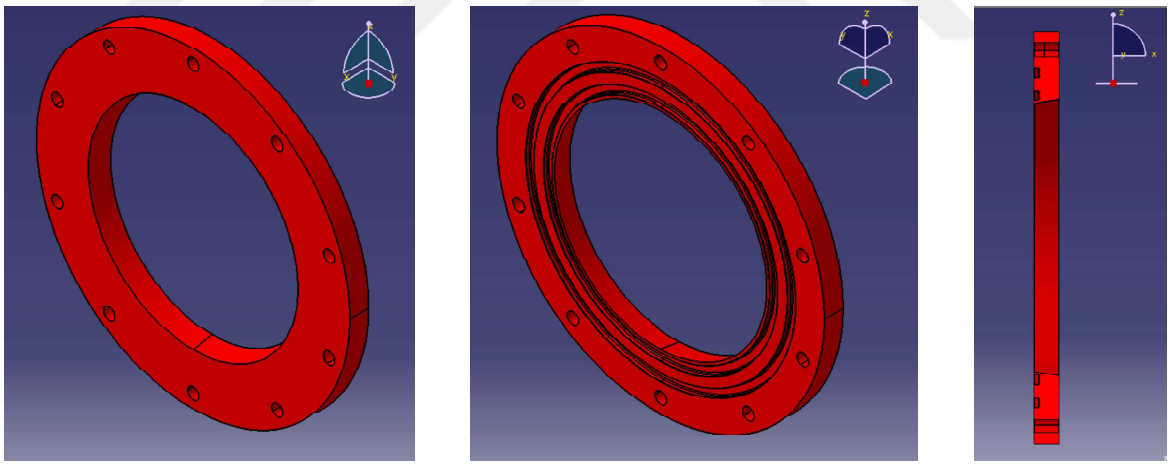

(a) (b) (c)

Figure 6.16. Designed cover from (a) front, (b) back and (c) cut views.

There are two o-rings that are squeezed between the cover and the nozzle, and between the cover and the jacket. The inner wall of the cover part is machined in such a way that it provides a natural extension to the copper nozzle of the rocket engine in order to provide a smoother transition from the nozzle to the cover. Stainless steel is

chosen for manufacturing the cover because it is exposed to high temperature at the exit of the nozzle and it is a small part that weight is not so important.



(a) (b)

Figure 6.17. (a) Combustion chamber side and (b) outer side of the manufactured cover.

In this design, the wall on the inner side of the inner o-ring is quite thin. Also, cover is located in a place that could be very hot during the firing. O-ring may fail because of these reasons. Designed and manufactured part can be seen in Figure 6.16 and Figure 6.17.

6.8. Sensors

There are four kinds of sensors that are used in the test system: pressure sensors, thermocouples, flow meters and load cells.

6.8.1. Pressure Sensors

KELLER PA-21Y series pressure sensors are chosen to measure the pressure. It is a piezoresistive pressure transmitter. Piezoresistive type is one of the most common pressure sensor type. Electrical resistance of the piezoresistive sensors on the diaphragm changes with the applied pressure because of the bending of the diaphragm.

That change of the resistance is used to measure the applied pressure. 60 bar and 100 bar types are used at different locations in the system. Sensor gives 4-20 mA output and its operating temperature range is -40°C to 100°C. 1/4" piping extensions are used where the fluid temperature is out of this temperature range. Temperature of the fluid decreases (where the pressure of the combustion chamber is measured) or increases (where the pressure of the cryogenic fluid is measured) before reaching the pressure sensor at this extensions because of the heat transfer with the ambient.



Figure 6.18. KELLER PA-21Y pressure sensor [25].

6.8.2. Flow Meters

Blancett turbine flow meter is used to measure the flow rate of the fuel. As the flow passes through the turbine flow meter, it rotates the turbine blades where the angular velocity of the blades is proportional to the flow velocity. An electrical pickoff mounted on the turbine casing senses the passes of turbine blades and creates an electric signal with the frequency proportional to the fluid flow rate. Volumetric flow rate of the fluid is calculated by multiplying the frequency with a calibration constant. Mass flow rate of the fluid can be found by multiplying volumetric flow rate with the density of the fluid. It can be used for both gas and liquid.

6.8.3. Load Cells

There are three load cells in the system. Two of them are used to measure the weight of the propellant tanks and one of them is used to measure the thrust in the thrust stand. Beam types load cells are used for tanks and S-type is used for the thrust measurement. Beam type load cells are mounted on weighing scale platforms to be able to place the tanks on them. Zemic L6G 300 kg load cells are used as beam type load cells and Delta MS-01 2000 kg load cell is used as a S-type load cell. They can be seen in Figure 6.19.

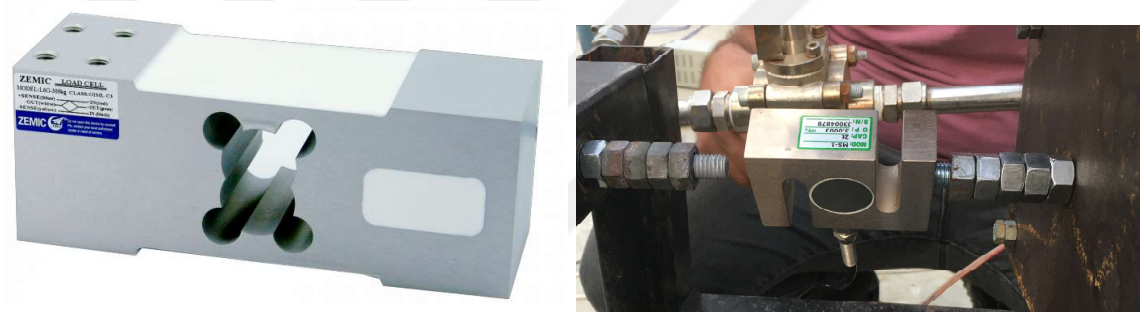

(a) (b)

Figure 6.19. (a) Beam type and (b) S-type load cells.

Load cells have analog voltage outputs which are in mV range. They can be measured easily by Fluke F15B+ multi-meter but they need to be amplified to be measured correctly by NI USB 6008 DAQ. Therefore, commercially available Delta brand load cell amplifier is used to amplify load cell output. Calibration of the load cell is made in several steps. Firstly, output from the amplifier is measured when the load cell is in unloaded position and knob on the amplifier is turned until the output is zero. Next step is placing a know weight on the load cell and measuring the output from the amplifier. Load cell output is assumed to be changing linearly with the applied load. Output of the idle state, which is zero, and output of the state loaded with a known weight can be used to calibrate the load cell and other unknown weights can be measured. More than one known weight can be used to make calibration and to

increase the accuracy. On the other hand, this amplifier is very sensitive to humidity of the environment. Test area is very humid and calibration of the load cells has to be made before each test. It is observed that a moisture layer is formed on the amplifier in a short time and a heat gun is used to remove moisture before the tests.

6.9. Actuators

Solenoid and pneumatic valves are used to control the ball valves. Actually, solenoid valve is used to control the pneumatic valve and pneumatic valve controls the ball valve directly.

6.9.1. Pneumatic Valves

There are two kinds of pneumatic actuators in the system: Swagelok 133 SR (spring return) and Swagelok 135 DA (double acting). Applied pressure, generally 6-8 bar, turns the shaft in pneumatic actuator. This shaft is connected to ball valve to open and close the ball valve. Spring return pneumatic actuator has single inlet port and shaft turns when an external pressure is applied from this inlet port. Spring loaded actuator returns its initial position when the applied external pressure is removed. Double acting valve has two inlet ports. Shaft turns when an external pressure is applied from one of the ports but it does not return its initial position when applied pressure is removed. Pressure has to be applied from other port in order to turn the shaft to its initial position. Therefore applying pressure from single pressure line is enough for spring return type but there must be two separate pressure lines for double acting type. Pneumatic actuator types can be seen in Figure 6.20.

6.9.2. Solenoid Valves

Solenoid valve is used to control fluid flow by an electrical signal. When it is energized, an electromagnet moves the actuator and when de-energized, a spring returns the actuator to its initial position. Solenoid valves can be classified by their number of



(a) (b)

Figure 6.20. (a) Swagelok 133 spring return type and (b) double acting type pneumatic actuators.

positions and number of ports. 3/2 and 5/2 types are used in the system. 3/2 or 5/2 represents that there are 3 or 5 ports and 2 positions in the solenoid valve.

Figure 6.21 (a) and Figure 6.21 (b) show the schematics of 3/2 and 5/2 type solenoid valves. There are 2 positions (left and right) and 3 ports (A, R and P) in Figure 6.21 (a). Port A is connected to port P when the actuator is de-energized and port A is connected with port R when the actuator is energized. If the pressurized gas is connected to port R and spring return pneumatic valve is connected to port A, pressurized gas is sent to pneumatic valve when the solenoid valve is energized. Pressurized gas in the pneumatic valve is discharged when the solenoid valve is de-energized and port A is connected with port R.

Similar principle is valid for 5/2 valve, which can be seen in 6.21 (b). The difference is there are 5 ports instead of 3 ports. Pressurized gas is connected to port 1 and two inlet ports of the double acting pneumatic valve are connected to ports 4 and 2. Ports 1 and 4 are connected with each other when the solenoid valve is de-energized

and pneumatic valve is in a certain position. When the solenoid valve is energized, port 1 is connected with port 2, pressurized air in port 4 is discharged from port 5 and other inlet of the double acting pneumatic valve is pressurized. Therefore, pneumatic valve changes its position. In summary, spring loaded pneumatic valve can be controlled with 3/2 way solenoid valve and double acting pneumatic valve can be controlled with 5/2 way solenoid valve. A similar 5/2 way solenoid valve that is used in the test system can be seen in Figure 6.21 (c) .

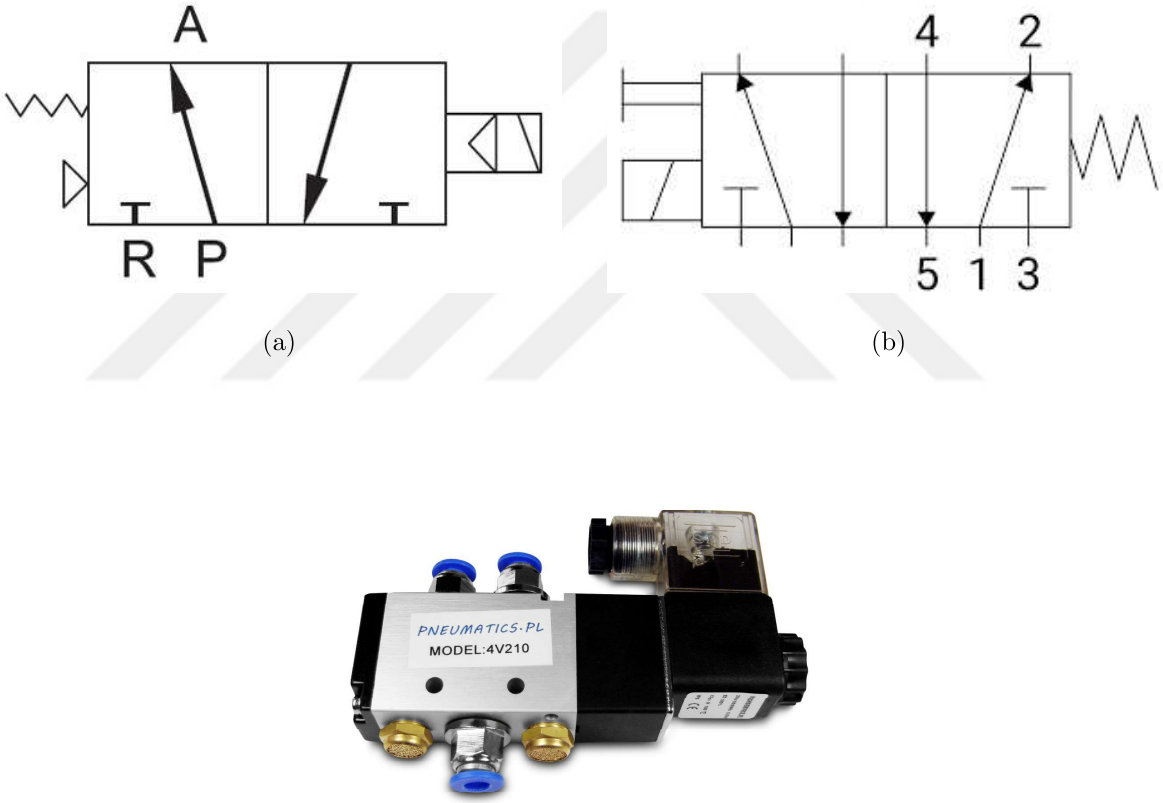

(a) (b)

(c)

Figure 6.21. (a) 3/2 type [26] and (b) 5/2 type [27] solenoid valve schematics are shown, (c) shows a representative solenoid valve [28].

6.10. Control System

Tests are conducted using a Labview Code. NI USB 6008 and USB 6009 Multifunction I/O Devices are used to read sensors and send signals to the actuators. Their input and output voltage range is -10/10 V. Therefore, all the sensor and actuator systems are designed to be used in this range. The difference between USB 6008 and USB 6009 is the resolution of the devices. USB 6008 is a 12 bit device whereas USB 6009 is 14 bit. Assuming a voltage range of 20 V, difference between the two devices can be seen expressed as

$$\frac{20V}{2^{12}} = 4.9mV, \tag{6.1}$$

$$\frac{20V}{2^{14}} = 1.2mV. \tag{6.2}$$

In other words, USB 6009 can sense more than 4 times smaller voltage changes than USB 6008. As mentioned before, raw output of the load cels are in mV range and neither USB 6008 nor USB 6009 can be used to get accurate measurement from the raw load cell output.

Text sequence is created in LABView. Table 6.1 shows which valve is opened at which time. "O", "C" and "NN" represent "opened", "closed" and "automatically controlled", respectively. First pressurization up to a certain pressure, activation of bang bang control, oxidizer line cooling, fuel line filling and injector cooling are conducted manually to observe the behaviour of the system, check and intervene if any problem occurs. For instance, first pressurization up to a certain pressure is done manually in several steps to see if any leakage occurs. Also, cooling of oxidizer line and injector is done until liquid is seen at the exit of the line and the injector. Therefore, times until "Firing sequence starts (t-3 s)" is given as estimation and they are not automatically controlled by the LABView sequence. LABView sequence starts after this point and continues until purging is finished. Depressurization of the tanks are done manually because if there is anything wrong, depressurization of oxygen to the ambient may cause fire.

Table 6.1. Test sequence that is used in LABView.

		Pressurizer Valve Fuel	Depressurizer Valve Fuel	Pressurizer Valve Oxidizer	Depressurizer Valve Oxidizer	Tank Valve Fuel	Tank Valve Oxidizer	Main Valve Fuel	Main Valve Oxidizer	Bleed Valve Fuel	Bleed Valve Oxidizer	Cooling Water Valve	Fuel Purge Valve	Igniter Up Pneumatic Valve	Igniter Down Pneumatic Valve	Igniter Electric
Time	**Action**	**BBCV-F1**	**BBCV-F2**	**BBCV-O1**	**BBCV-O2**	**TPV-F**	**TPV-O**	**MPV-F**	**MPV-O**	**BPV-F**	**BPV-O**	**TPV-W**	**LPPV-F**	**IUPV**	**IDPV**	**IER**
t-50 s	System at rest	C	C	C	C	C	C	C	C	C	C	C	C	C	O	C
t-41 s	Test sequence starts	C	O	C	O	C	C	C	C	C	C	C	C	C	O	C
t-40 s	Pressurization starts	O	C	O	C	C	C	C	C	C	C	C	C	C	O	C
t-36 s	Bang bang control activated, lines are pressurized	NN	C	NN	C	O	O	C	C	C	C	C	C	C	O	C
t-35 s	Oxidizer line cooling starts	NN	C	NN	C	O	O	C	C	C	O	C	C	C	O	C
t-21s	Oxidizer line cooling finished	NN	C	NN	C	O	O	C	C	C	C	C	C	C	O	C
t-20s	Injector cooling starts	NN	C	NN	C	O	O	C	O	C	C	C	C	C	O	C
t-7s	Injector cooling finished	NN	C	NN	C	O	O	C	C	C	C	C	C	C	O	C
t-6s	Fuel line filling	NN	C	NN	C	O	O	C	C	O	C	C	C	C	O	C
t-4 s	Fuel line filling completed	NN	C	NN	C	O	O	C	C	C	C	C	C	C	O	C
t-3 s	Firing sequence starts	NN	C	NN	C	O	O	C	C	C	C	O	C	O	C	O
t-1 s	Oxidizer main valve opened	NN	C	NN	C	O	O	C	O	C	C	O	C	O	C	O
t	Fuel main valve opened and ignition	NN	C	NN	C	O	O	O	O	C	C	O	C	O	C	O
t+5 s	Igniter goes down	NN	C	NN	C	O	O	O	O	C	C	O	C	C	O	C
t+20 s	Test is finished and purging starts	C	C	C	C	C	C	C	C	C	C	O	O	C	O	C
t+25 s	Purging is finished and lines are depressurized	C	C	C	C	C	C	C	C	O	O	C	C	C	O	C
t+30 s	Tanks are depressurized	C	O	C	O	C	C	C	C	C	C	C	C	C	O	C

Overview of the LABView panel is given in Figure 6.22. Time elapsed since the start of the NI is given at the top. There are pressure gauges for all of the pressure sensors and the thermocouple. Each of the pneumatic valve can be controlled manually with switches. Below the switches, bang bang control is placed. Desired pressure and hysteresis can be adjusted there. Hysteresis is used to prevent too many on and off of the bang bang control valves because the measured pressure cannot be exactly the same as the set pressure.

0.2 bar hysteresis is used to prevent too many valve actions. Set pressure and measured pressure for the LOX tank and fuel tank can be seen in graphs at left and right side, respectively. "LOX Pressurizer" and "Fuel Pressurizer" knobs between the graphs are used to active the bang bang control. All of the measured pressures can be observed below the LOX bang bang control graph. Right next to pressure graph, there are test control buttons. "Test Mode" button disables the manual control and activates automatic control. "Fuel line test", "LOX line test" or "Firing Test" can be chosen from the "Test Type" for different tests and test time is determined. Test starts when the "TEST" button is pressed. This button works only if the "Test Mode" knob is in active position. "EMERGENCY" button stops the test immediately in case of an emergency situation.

Data measured from the load cells are located below the test buttons. Fuel tank mass, LOX tanks mass and measured thrust values are visualised as bars and mass data is given with respect to time in the graph just at the left side of the bars. As mentioned before, mass flow rate can be calculated using the data from load cells located below the tanks to measure their mass or by a turbine mass flow meter. Both of these methods are given in the LABview panel in case any problem occurs at the load cells or the turbine flow meter. Thermocouple data can be observed below the mass graph. However, temperature data could not be measured during the tests due to the faulty connection of the thermocouple.



Figure 6.22. Appearance of the LABView panel.

Mass flow rate data obtained from the turbine mass flow meters are given below the temperature graph and calculated passed total mass through the turbine flow meter is given at the right side of the temperature graph. "Total Fuel Mass Count" and "Total LOX Mass Count" data show the raw turbine flow meters data to double check the calculated total mass data. Thrust data with respect to time is given at the bottom right side of the panel.

7. TESTS

Tests are divided into two categories: component tests and thrust chamber tests. Individual components tests like cooling channel test and injector water test are investigated in Section 7.1. Cold flow tests of the injector with liquid nitrogen and water, open fire tests and complete thrust chamber tests are discussed in Section 7.2.

7.1. Component Tests

Every part of the full system is tested individually before the full system test. Each part is tested after manufacturing and revisions are made if needed. Test procedures and results of the tests for main parts of the system are given in this section.

7.1.1. Cooling Water Mass Flow Rate Test

Heat transfer analyses are conducted assuming that the given water mass flow rate can be passed through the cooling channels. However, there is not an easy way to calculate the pressure drop across the cooling channels because channels are so narrow that very small manufacturing defects causes significant pressure drop. Also, a satisfactory CFD results could not be achieved for the cooling channels. Therefore, pressure drop to pass the needed mass flow rate had to be determined experimentally.

A test setup with a commercially available Karcher BP 2 Garden water pump is prepared for the test. Suction side of the pump is connected to the water tank and discharge side is connected to the inlet of the cooling channel. Exit of the cooling channel is connected back to the water tank so that a circulating water flow is achieved. Pump's max power is 700 W, max flow rate is 3000 l/h and max pressure is 3.5 bar.

Tests showed that mass flow rate of the water is 0.35 kg/s and inlet pressure of the cooling channel is 1.5 bar. This mass flow rate is significantly lower than the

assumed mass flow. It is noticed that water pump cannot supply enough water and another method has to be used for the cooling.

A water tank with an external pressurizer is used for cooling. 235 bar pressurized nitrogen cylinder is connected to a 100 L water tank by a pressure regulator system. 235 bar pressure is reduced to 40 bar by a spring loaded Linde pressure regulator. After that, a dome type pressure regulator and TESCOM ER5000 electropneumatic actuator is used to keep pressure in the water tank at 15 bar regardless from the pressure at the nitrogen cylinder and the water mass flow rate. This system can be controlled from a computer to adjust pressure as desired in the water tank without any physical adjustment. 15 bar pressure in the water tank cannot be exceeded because of the mechanical limitation of the water tank. This system showed that 1 kg/s water mass flow rate can be achieved with 15 bar water tank pressure.

7.1.2. Injector Water Tests

As mentioned before, two injectors are manufactured. At first, water is used as working fluid to calculate C_d of the injector. C_d is calculated as

$$C_d = \frac{\dot{m}}{A_{flow}\sqrt{2\rho(P_{up} - P_{down})}}, \tag{7.1}$$

where injection area (A_{flow}) and density (ρ) are known; mass flow rate ($\dot{m}$), upstream pressure (P_{up}) and downstream pressure (P_{down}) pressure are measured during the test. C_d can be calculated using known and measured values in Equation 7.1.

C_d of the fuel line and oxidizer line for the first injector (Injector V1) are calculated as 0.72 and 0.69, respectively. Test results of the first injector showed that oxidizer pressure drop of the injector is too low for the desired 1.25 kg/s oxidizer mass flow rate and fuel pressure drop is larger than the expected for the desired 1.01 kg/s fuel mass flow rate. It is seen that pressure drop is 0.72 bar and 11.9 bar for 1.25 kg/s LOX mass flow rate and 1.01 kg/s ethanol mass flow rate, respectively. Therefore, another injector (Injector V2) is designed with larger fuel injection area and smaller oxidizer

injection area. C_d results of the Injector V1 are used for the new design to achieve desired mass flow rates at %15-20 pressure drop.

Water test results of the injector V2 showed that C_d of the fuel and oxidizer line are 0.52 and 0.69, respectively. It is observed that C_d of the oxidizer line is almost the same for two injectors but C_d of the fuel line of the injector V2 is significantly lower than the injector V1. This difference may be cause from a manufacturing defect. Pressure drop of fuel and oxidizer lines for 1.25 kg/s LOX mass flow rate and 1.01 kg/s ethanol mass flow rate are calculated as 5.0 bar and 9.9 bar, respectively. Pressure drop of the fuel line is higher than the expected value but it is decided that 9.9 bar pressure drop is acceptable.

7.2. Thrust Chamber Tests

BUSTLab V1 Liquid Rocket Engine is tested under different conditions in an open area test facility. Gaseous and liquid oxygen are used as the oxidizer for different tests and %75 ethanol-%25 water mixture is used as the fuel.

Cold flow and open fire test are conducted before the actual engine test. Open fire tests, using only the injector without the combustion chamber, with gaseous oxygen at 10 bar and 30 bar; and open fire test with liquid oxygen at 80 bar tank pressure are completed successfully. Thereafter, final test is conducted with combustion chamber attached at 80 bar tank pressure using liquid oxygen.

7.2.1. Cold Flow Tests

After the tests of individual components like pipes, cavitating venturis and injector, the full system is tested with liquid nitrogen and water instead of liquid oxygen and ethanol. Tests are conducted at different tank pressures up to 80 bar. These tests are conducted to examine all the components and fluid lines under high pressure and low temperature flow conditions. Both of the tanks are pressurized with the gaseous

nitrogen bundles at 235 bar. A photo of the cold flow test using liquid nitrogen and water is given in Figure 7.1.



Figure 7.1. BUSTLab V1 rocket engine cold flow test.

Final cold flow test is conducted at 80 bar tank pressure and pressures at different locations during the test are given in Figure 7.2. The test starts at t=207.5 s and it continues for 21 seconds. Initially, the LOX tank is at 80 bar but the fuel tank is over-pressurized to 85 bar. Tank pressures are set to 80 bar in the LabVIEW but the system only tries to keep the pressure at 80 bar if it goes below 80 bar by opening the pressurizer valve. If the pressure is higher than the set pressure initially, the system does not depressurize the tank automatically. Depressurizer valves can only be opened manually in the LabVIEW. Pressure in the fuel tank decreases to 80 bar and stays there as soon as the main valve is opened.

At first, both of the tank valves are opened simultaneously at t=207.5 s and both of the lines are pressurized instantaneously up to the main valve, as can be noticed in Figure 7.2. Oxidizer and fuel dome pressures starts increasing after the main valves are opened. It is seen that constant 80 bar tank pressure can be provided for both of the

tanks during the test. However, there are some pressure fluctuations that are caused by the bang-bang control system and measurement errors.

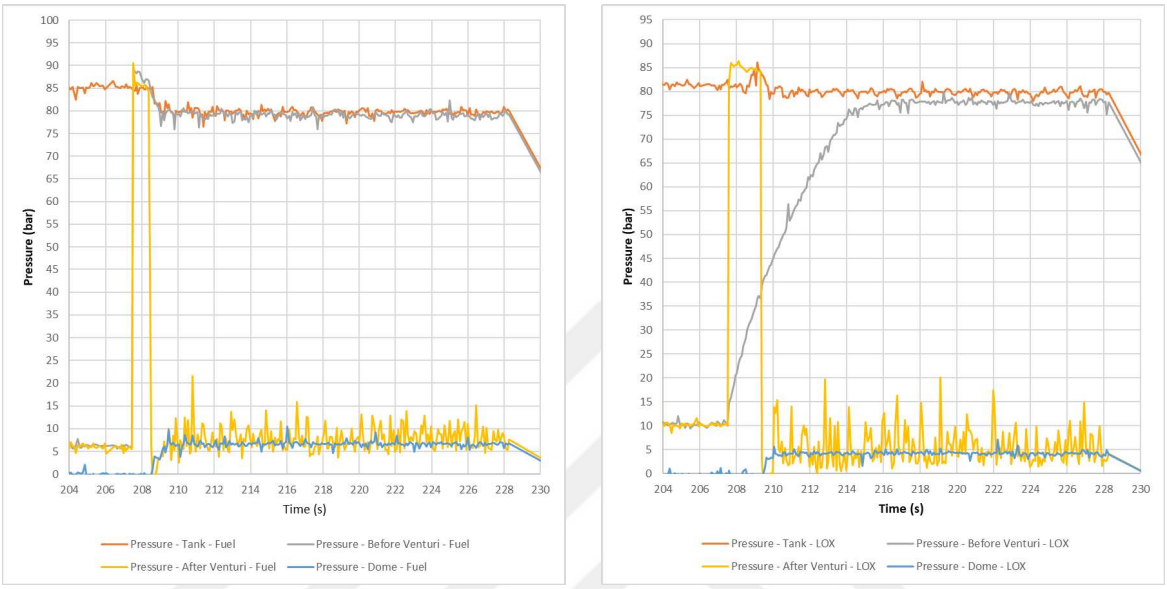

(a) (b)

Figure 7.2. Pressure graphs of the cold flow test with 80 bar tank pressures for (a) the fuel line and (b) the oxidizer line.

Fuel and LOX dome pressures are 6.5 bar and 4 bar during the test, respectively. There are high pressure fluctuations at "After Venturi" locations in both of the lines. "After Venturi" pressure sensors are just at the exit of the cavitating venturi and these fluctuations may be caused by unsteady flow at downstream of the venturi. Also, it is observed that the pressure sensor at the "Before Venturi" location in the LOX line is faulty.

This test showed that all the valves work seamlessly under high pressure and low temperature conditions, proper working conditions (within the temperature limits of the manufacturer) could be provided by extending the pipelines for the pressure sensors in the cryogenic lines. Also, it is observed that fuel lines in the injector are not frozen although there is cryogenic liquid on the other side of the injector.

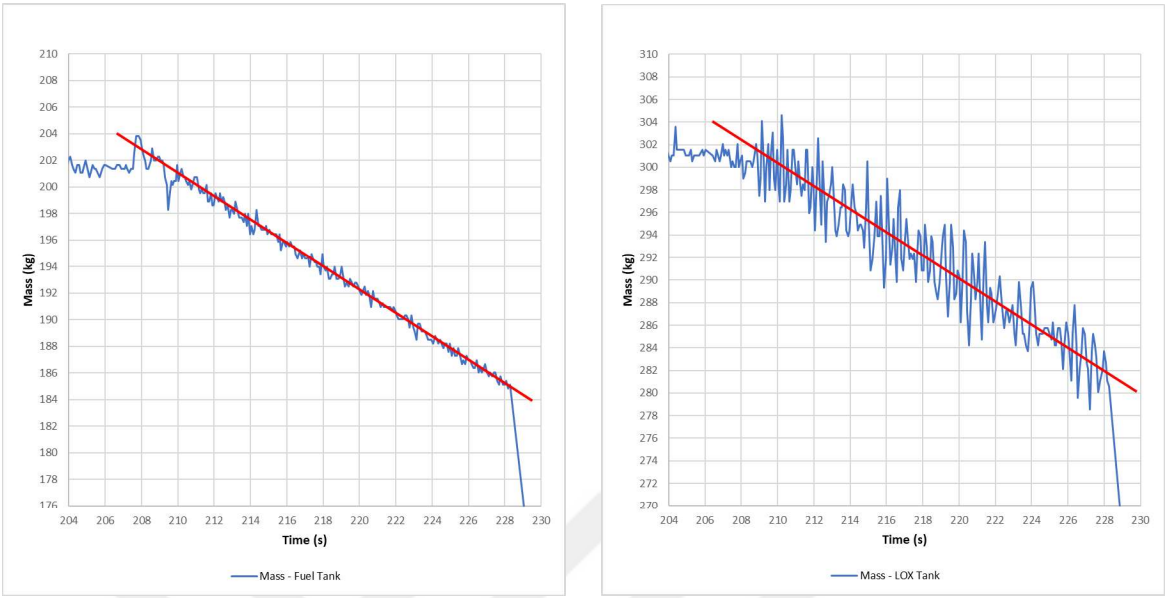

(a) (b)

Figure 7.3. Change of the tank masses during the cold flow test with 80 bar tank pressures for (a) the fuel tank and (b) the oxidizer tank.

Because of the lack of a cryogenic flow meter and the problems at the turbine flow meter in the fuel line, the mass flow rate can only be calculated by the change of the masses of the propellant tanks. Tank mass measurements are not very accurate because of the measurement errors and the effect of the bang-bang control. Sudden high pressure supply from the 235 bar pressurized nitrogen bundle causes a hitting effect in the propellant tanks. However, they give usable results for calculating mass flow rate for the long tests like 20 seconds. Change of the tank masses with respect to time are given in Figure 7.3 and red lines can be used to calculate the mass flow rates. LOX tank mass has significantly higher fluctuations but still, it can be used for mass flow rate calculation for the 20 seconds test. Mass flow rates for the fuel line (water in this test) and the LOX line (liquid nitrogen in this test) are calculated as 0.88 kg/s and 1.06 kg/s, respectively.

CFD analyses show that the water mass flow rate through the fuel cavitating venturi for the upstream pressure of 80 bar at cavitating mode is 1.06 kg/s. Also, the LN2 mass flow rate through the LOX cavitating venturi for the upstream pressure of

80 bar at cavitating mode is 1.02 kg/s. It should be noted that cavitating venturis are designed so that the mass flow rates through them are 1.01 kg/s (ethanol) and 1.26 kg/s (LOX) for the fuel and oxidizer cavitating venturies, respectively. Other CFD analyses are conducted to examine the mass flow rate when water and LN2 are used instead of ethanol-water mixture and LOX, so that venturies can be tested without using ethanol and LOX which can be dangerous.

LN2 mass flow rate for the cold flow test (1.06 kg/s) is almost the same as the CFD results (1.02 kg/s). However, the water mass flow rate for the cold flow test (0.88 kg/s) is significantly lower than the CFD results (1.06 kg/s).

CFD results coincide with the water tests of the cavitating venturies. In other words, there is no significant difference between the CFD results and the test results when the fuel and LOX cavitating venturies are tested with water. There might be some kind of a blockage, like a small particle, inside the cavitating which causes the mass flow rate to be lower than expected.

17% lower mass flow of the water in the fuel line may cause 0.84 kg/s instead of 1.01 kg/s fuel (ethanol-water mixture) mass flow rate at the actual firing. It is still in the acceptable range and it makes the OF ratio 1.5. Also, it is seen that the pressure drop at the injector is 4 bar and 6.5 bar for the LOX and fuel lines, respectively.

7.2.2. Open Fire Tests

The system is tested with an open fire test where the combustion chamber is detached from the injector and injected fluids are ignited. Test setup for open fire tests is shown in Figure 7.4. Igniter just in front of the injector can be seen in the figure. Ignition occurs at ambient conditions, therefore it is safer than the actual engine test. Also, actual mass flow rates as the full engine test can be measured because mass flow rates through the cavitating venturies are not affected from the downstream conditions.

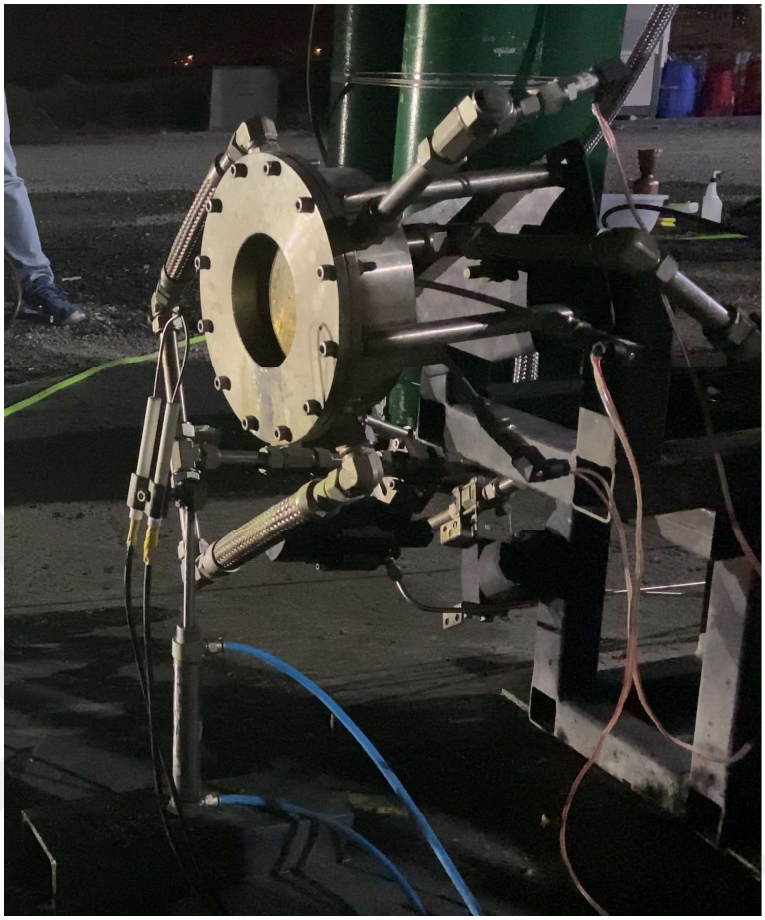

Figure 7.4. BUSTLab V1 rocket engine open fire test setup.

The igniter has to be tested before the full engine test. The igniter used in the actual engine is a commercial spark igniter that is used in metal casting furnaces to ignite natural gas. It is moved up and down with a pneumatic actuator. Its behaviour while propellants at high velocities and oxidizer at cryogenic condition flowing towards it has to be observed.

Three open fire tests at 10 bar, 30 bar and 80 bar tank pressures are conducted. GOX is used instead of LOX for 10 bar test and LOX is used for 30 bar and 80 bar tests. 10 bar test is conducted to test the igniter and to identify safety deficiencies. Main focus is observing the ignition. So, GOX is chosen instead of LOX to prevent any problems caused from cryogenic conditions. Results of 30 bar and 80 bar tests are given in the following sections.

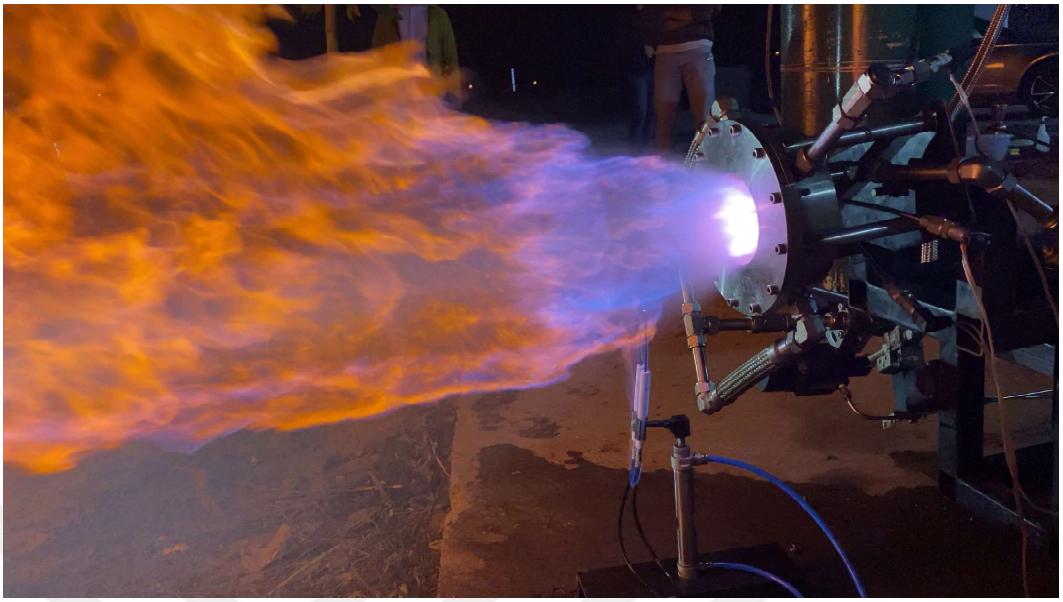

Figure 7.5. BUSTLab V1 10 bar open fire test.

10 bar open fire test showed that ignition is achieved successfully. There was a small fire around the test stand after the test is finished which can also be seen in Figure 7.5. It was extinguished quickly and required precautions are taken before the next 30 bar test. It is thought that fuel spread around the test stand just before the ignition, is the reason of the fire. This fire damaged the igniter and the pneumatic pipes that are used to move the igniter up and down. They are replaced before the next test.

7.2.2.1. 30 Bar Test. An open fire test at 30 bar tank pressure is conducted before the actual test pressure, 80 bar. One of the main reasons is to test the spark injector while fluid flows against it with a high velocity and to observe ignition. LOX is used as an oxidizer in this test. A photo taken during the test is given in Figure 7.6.

Just as the cold flow test, the pressure sensor at "Before Venturi - LOX Line" was not working properly in this test, too. Reason for the faulty pressure sensor may be the damaging of the sensor from cryogenic flow. Resulting pressures of the test can be seen in Figure 7.7.

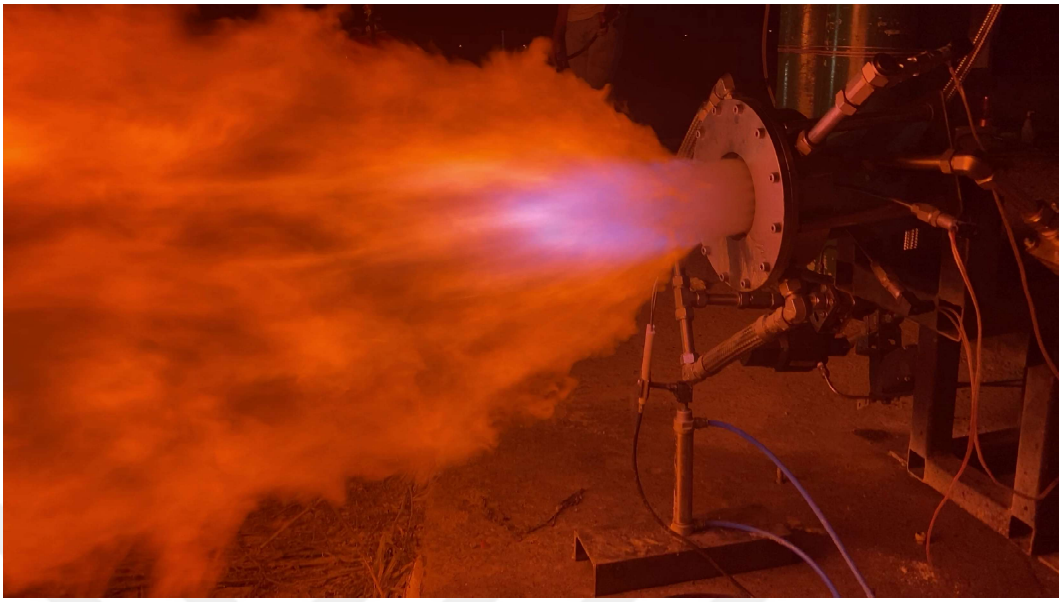

Figure 7.6. BUSTLab V1 30 bar open fire test.

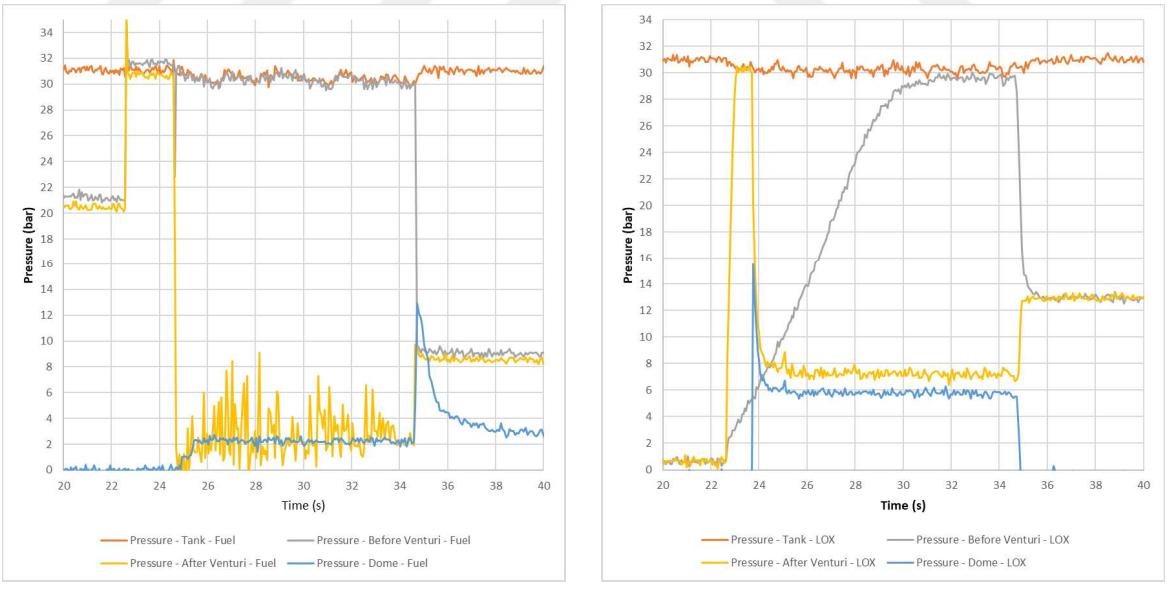

(a) (b)

Figure 7.7. Pressure graphs of the open fire test with 30 bar tank pressures for (a) the fuel line and (b) the oxidizer line.

Both of the tank valves are opened at t=22.6 s. After 1 second, LOX main valve is opened at t=23.6 s and the fuel main valve is opened 1 second later than LOX main valve, at t=24.6 s. Both of the main valves are closed at t=34.6 s and the test is finalized as planned.

Pressure spikes at "After Venturi - LOX Line" and "Dome - LOX Line" can be identified easily from Figure 7.7 when the tank valve and LOX main valve are opened, respectively. Pressure at the LOX dome increases up to 15 bar when the main valve is opened and stabilizes at 6 bar after about 0.5 s.

Even if the fuel main valves are fully opened at t=24.6 s, fuel dome pressure does not build up immediately and it takes about 0.8 seconds to stabilize around 2.25 bar. There is a sudden increase in the fuel dome pressure when the main valves are closed at t=34.6 s. This is caused by the purge of the fuel line starting from just after the fuel main valve.

7.2.2.2. 80 Bar Test. Open fire at 80 bar tank pressure with the actual propellant combination, %75 ethanol - %25 water mixture and LOX, is the last test before the final firing of the engine. This test's results give the actual mass flow rates of the propellants and the pressure drop at the injector. Also, the igniter is tested under the real test conditions to be able to see how it does behave while there is a LOX flow with a high velocity against the igniter.

Both of the tank valves are opened at t=54.1 s and the lines are pressurized up to the main valves. LOX main valve and fuel main valve are opened after 1 and 2 seconds, respectively.

Fuel line pressure during the test can be seen in Figure 7.8. Just like the 30 bar LOX test, fuel dome pressure stabilizes at 7 bar 1 second after the ignition and stays almost the same during the test. There is again a pressure spike at the end of the test because of the purge. Also, fuel tank pressure stays at almost 80 bar during the test.

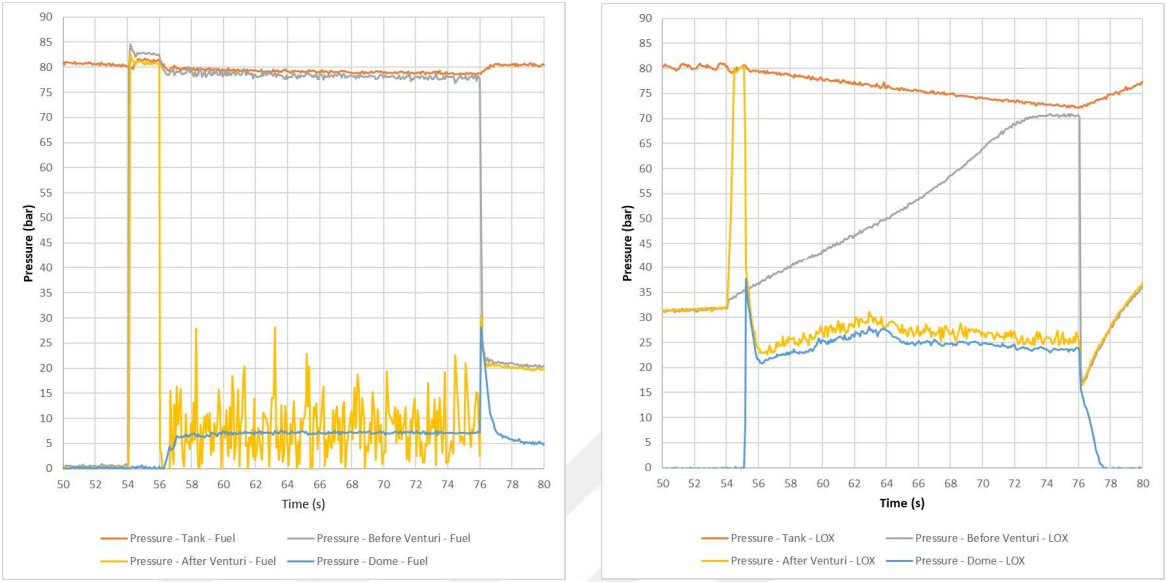

(a) (b)

Figure 7.8. Pressure graphs of the open fire test with 80 bar tank pressures for (a) the fuel line and (b) the oxidizer line.

LOX line pressure is not as stable as the fuel line which can be seen in Figure 7.8. First of all, LOX tank pressure decreases from 80 bar to 73 bar almost linearly during the 20 seconds test. The reason is, not being able to supply enough pressurizer gas from the nitrogen bundle to the LOX tank because the temperature of the nitrogen gas drops significantly when it enters the cold LOX tank and more nitrogen gas than expected is needed to maintain the 80 bar pressure. This problem is identified in this test and solved in the actual engine test by increasing the supply pressure of the nitrogen gas.

Apart from the change of the LOX tank pressure, LOX dome pressure increases from 21 bar to 27 bar at the first 9 seconds of the test. It decreases to 25 bar between t=63 s and t=65 s and stays between 25 bar and 23 bar throughout the rest of the test. Achieved LOX dome pressure is much higher than the expected LOX dome pressure for the open fire test. Dome pressure was expected to be around 5 bar according to the results of the cold flow test. Reason for this situation may be the insufficient cooling of

the injector and evaporation of the LOX while flowing through the thin injector holes. Higher pressure difference is needed to pass gaseous oxygen through the injector with respect to the liquid oxygen.

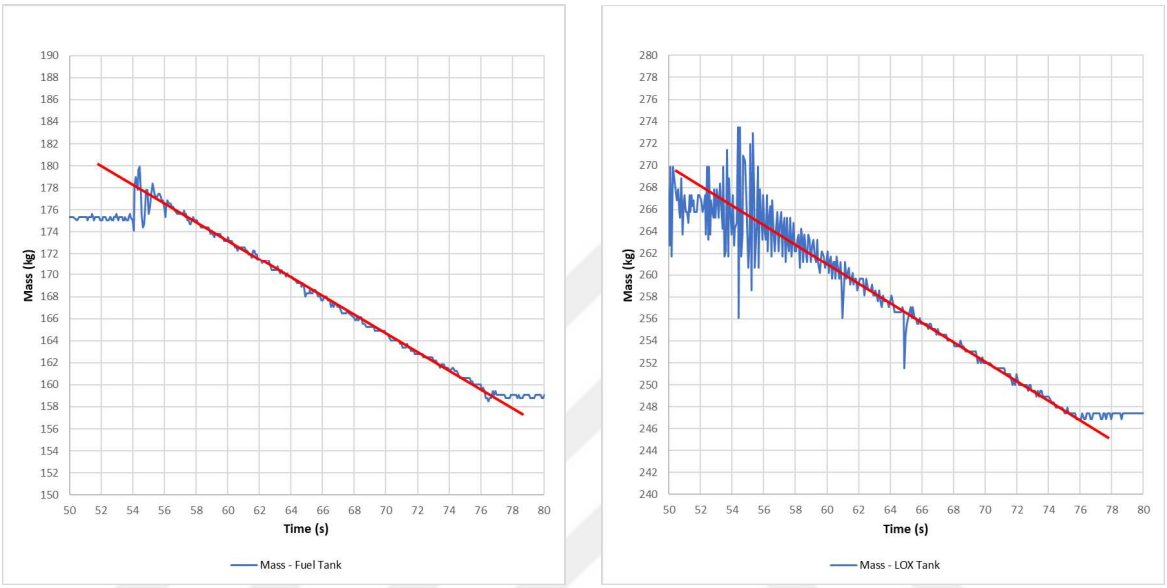

(a) (b)

Figure 7.9. Change of the tank masses during the open fire test with 80 bar tank pressures for (a) the fuel tank and (b) the oxidizer tank.

Mass flow rates can be calculated by tank masses using Figure 7.9. Even if the tank mass calculations are not so stable and there are fluctuations especially in the LOX tank measurements at the beginning of the test, a linear line can be drawn for the last half of the test and the mass rates can be calculated from the slope of this line. Mass flow rates of the LOX and fuel are calculated as 0.88 kg/s and 0.84 kg/s, respectively. So the OF ratio is 1.04. 0.84 kg/s fuel mass flow rate coincides with the cold flow test results but 0.88 kg/s LOX flow rate significantly deviates from the cold flow test and CFD results. It had to be about 1.26 kg/s. Decreasing LOX tank pressure during the test might have an effect on this result but it cannot be the only reason because this would only result in a 5 % decrease in the mass flow rate.

Measured mass flow rates are lower than the design mass flow rates of 1.26 kg/s for the LOX and 1.01 kg/s for the fuel, and OF ratio is lower than the designed value 1.25. However, it is decided that a complete thrust chamber engine test can be conducted even if the mass flow rates are lower than the expected. This would result in lower chamber pressure and lower thrust.



Figure 7.10. BUSTLab V1 80 bar open fire test.

The expected OF ratio was 1.25 but 1.04 is still reasonable for the test and this setup can be used in the actual test. More precise adjustments can be made for the tank pressures and the 1.25 OF ratio can be achieved with further testing but that setup is accepted as eligible because of the insufficient LOX supply for further tests and time constraints. A photo taken during 80 bar open fire test can be seen in Figure 7.10.

7.2.3. BUSTLab V1 Complete Thrust Chamber Test

After the successful completion of the 80 bar open fire test, the combustion chamber is attached to the injector for the full test and fixed to the test stand. The com-

bustion chamber is cooled with an external water source maintained at 15 bar during the test. Cooling water enters the combustion chamber from the nozzle side and exits from the injector side. 20 seconds test is planned. Test setup after cooling the system with LN_2 is shown in Figure 7.11.

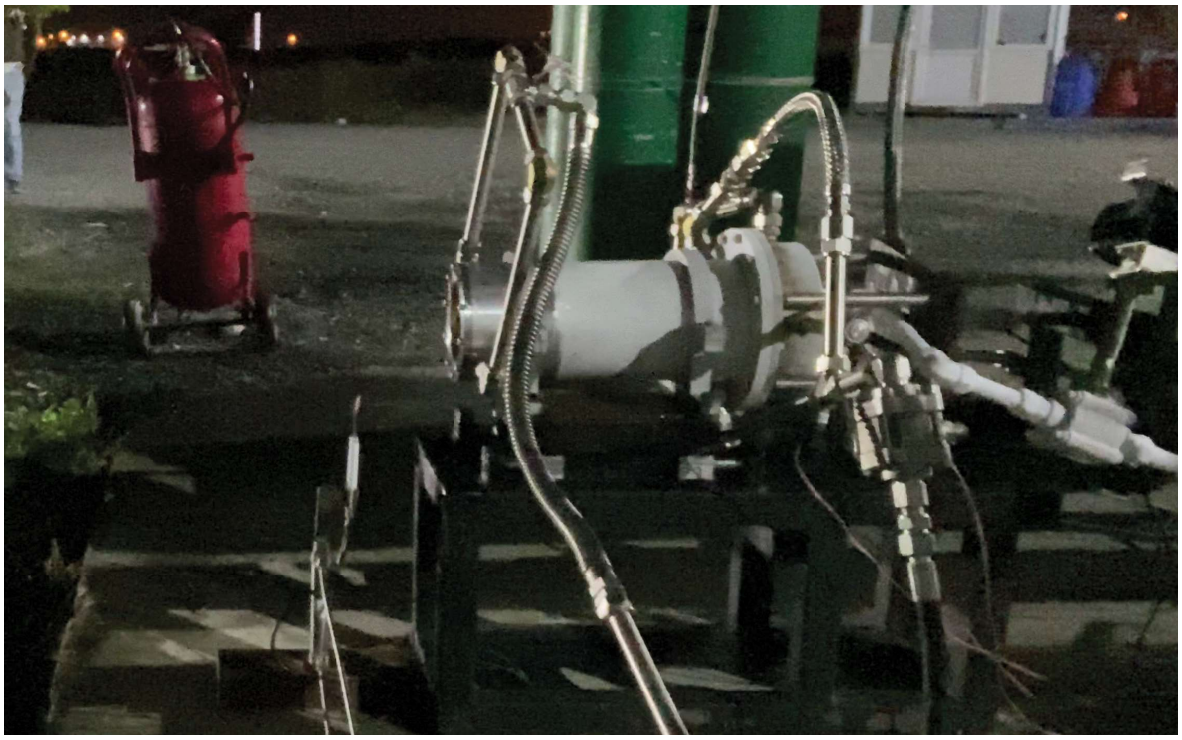

Figure 7.11. BUSTLab V1 rocket engine after cooling the system.

Test setup from a different view angle is given in Figure 7.12. Propellant tanks, control table, pressurizer system, some parts of the cooling system and test stand can be seen in the figure.

Figure 7.13 shows the pressure data taken during the test. Test is terminated unexpectedly after 12 seconds from the ignition. Test starts at t=913 s with opening the tank valves and ignition occurs at t=915 s as soon as the fuel main valve is opened.

Pressure at the LOX dome develops in less than 0.5 second after opening the LOX main valve. LOX dome pressure fluctuates around 65 bar until t=924 s and there

occurs a sudden 3 bar drop after this time. The same drop can be observed at LOX tank pressure as well.

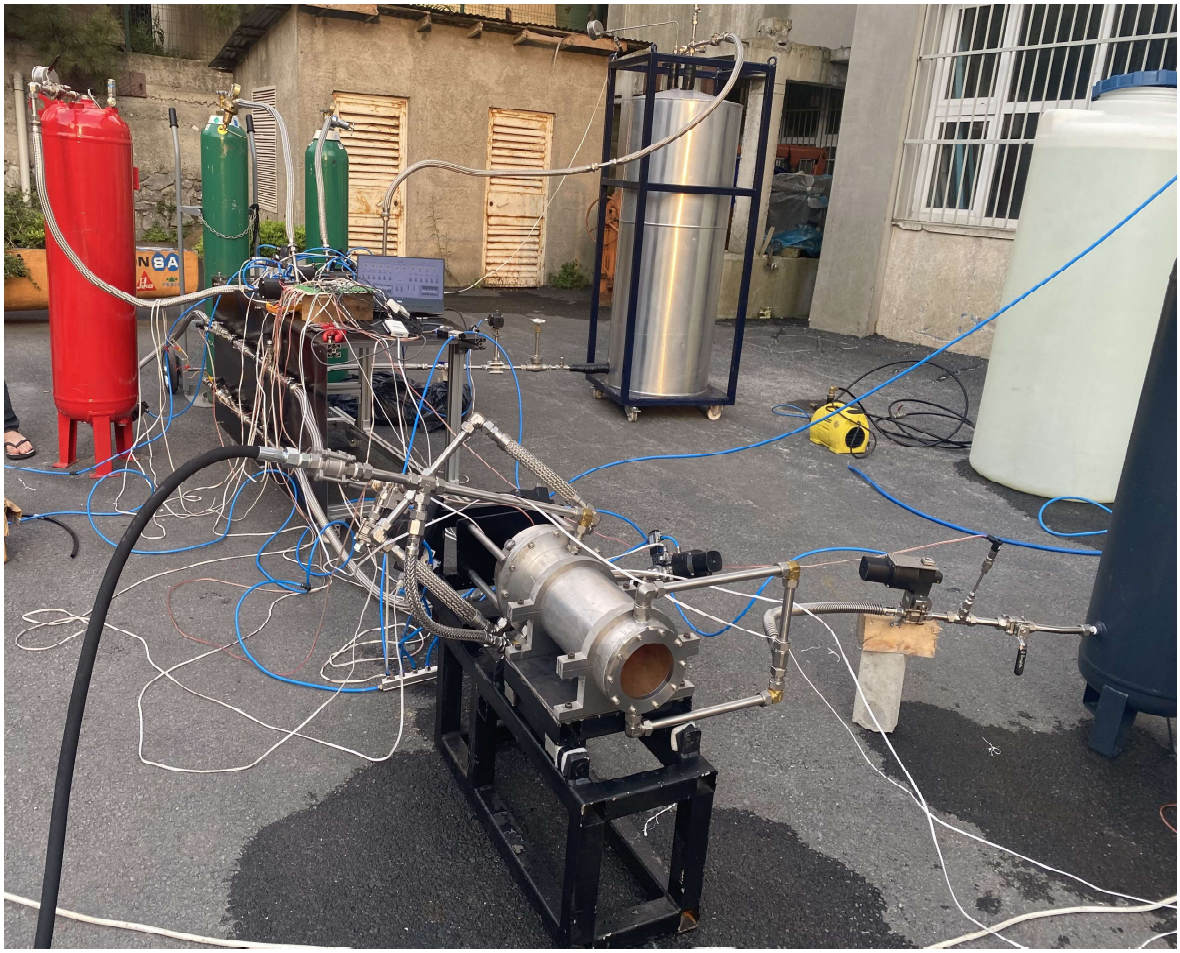

Figure 7.12. BUSTLab V1 rocket engine complete thrust chamber test setup.

Fuel dome pressure shows an unexpected behaviour. Even if the mass flow rate is almost the same throughout the test, it takes around 7 seconds to stabilize around 43 bar. It can be caused from the vaporization of the ethanol inside the dome. Ethanol may have become saturated liquid-vapor mixture and its density may have decreased significantly. Since the mass flow rate is controlled by the cavitating venturi, pressure drop at the injector increases to pass the same mass flow rate with the cavitating venturi.

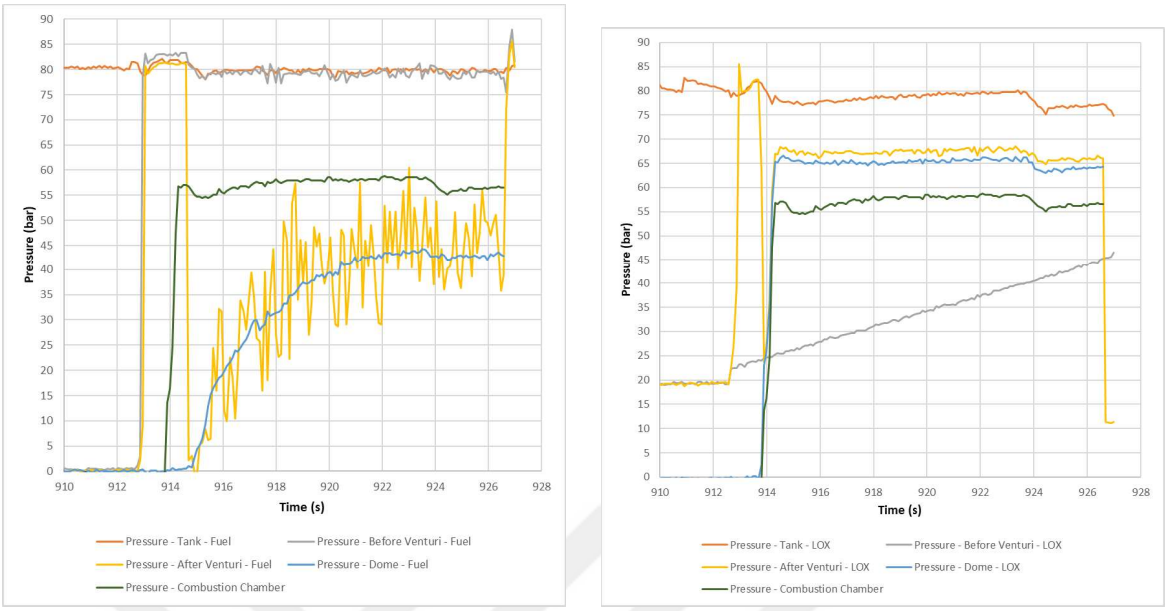

(a) (b)

Figure 7.13. Pressure graphs of the engine test with 80 bar tank pressures for (a) the fuel line and (b) the oxidizer line.

Sudden pressure drop at t=924 s can be observed at fuel dome pressure, too. However, the fuel dome pressure drop is less severe than the LOX dome pressure, around 1.5 bar. This pressure drop might be caused by the insufficient pressurizer supply to the LOX tank, pressure drop in the LOX tank, lower LOX mass flow through the cavitating venturi, pressure drop in the LOX dome, as a result, drop in the combustion chamber pressure. Lower combustion chamber pressure causes a drop in the fuel dome pressure since the fuel mass flow rate is only regulated by the cavitating venturi and there must be a drop in the fuel dome pressure to be able to maintain the same pressure drop at the injector.

Undesired decrease of the LOX tank pressure problem in the 80 bar open fire test seems to be solved by increased nitrogen supply pressure until the t=924 s where a sudden pressure drop is observed.

A photo taken during the test is given in Figure 7.14. Test is stopped unexpectedly at 927th second because of an explosion. Exact reason of the explosion could not be determined. One possibility is a failure of the o-ring between the ethanol and the LOX. Injector shape may have deformed due to the high temperature difference between the two sides of it and o-ring may have leaked.



Figure 7.14. BUSTLab V1 engine firing test.

Tank mass data taken during the test can be seen in Figure 7.15. Mass flow rates can be calculated by using tank mass graphs just like the 80 bar open fire test. Mass flow rates are calculated as 0.83 kg/s and 0.89 kg/s for the LOX and fuel, respectively. This results in an OF ratio of 0.93. LOX mass flow rate is 5.5 % higher and fuel mass flow rate is 6 % lower than the 80 bar open fire test which results in a lower OF ratio.

As can be seen from Figure 7.13, combustion chamber pressure could not be measured correctly. Combustion chamber pressure seems higher than the fuel dome pressure throughout the entire test which is not possible. After examining the 80 bar open fire results, the same situation is observed at that test, too. Even if there was no chamber attached, in other words, "Pressure - Combustion Chamber" sensor

was at open air, it was showing slightly lower pressure values than the LOX dome. There might be leakage between the LOX dome and the position of the "Pressure - Combustion Chamber" pressure sensor caused by a faulty o-ring. Also, there was a problem at the load cell which measures the generated thrust. Thrust could not be measured correctly during the test.

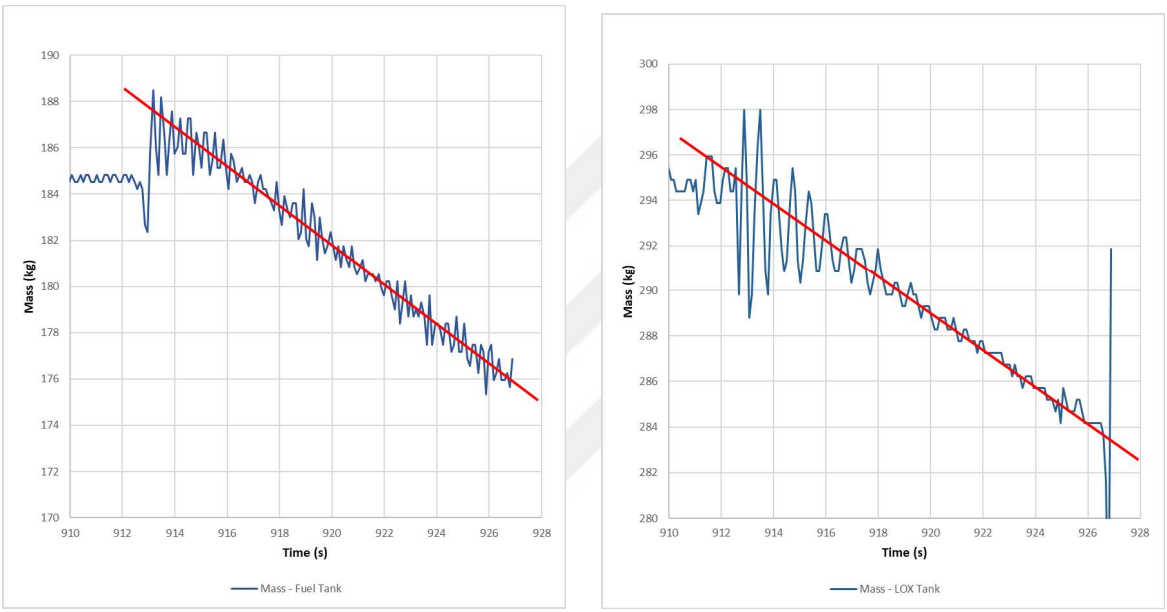

(a) (b)

Figure 7.15. Change of the tank masses during the engine test with 80 bar tank pressures for (a) the fuel tank and (b) the oxidizer tank.

Since the combustion chamber pressure could not be measured correctly, the combustion chamber pressure can be calculated from the mass flow rates and the OF ratio. Given the 0.93 OF ratio, 0.83 kg/s LOX flow rate and 0.89 kg/s ethanol flow rate, given chamber geometry would result in 21 bar chamber pressure. Thrust of the engine can be calculated theoretically. Mass flow rate is know and exit velocity can be calculate from isentropic flow relations. Thrust is calculated to be 3.62 kN for 21 bar chamber pressure. Design mass flow rate and the results of the cold flow, open fire and engine test are summarized in Table 7.1.

Both the fuel dome and the LOX dome pressures are higher than the expected for the estimated 21 bar combustion chamber pressure. High LOX dome pressure is also mentioned in the 80 bar open fire test. Reason may be the phase change of ethanol and LOX at the dome. Heat from the combustion may cause ethanol and LOX to change phase and become saturated liquid-vapor mixture. Since the mass flow rate is determined by the cavitating venturi, pressure difference across the injector increases to pass the same mass flow rate even if the density of the fuel and the oxidizer change.

Table 7.1. Designed and measured mass flow rates in the fuel and the oxidizer lines.

	Mass Flow Rate (kg/s)		**OF Ratio**
	Fuel Line	**Oxidizer Line**	
Design (Ethanol (fuel) - LOX (oxidizer))	1.01	1.26	1.25
Design (Water (fuel) - LN_2 (oxidizer))	1.06	1.02	
Cold Flow (Water (fuel) - LN_2 (oxidizer))	0.88	1.06	
80 Bar Open Fire Test (Ethanol (fuel) - LOX (oxidizer))	0.84	0.88	1.04
Complete Thrust Chamber Test (Ethanol (fuel) - LOX (oxidizer))	0.89	0.83	0.93

8. CONCLUSION

In this research, a bi-propellant rocket engine is designed, manufactured and tested. Firstly, it is designed to generate 10 kN thrust at 50 bar combustion chamber pressure. Kerosene as the fuel and gaseous oxygen as the oxidizer are used. It is decided to use an external water supply for the cooling. Even if the water cooling is used, design is optimized so that it can be easily converted to regenerative cooling with minimal changes. Thrust chamber and cooling channels are designed and manufactured based on this configuration. However, it is found out that 10 kN thrust and 50 bar combustion chamber pressure are not achievable with the available pressurization system. Also, it is noticed that ethanol is easier to find than kerosene for lab-scale experiments and performance of the ethanol is not so different than kerosene. It is decided to test the engine at 30 bar combustion chamber pressure to achieve 5.7 kN thrust with %75 ethanol-water mixture as the fuel and liquid oxygen as the oxidizer. For this configuration, resulted mass flow rates are 1.01 kg/s and 1.26 kg/s for the fuel and the oxidizer, respectively.

Combustion chamber temperature can be adjusted by changing the concentration of the ethanol-water mixture. Increasing the water concentration in the mixture decreases the maximum combustion chamber temperature for the optimum OF ratio. Furthermore, changing the ethanol concentration shifts the OF ratio that maximum I_{sp} is achieved. Increasing water concentration decreases the optimum OF ratio. Optimum OF ratio for %75 concentrated ethanol is around 1.25 whereas optimum OF ratio for %100 concentrated ethanol is around 1.50. Also, adding water to the ethanol decreases the maximum achievable I_{sp}.

Propellants are pressurized by external high pressure nitrogen cylinders. They are available as bundles where 15 pieces high pressure nitrogen cylinders are connected with each other in parallel. It is not possible to control the pressure at the propellant tanks by standard spring loaded pressure regulators. They cannot supply enough

pressurization gas to the propellant tanks. Also, their exit pressure depends on the inlet pressure (pressure of the nitrogen cylinder) and even if the setting of the regulator is not changed, exit pressure decreases with the decreasing inlet pressure. Therefore, two actively controlled pressure control systems are used in the test system. One of them is a commercially available PID controlled electropneumatic controller (TESCOM ER5000) and a dome-loaded pressure regulator. Electropneumatic controller measures the pressure at the outlet of the dome-loaded pressure regulator and adjusts the dome pressure according to the outlet pressure to keep the pressure constant. Pressure can also be controlled by a computer. This system is used for the cooling water pressurization. Another pressure control system is the bang bang control to adjust the pressure at the propellant tanks. Standard on-off pneumatic controlled ball valves are used in the bang bang control system. Pressure at the propellant tank is measured and pressurization valve is opened if the pressure at the tank if lower than the set pressure. De-pressurization valves also can be used to decrease the pressure if the tank pressure is higher than the set pressure. Bang bang control creates a hammering effect at the tank because high pressure from the nitrogen cylinders is supplied suddenly with the opening of the pressurization valve. This effect creates fluctuations at the weight measurements of the tanks.

Mass flow rate is controlled by cavitating venturies. Throat of the cavitating venturi acts like the throat of the nozzle for the gases. When the pressure ratio between the downstream and upstream of the venturi reaches a certain value, around 0.8, mass flow rate through the cavitating venturi stays the same for the same upstream pressure even if the downstream pressure is lowered. In other words, mass flow rate through the venturi does not depend on the downstream pressure in the cavitating mode and mass flow rate can be controlled as desired just by changing the upstream pressure. Other than providing mass flow control, cavitating venturi acts like a buffer zone against the pressure fluctuations in the combustion chamber. Fluctuations in the combustion chamber does not affect the mass flow rate because mass flow rate through the cavitating venturi does not depend on the downstream conditions in the cavitating mode.

Cavitating venturies are designed using CFD analyses. Analyses are also conducted for water and liquid nitrogen as the working fluids because testing the cavitating venturies with the actual fuel (ethanol) and oxidizer (liquid oxidizer) is costly and more safety precautions are needed. Instead, their first tests are conducted with water to validate the CFD analyses. Four cavitating venturies are manufactured, two for the fuel and two for the oxidizer. First fuel and oxidizer cavitating venturies are only used to verify the CFD results. Second set of cavitating venturies are designed and manufactured using the test results of the first set. Final cavitating venturies are designed with 3.52 mm throat diameter for the fuel and 3.72 mm throat diamater for the oxidizer. They are designed for 1.01 kg/s ethanol and 1.26 kg/s oxidizer mass flow rates at 80 bar upstream pressure. However, cold flow tests with water as the fuel and liquid nitrogen as the oxidizer showed that mass flow rate through the fuel cavitating venturi for water is %17 lower (0.88 kg/s instead of 1.06 kg/s) and mass flow rate through the oxidizer cavitating venturi for liquid nitrogen is %4 higher (1.06 kg/s instead of 1.02 kg/s) than the expected mass flow rates. OF ratio for the actual fuel and oxidizer becomes 1.57 with this results and it is thought to be acceptable to conduct firing tests.

Open fire tests without the combustion chamber connected to the injector are conducted before the full engine test. These test are done in different tank pressures to check if everything is working fine. The last open fire test at 80 bar tank pressure represents the same working conditions with the full engine test. Results showed that ignition is achieved successfully. However, mass flow rates can only be measured by the tank weights because turbine flow meter at the fuel line had problems during the tests and and cryogenic flow meter was not available for the oxidizer line. Tank weight measurements has some fluctuations due to the hammering effect of the bang bang control. However, filtered tank weight data can be used to measure the mass flow rates. 80 bar open fire test showed that only 0.88 kg/s and 0.84 kg/s can be achieved for the fuel and the oxidizer, respectively. These results are far below the expected and makes the OF ratio 1.04. However, it is decided to conduct the full engine test with these mass flow rates due to the lack of time and the budget.

Complete thrust chamber test is conducted at 80 bar tank pressures. Expected mass flow rates from the 80 bar open test results are 0.84 kg/s and 0.88 kg/s for the fuel and the oxidizer, respectively. OF ratio becomes 1.04 for these mass flow rates. Firing test showed that 0.89 kg/s fuel mass flow rate and 0.83 kg/s oxidizer mass flow rate are achieved. These results are quite different from the 80 bar open fire test results. OF ratio is calculated to be 0.93. There was a problem at the combustion chamber pressure sensor in this test. Therefore, combustion chamber pressure cannot be measured. Also, there was a malfunction at the load cell that is used for the thrust measurement and thrust could not be measured. Combustion chamber pressure is calculated from the mass flow rates, OF ratio and the throat area as 21 bar. Calculated thrust with the achieved mass flow rates and the calculated combustion pressure is 3.64 kN. Expected test time was 20 seconds. An explosion had occurred at the 12th second of the test and test was stopped. The exact cause of the explosion was not found. One guess is the sealing problem at the o-ring between the LOX dome and the fuel dome. Some locations on the injector might be expanded and contracted due to the high temperature difference between the combustion chamber side and the LOX side. This may cause a leakage problem between the fuel and the oxidizer and resulted in explosion.

Water test results of the cavitating venturies were satisfactory with respect to CFD results. However, mass flow rates were lower than expected at cold flow and hot fire tests. Therefore, there might be another reason than the sizing of the venturi for this problem. Lower propellant mass flow rates than the expected during the tests may be caused from the blockage of the cavitating venturies by external particles or formation of ice at the throat. Moisture in the oxidizer line may transform to ice when the cryogenic flow passes through the venturi. Lower mass flow rates resulted in lower thrust and OF ratio to be different than the design.

The reason for the much higher pressure drop than expected at the injector during the hot fire and complete thrust chamber tests is thought to be the evaporation of the propellants inside the dome before entering the combustion chamber. Since the mass flow rate is regulated by cavitating venturi, pressure drop at the injector increases to

pass the same mass flow rate with a lower density fluid, saturated liquid-vapor mixture. Also, it is observed that cavitating venturi in the oxidizer line may not be working in cavitating mode during the complete thrust chamber test because the pressure ratio across the cavitating venturi reaches 0.8.

8.1. Future Work

BUSTLab V1 rocket engine is designed to be water cooled. However inlet and outlet ports of the water are placed so that it can be transformed into a regeneratively cooled engine. Fuel enters the dome through 4 ports around the dome in the current design and water enters the cooling channels through the ports on the jacket part. Fuel pipeline from the main fuel valve can be connected to the current water inlet port and current water outlet port can be connected to the current fuel inlet ports on the sides of the dome. In this way, fuel enters the cooling channels through the port at the aft size of the jacket, cools the nozzle and the combustion chamber while flowing in cooling channels, exits the cooling channels through the port at the dome side of the jacket and enters the fuel dome through the four fuel inlet ports. Furthermore, cooling channels may need to be redesigned considering the temperature increase of the propellant used for the regenerative cooling and the pressure drop of it at the cooling channels. Current water cooled design cannot be used for the flight test because it needs an external water supply. It can be used for flight test if the regenerative cooling design is adapted.

Another important point for being able to achieve vertical take of and vertical landing is the throttleability. Thrust of the current design cannot be actively controlled. One of the easiest way of controlling the thrust is the mass flow rate control. Cavitating venturies are used in the current design to determine the mass flow rates. Mass flow rate through cavitating venturi can be controlled by changing its upstream pressure or the throat area. As mentioned before, there are two critical points where the mass flow rate can be restricted: throats of the cavitating venturi and the nozzle. Mass flow rate through the cavitating venturi changes with the square root of the upstream pressure. However, mass flow rate through the nozzle of the thrust chamber changes

proportionally with the chamber pressure. Main aim of using cavitating venturi is limiting the mass flow rate at the cavitating venturi by keeping the downstream pressure of the venturi below a certain level of the upstream pressure. If the ratio of the downstream pressure and the upstream pressure of the cavitating venturi exceeds a certain limit, mass flow rate is not choked at the cavitating venturi anymore and mass flow rate cannot be only controlled by the upstream pressure of the cavitating venturi. If the upstream pressure of the cavitating venturi is reduced, mass flow rate and the combustion chamber pressure decreases with the square root of the cavitating venturi upstream pressure. In other words, combustion chamber pressure decreases slower than the upstream pressure of the cavitating venturi. For instance, if the upstream pressure of the cavitating venturi is reduced to one quarter, mass flow rate and the combustion chamber pressure is halved. Therefore, ratio of the downstream pressure and the upstream pressure of the cavitating venturi may exceed the critical limit while trying to reduce the mass flow rate. Cavitating venturi upstream pressure control is not a preferred method because of this reason.

Another way of changing the mass flow rate through the cavitating venturi is changing the throat area of it. Mass flow rate changes proportionally with the cavitating venturi throat area. Upstream pressure of the cavitating venturi can be kept constant while changing the mass flow rate in this way. This guarantees that pressure ratio both sides of the venturi stays below critical limit while changing the mass flow rate. A variable area cavitating venturi can be designed and used in the system to make the engine throttleable.

Mass flow rate of the engine can also be controlled by the injector instead of using cavitating venturi. Mass flow rate through the injector depends of the pressure at the both sides of the injector and the injector area. Mass flow rate can be controlled if the injector area can be controlled actively. A pintle injector designed can be used for this purpose. Cavitating venturies are not needed anymore if the pintle injector is used.

The most problematic point during the tests was the sensor measurement. Thrust load cell was faulty during the complete thrust chamber test. Also, there were faulty pressure sensors during the hot fire tests. It is realized that one of the most important point of testing is making sure that all of the measurement devices are working properly before each test. Cryogenic flow near the pressure sensors and high loads at the load cells may cause sensors to become faulty. A measurement pre-check system can be developed to test measurement devices before each test. A secondary pressure line can be constructed so that all of the pressure sensors are connected to this line. Before each test, lines to which the pressure sensors are actually connected can be closed by manual or remote controlled valves and sensor connections to the secondary pressure line can be opened. Pressure sensors can be checked in this way before each test. A pre-loading mechanism can be developed to check thrust load cell. It can be pre-loaded with a known load before the test to see if it gives the correct measurement.

REFERENCES

1. Kokal, U., *Development of a Mili-Newton Level Thrust Stand for Thrust Measurements of Electric Propulsion Systems and UK90 Hall Effect Thruster*, M.S. Thesis, Bogazici University, 2019.

2. Haidn, O. J., "Advanced Rocket Engines", *Advances on Propulsion Technology for High-Speed Aircraft*, Vol. 1, pp. 6–1, 2008.

3. Sutton, G. P. and O. Biblarz, *Rocket Propulsion Elements*, John Wiley & Sons, New Jersey, 2016.

4. Bills, J. D., *Liquid Fuel Film Cooling: a CFD Analysis with Hydrocarbon Fuel*, M.S. Thesis, Air Force Institute of Technology, 2016.

5. Salvatore, V., F. Battista, P. De Matteis and L. Rose, "Current Activities for the Development of a LOX/LCH4 Regenerative Thrust Chamber at the Italian Aerospace Research Centre", paper presented at the *Space Propulsion Conference*, Cologne, 2014.

6. Goddard, C. H., "Scientific Identification of Firearms and Bullets", *American Institute of Criminal Law and Criminology*, Vol. 17, p. 254, 1926.

7. Betts, E., "Waking a Giant: Bringing the Saturn F-1 Engine Back to Life", `https://ntrs.nasa.gov/api/citations/20140011656/downloads/20140011656.pdf`, accessed on May 5, 2022.

8. Marques, M. P. P. M., *Small Liquid Propellant Rocket Engine*, M.S. Thesis, Técnico Lisboa, 2016.

9. Delpy, R. and J. Oswald, "PERSEUS Project 5kN LOX/Ethanol Rocket Engine Fire Tests", paper presented at the *7th European Conference for Aeronautics and*

Space Sciences (EUCASS), Milan, 2017.

10. Andersson, E., *Preliminary Design of a Small-Scale Liquid-Propellant Rocket Engine Testing Platform*, M.S. Thesis, Luleå University of Technology, 2019.

11. Trillo, J. E., *Design of a 500 lbf Liquid Oxygen and Liquid Methane Rocket Engine for Suborbital Flight*, M.S. Thesis, University of Texas at El Paso, 2016.

12. Herrera, M. J., *Design and Testing of a 500 lbf Liquid Oxygen/Liquid Methane Engine*, M.S. Thesis, University of Texas at El Paso, 2019.

13. Lopez, I., *Design of a 2000 lbf LOX/LCH4 Throttleable Rocket Engine for a Vertical Lander*, M.S. Thesis, University of Texas at El Paso, 2017.

14. Tokudome, S., T. Yagishita, K. Goto, N. Suzuki, T. Yamamoto and Y. Daimoh, "An Experimental Study of an N2O/Ethanol Propulsion System with 2 kN Thrust Class BBM", *Transactions of the Japan Society for Aeronautical and Space Sciences, Aerospace Technology Japan*, Vol. 19, No. 2, pp. 186–192, 2021.

15. Pizzarelli, M., F. Nasuti and M. Onofri, "Trade-Off Analysis of High-Aspect-Ratio-Cooling-Channels for Rocket Engines", *International Journal of Heat and Fluid Flow*, Vol. 44, pp. 458–467, 2013.

16. Bergman, T. L., F. P. Incropera, D. P. Dewitt and A. S. Lavine, *Fundamentals of Heat and Mass Transfer*, John Wiley & Sons, New Jersey, 2011.

17. "Chemical Equilibrium with Applications", `https://www1.grc.nasa.gov/research-and-engineering/ceaweb/`, accessed on May 21, 2022.

18. Nardi, R., V. Perez and A. Pimenta, "Experiments with Pintle Injector Design and Development", paper presented at the *51st AIAA/SAE/ASEE Joint Propulsion Conference*, Orlando, 2015.

19. Yang, L.-J. and Q.-F. Fu, "Theoretical Investigation on the Dynamics of a Gas-Liquid Coaxial Swirl Injector", *Journal of Propulsion and Power*, Vol. 27, No. 1, pp. 144–150, 2011.

20. Lee, I., D. Kim and J. Koo, "Breakup Structure of Two-Phase Jets with Various Momentum Flux from a Porous Injector", *Journal of Thermal Science*, Vol. 23, No. 1, pp. 60–67, 2014.

21. Stark, R., "Flow Separation in Rocket Nozzles, a Simple Criteria", paper presented at the *41st ASME/SAE/SEE Joint Propulsion Conference*, Tucson, 2005.

22. Ingle, M. A., *Characterizing Cryogenic Propellant Flow Behavior Through a Cavitating Venturi in Comparison to Alternative Flow Control Mechanisms*, M.S. Thesis, The University of Texas at El Paso, 2014.

23. Yazıcı, B., *Numerical and Experimental Investigation of Flow Through a Cavitating Venturi*, M.S. Thesis, Middle East Technical University, 2015.

24. Kang, D., K. Ahn, B. Lim, S. Han, H.-S. Choi, S. Seo and H. Kim, "Flow Control Characteristics of Cavitating Venturi in a Liquid Rocket Engine Test Facility", *Journal of the Korean Society of Propulsion Engineers*, Vol. 18, No. 3, pp. 84–91, 2014.

25. KELLER AG für Druckmesstechnik, "Piezoresistive Pressure transmitters for Industrial Applications, Series 21Y", `https://download.keller-druck.com/api/download/8Ls5MtHNCdS8NgffyPLvee/en/latest`, accessed on April 12, 2022.

26. "Pneumatic Solenoid Valve, 3 Way, Normally Open, 12V/24V/110V/220V", `https://www.ato.com/pneumatic-solenoid-valve-3-way-normally-open-12v-24v-110v-220v`, accessed on April 20, 2022.

27. "5/2 Single Solenoid Valve With Spring Return", `https://www.uflowvalve.com`

/pneumatic-valve/product/5-2-single-soleno id-valve-with-spring-return, accessed on April 15, 2022.

28. "Solenoid valve 5/2 4V210 1/4 inch for pneumatic cylinders + connectors 6mm", https://hpcontrol.eu/elektrozawor-silownikow-5-2-4v210-1-4-zlaczki-6mm.html, accessed on April 12, 2022.

APPENDIX A: CAVITATING VENTURI TESTS

Cavitating venturies OCV-V0 and FCV-V1 are tested with water to verify CFD analyses results. Most important results are given in section 4.3 and the rest of them are given in this chapter.

A.1. OCV-V0 Water Tests

OCV-V0 - Test 2 water test results are given in Figure A.1. Manual valve is closed gradually in this test, which can be seen between 20th and 50th seconds. However, there are quite high pressure fluctuations observed especially in the downstream pressure. Ball valve is opened fully in 18th second and cavitating mode can be observed in 19th second.

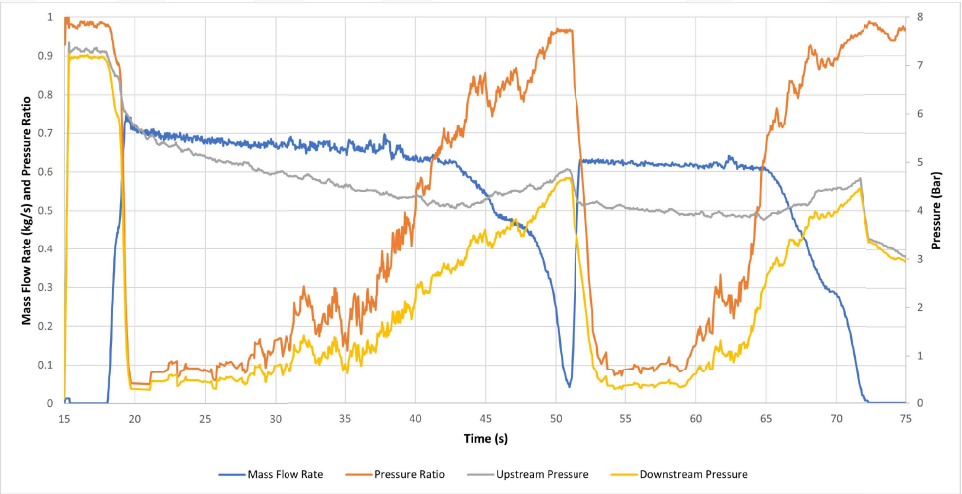

Figure A.1. Water test results of the oxidizer cavitating venturi OCV-V0 for the upstream pressure of 4 to 6 bar (OCV-V0 - Test 2)

Ball valve is closed gradually after this point. Cavitating mode continues until 43th second where the pressure ratio reaches around 0.8. Ball valve is closed furthermore and decrease in the mass flow rate can be seen clearly with the increasing pressure ratio.

Fluctuations in the pressure ratio is quite high especially when it is below 0.2. There are measurement fluctuations in upstream pressure and downstream pressure and they are magnified when the pressures are divided to each other to calculate pressure ratio.

A.2. FCV-V1 Water Tests

Upstream pressure decreases from 5.5 bar to 4 bar and mass flow rate decreases from 0.7 kg/s to 0.64 kg/s between 20th and 43th seconds. Upstream pressure is almost constant at 3.9 bar and mass flow rate is 0.62 kg/s between 52th and 65th seconds.

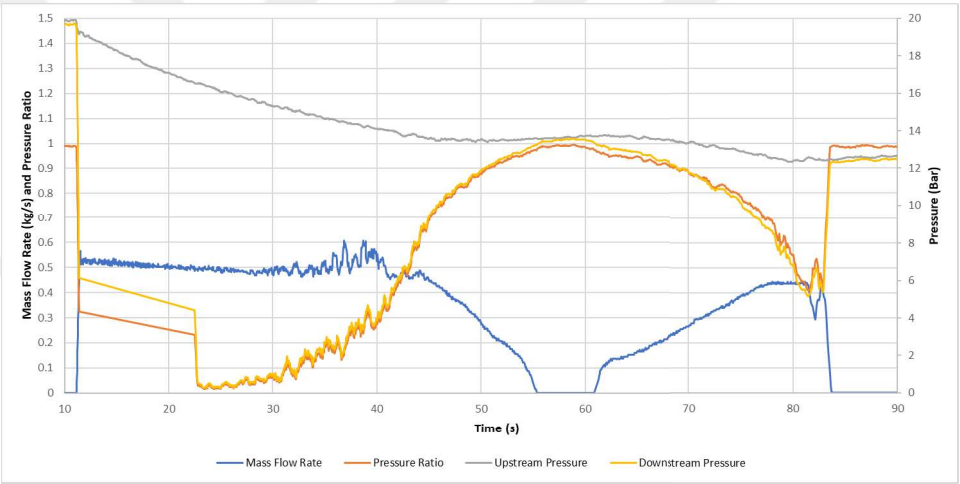

Figure A.2. Water test results of the fuel cavitating venturi FCV-V1 for the upstream pressure of 20 bar (FCV-V1 - Test 2).

Figure A.2 shows the water test results for FCV-V1. The tank pressure is set to 20 bar before the test. FCV-V1 is tested for 20 bar upstream pressure and different downstream pressure by changing the opening of the ball valve at the downstream of the cavitating venturi. Pressure in the tank starts to decrease when the pneumatic valve is opened at t=11 s. It starts stabilizing after t=45 s and stays almost constant at around 14 bar for 25 seconds. Pressure ratio changes between 0.35 and 1 during this section of the test. So, both the cavitating and the non-cavitating modes can be analysed. It decreases to 12.5 bar after 70th due to the insufficient pressurizer gas

supply. 0.47 kg/s water mass flow rate at 13.5 bar upstream pressure and 0.44 kg/s water mass flow rate at 12.6 bar upstream pressure are measured in this test.

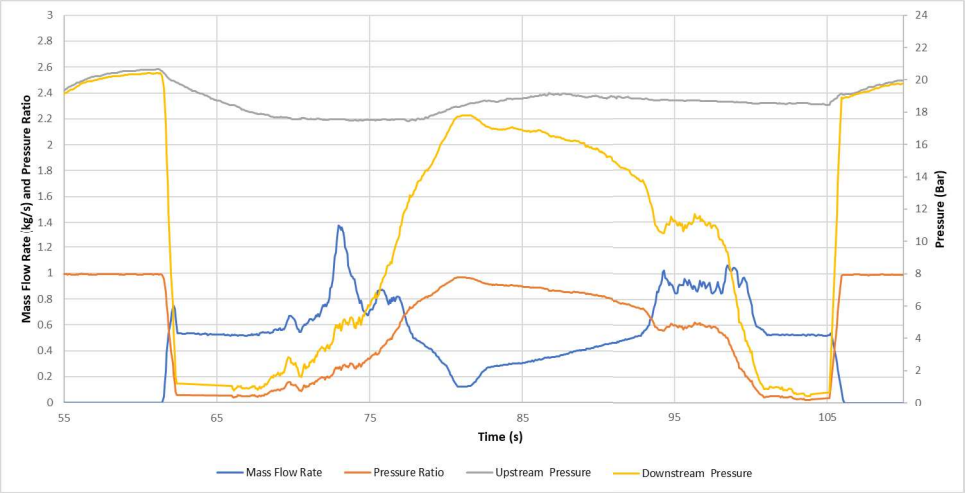

Figure A.3. Test results of the fuel cavitating venturi FCV-V1 for the upstream pressure of 18.5 bar (FCV-V1 - Test 3).

Figure A.3 shows another water test for FCV-V1. It starts with a water tank pressure of 20.5 bar, initially. It is almost constant at 18.5 bar between 87th and 105th seconds. Mass flow rate fluctuates around 0.9 kg/s where the pressure ratio is around 0.6. 0.9 kg/s is very high for 18.5 bar upstream pressure when compared with CFD analysis results and the other tests. It can be said that there is a measurement error during this period. When the pressure ratio is decreased further by opening the manual ball valve, mass flow rate stabilizes at around 0.53 kg/s with almost no fluctuations. A flow rate of 0.53 kg/s is an expected results for 18.8 bar upstream pressure.

APPENDIX B: TECHNICAL DRAWINGS

Technical drawings of the cavitating venturies FCV-V1 and OCV-V1, the combustion chamber, and the dome andare given in this chapter.

B.1. Fuel Cavitating Venturi FCV-V1

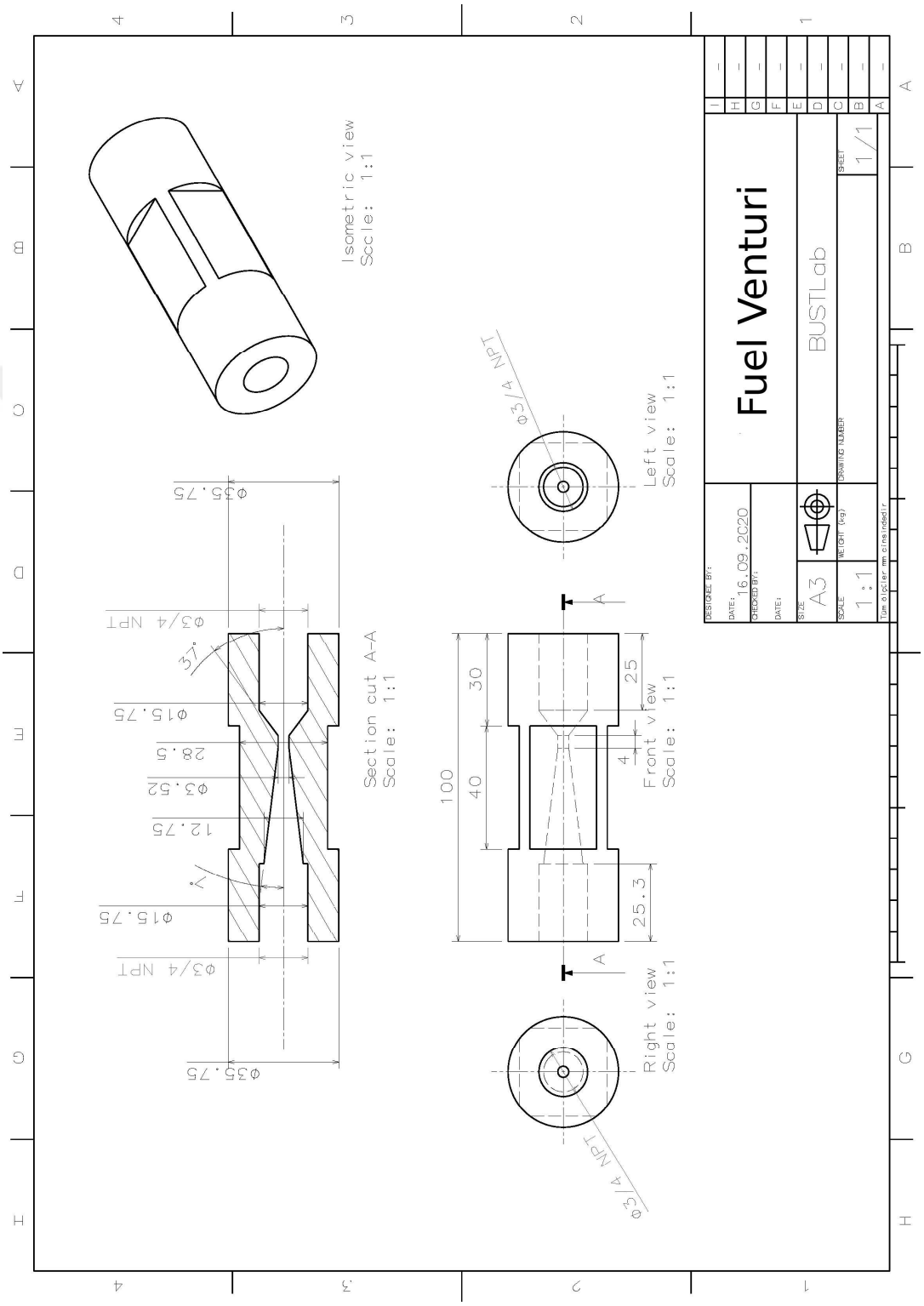

Figure B.1. Technical drawing of the fuel cavitating venturi FCV-V1.

B.2. Oxidizer Cavitating Venturi OCV-V1

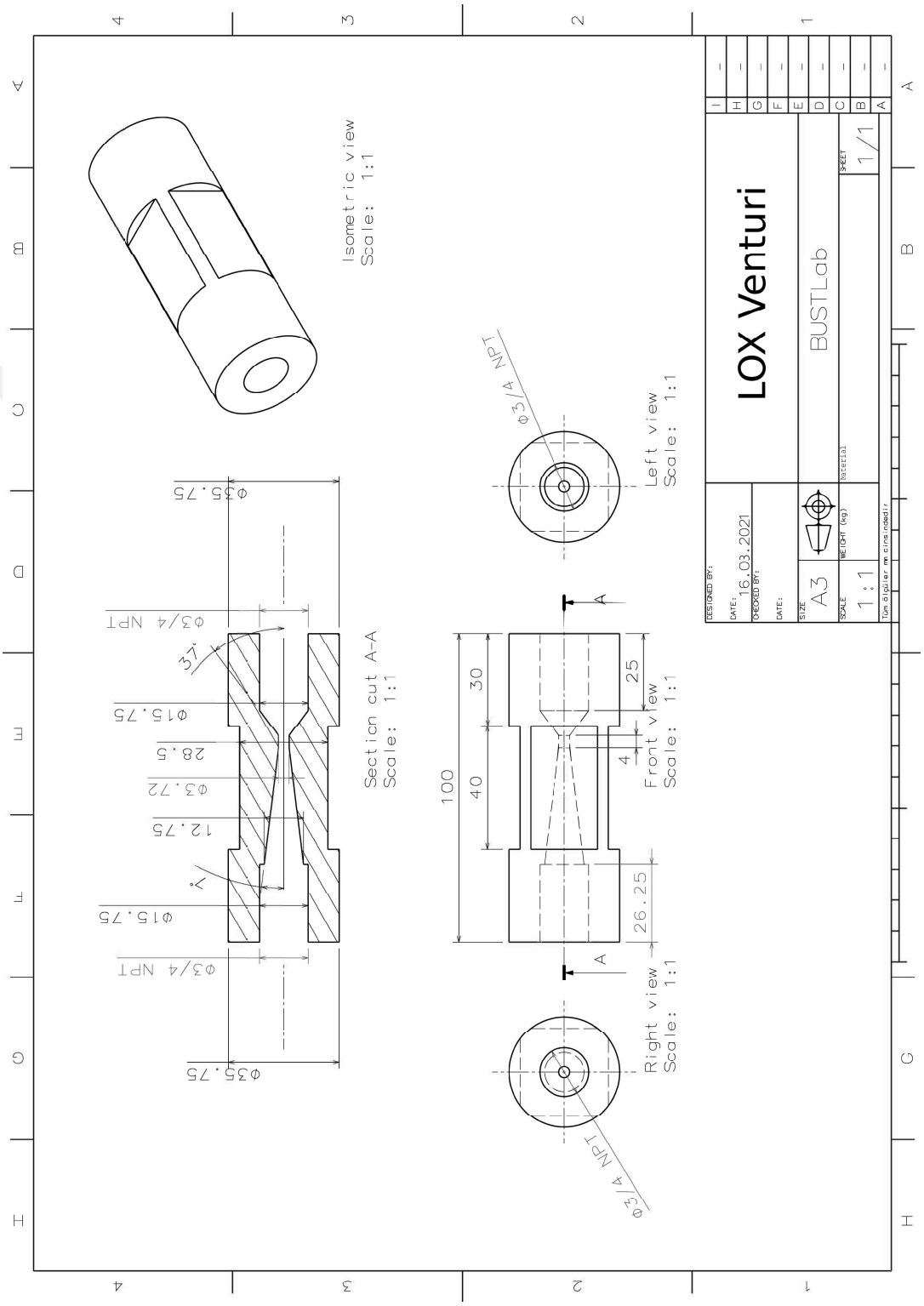

Figure B.2. Technical drawing of the oxidizer cavitating venturi OCV-V1.

B.3. Combustion Chamber

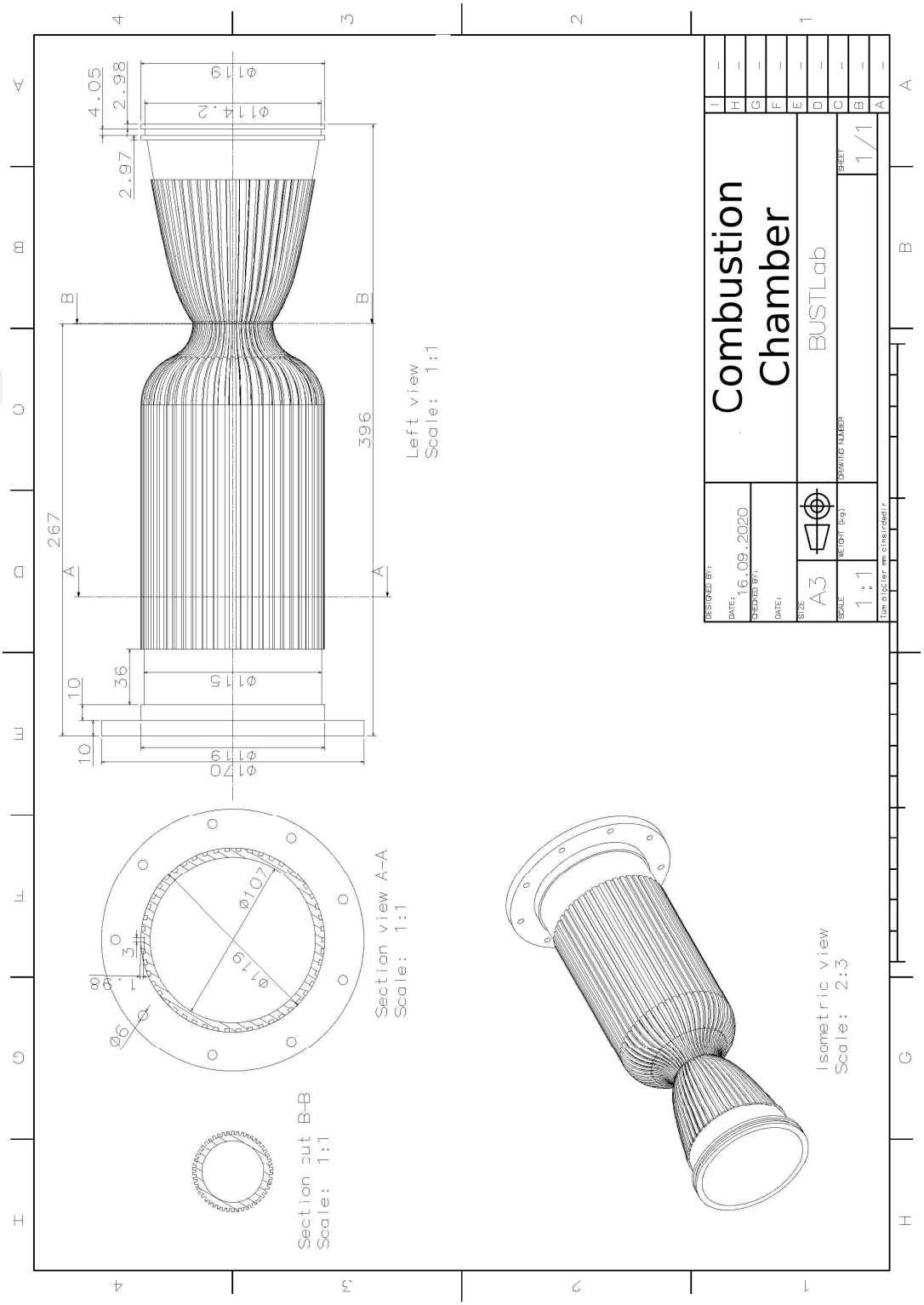

Figure B.3. Technical drawing of the combustion chamber.

B.4. Dome

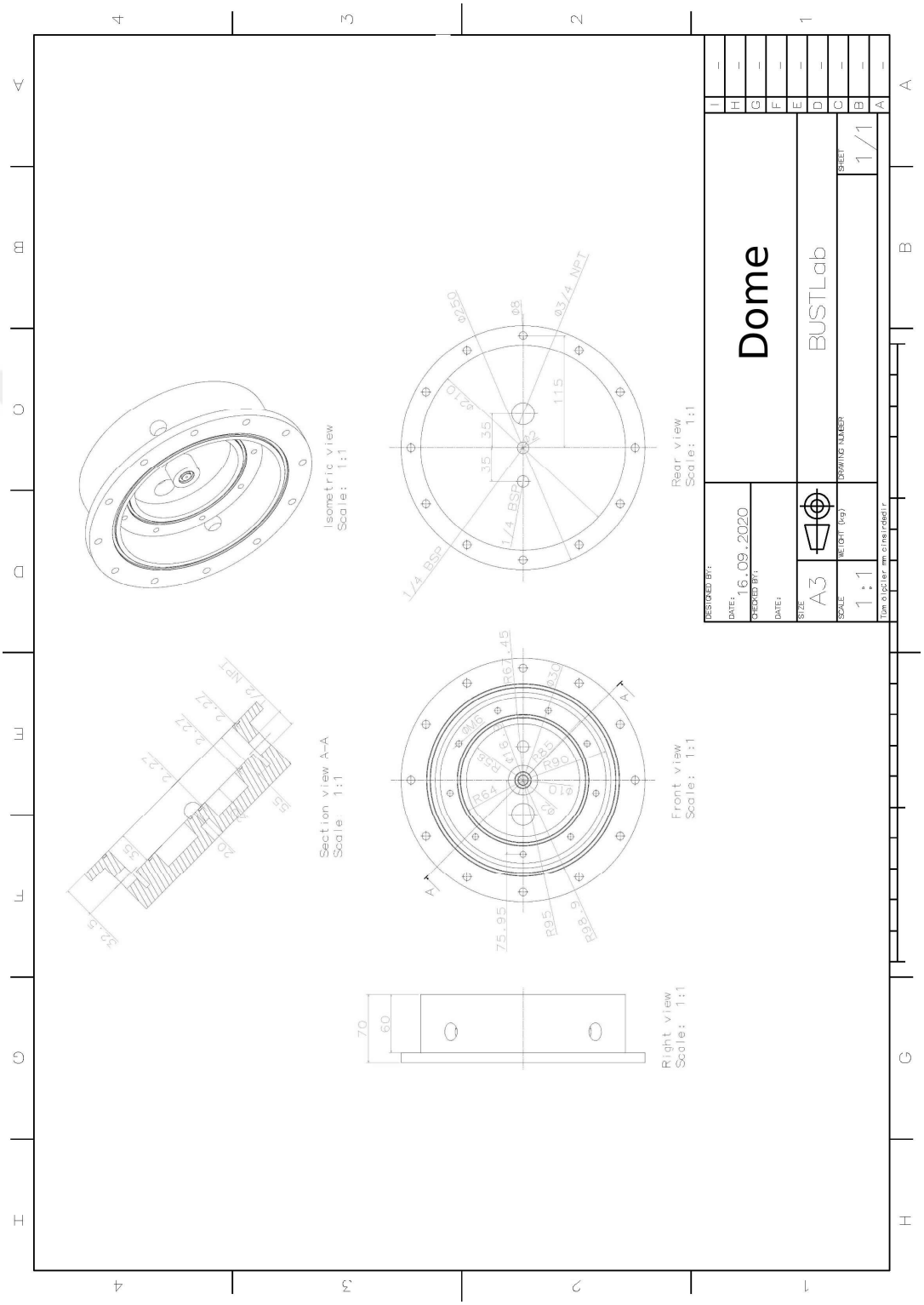

Figure B.4. Technical drawing of the dome.